A PETROLOGIC AND DIAGENETIC STUDY OF THE ONONDAGA FORMATION, NEW JERSEY

By

Kelsey L. McGee

July, 2017

Director of Thesis: Dr. Donald W. Neal

Major Department: Geological Sciences

A petrologic investigation of the Onondaga Formation in New Jersey has never been conducted, although similar studies have taken place in the surrounding states of New York and Pennsylvania. Thirteen sample sites from the formation in New Jersey were analyzed using thin section point counting, insoluble residue analysis, X-ray Diffraction, and Scanning Electron Microscopy/Energy Dispersive X-ray microanalysis. These methods gave insight into the lithology, mineralogy, diagenesis, and depositional environment of the Onondaga Formation.

Five main lithofacies were identified. These are two limestones including siliceous mudstones and siliceous mudstones with nodular chert, and three siliceous mudrocks including calcareous mudrocks, calcareous mudrocks with nodular chert, and cherty calcareous mudrocks. The mineralogy of these five lithofacies is roughly consistent amongst the sites. Carbonate minerals (calcite and dolomite), silica, alkali feldspars, and phyllosilicates are the main mineralogical groups with silica being by far the most abundant. Albite was the main alkali feldspar identified and illite, chlorite, and minor kaolinite, were the three main phyllosilicates.

Carbonate mud and terrigenous sediments forming the Onondaga Formation were deposited in a carbonate ramp environment. After deposition, these sediments underwent burial and compaction, cementation, dissolution of fossils, chert nodule growth and dolomite formation

at the expense of the carbonate mud, further burial and compaction in the form of fractures, stylolites, and pressure seams, and finally healing of these fractures by sparite. The source of silica for chert nodule growth consisted of sponge spicules, dissolution of terrigenous sediment, influx of silica rich fluids from meteoric waters, and minor volcanic ash dissolution. These sediments were formed close to their source of origin during the incipient Acadian Orogeny. The small amount of clay minerals present, with respect to silica, in the samples points to not much weathering of the newly formed mountains during sediment accumulation.

A Petrologic and Diagenetic Study

of the Onondaga Formation, New Jersey

A Thesis

Presented To the Faculty of the Department of Geological Sciences

East Carolina University

In Partial Fulfillment of the Requirements for the Degree

Master of Science in Geology

By

Kelsey L. McGee

July, 2017

A Petrologic and Diagenetic Study

of the Onondaga Formation, New Jersey

By

Kelsey L. McGee

APPROVED BY:

DIRECTOR OF
THESIS: _____
Donald W. Neal, PhD

COMMITTEE MEMBER: _____
Richard K. Spruill, PhD

COMMITTEE MEMBER: _____
Terri L. Woods, PhD

COMMITTEE MEMBER: _____
Katharine Lee Avary, MS

CHAIR OF THE DEPARTMENT
OF GEOLOGICAL SCIENCES:_____
Stephen J. Culver, PhD

DEAN OF THE
GRADUATE SCHOOL: _____
Paul J. Gemperline, PhD

Dedicated

To my father, who is the most inquisitive person I know and always pushed me to ask the questions I never thought of in my research.

Acknowledgements

I would like to thank Dr. Donald Neal for taking me on as one of his last graduate students and putting up with my endless amount of questions. I would also like to thank my committee members for their insight, critiques, and edits in helping me complete my thesis. A special thanks goes to Dr. Richard Mauger for his help in running the XRD and interpreting those results. Thanks to Dr. Tom Fink for his time and patience in running the SEM-EDS. Also, many thanks go to James Watson and John Woods for all their help with my lab work.

I could not have completed this project without the help and support from all my friends, family, and colleagues along the way. Finally, a very special thanks goes to my fiancé Justin who was my rock through all of this work and helped me with numerous edits along the way.

Table of Contents

List of Tables

List of Figures

I. Introduction and Geologic Background

The Onondaga Formation dates from 390-383 million years ago during the Early-Middle Devonian in the Eifelian Age (USGS, n.d.). It is located in present day Virginia, West Virginia, Maryland, Ohio, Pennsylvania, New Jersey, New York, and Ontario (Figure 1) (Kindle, 1912; Dennison, 1961; Brett and Ver Straeten, 1994; Ver Straeten, 1996, 2001; Clark, 2003).

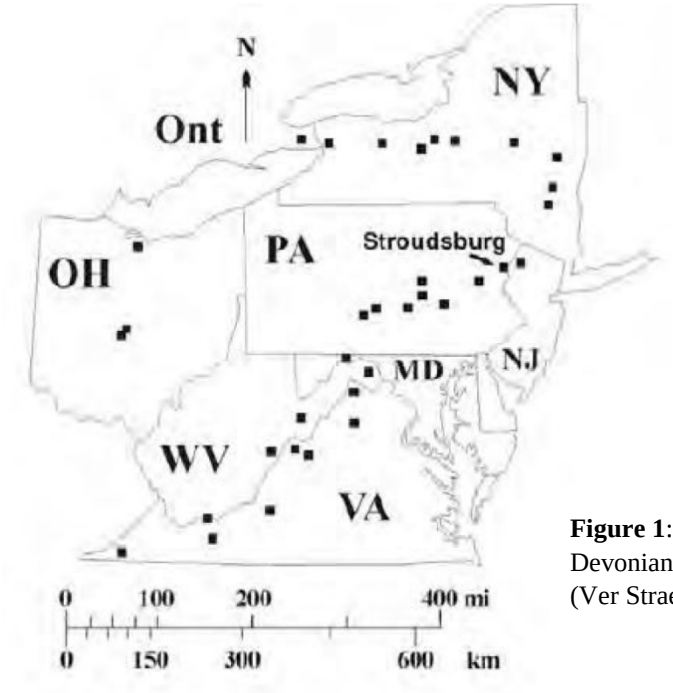

Figure 1: Key outcrops of upper Lower to lower Middle Devonian Onondaga Formation, Appalachian foreland basin. (Ver Straeten, 2001)

The Onondaga Formation has conformable boundaries everywhere with the overlying Marcellus Shale. The Schoharie and Esopus formations lie conformably below the Onondaga in eastern Pennsylvania, New Jersey, and southeastern New York (Epstein, 1984; Ver Straeten, 2001). The Schoharie and Esopus units are calcareous siltstones and mudstones grading downward into shales and sandy siltstones, and the Marcellus is a hydrocarbon-rich black shale (Epstein, 1984; Ver Straeten, 2001). These formations formed during the onset of the Acadian Orogeny in a foreland basin located under an ancient epicontinental sea, the Kaskaskia Sea (Fichter and Baedke, 2000). As the sea lapped onto the land, sediment was deposited in the shallow water

environment and limestones built up in the highly saturated water (Figure 2). These deposits were lithified to what is now known as the Onondaga Formation.

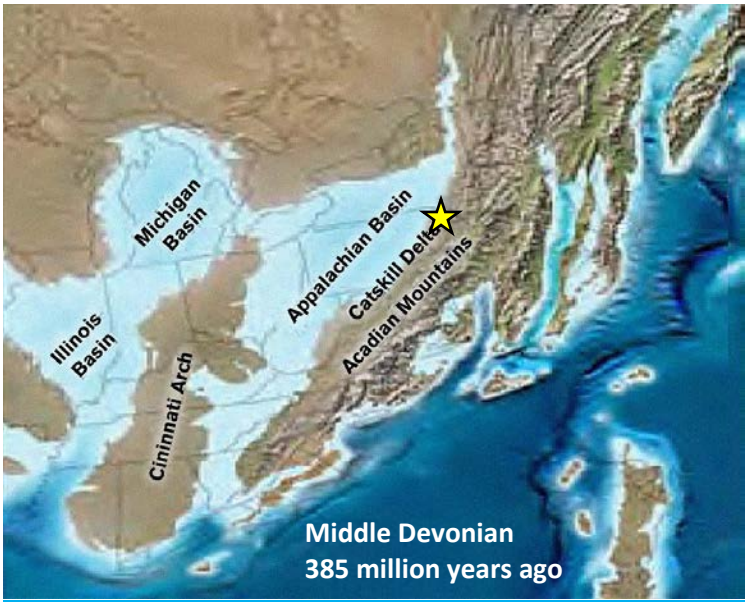

Figure 2: Paleogeographic reconstruction of the Devonian landscape in North America. Appalachian Basin represents the Kaskaskia Sea where the Onondaga Formation formed around the basin's edge. Star indicates location of study area. Modified from original map by Ron Blakey. (Blakey, 2009)

The Onondaga Formation is divided into four members which are, from oldest to youngest, Edgecliff, Nedrow, Moorehouse, and Seneca. In the Moorehouse, Nedrow, and upper Edgecliff members, nodules of dark gray to black chert are found (Oliver, 1956). These chert-bearing units correlate from New York into eastern Pennsylvania. The chert-bearing zones pinch out to the southwest, and are no longer seen in central Pennsylvania (Figure 3) (Willard, 1936). Further south, the Onondaga crops out again in western Virginia, West Virginia, and Ohio (Dennison, 1961). The chert-bearing interval is again found in these southern states. This chert appears very homogenous in nature and can be traced in the Onondaga through several states (Jarvis, 1988; Clark, 2003).

No petrologic investigation has been conducted on the Onondaga Formation in New Jersey. Understanding the petrology of the formation in New Jersey, as well as its diagenetic history, is important in understanding the depositional environment in which the chert and

limestone formed. It will also aid in the paleoclimate reconstruction of the Devonian in New Jersey. Further, a reconstruction of where the sites were located with reference to the thickness of the formation would help with member identification in New Jersey, which is lacking due to the absence of outcrops.

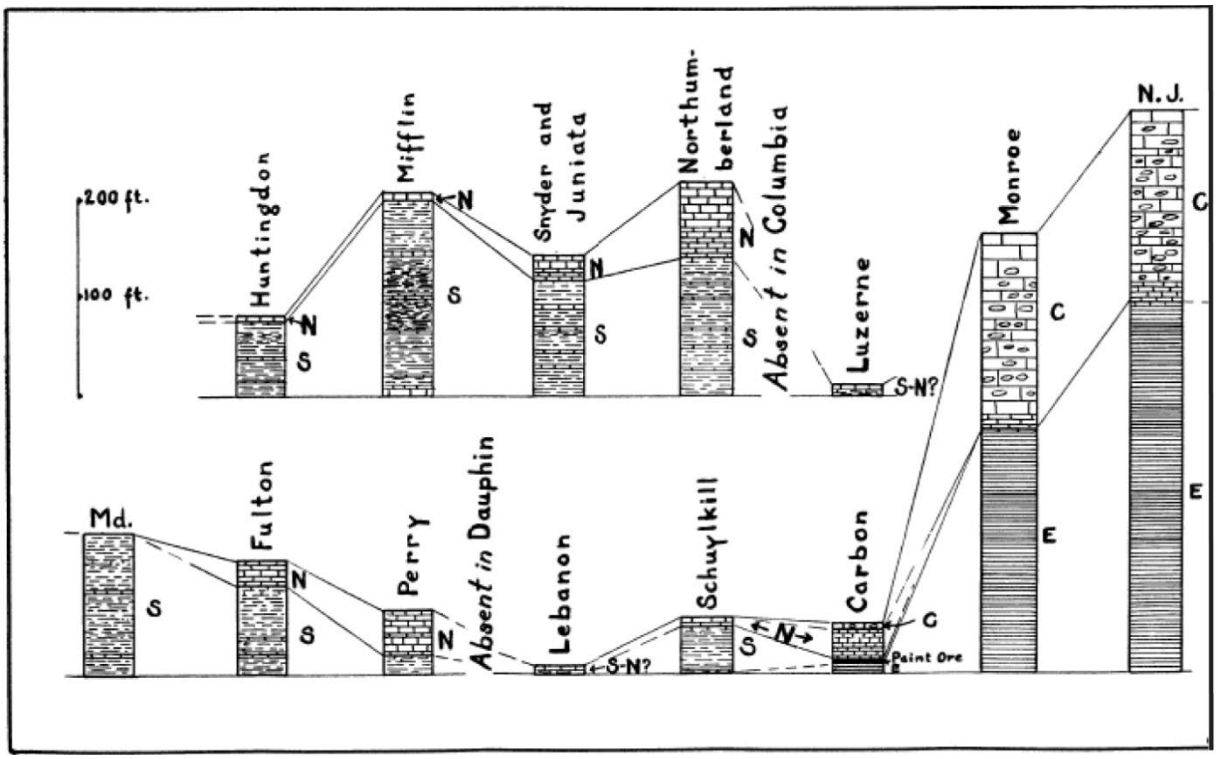

Figure 3: Correlation chart of the Onondaga Formation in Pennsylvania. Two series of columnar sections are drawn, the lower representing Onondaga in the more southern counties; the upper, the formation across central Pennsylvania. C=cherty limestone, E=Esopus, N=non-cherty limestone, S=limy shale. New Jersey and Maryland sections are included for comparison. (Willard, 1936)

II. Previous Research

The Onondaga Formation

The Onondaga Formation was originally named by James Hall in a report done for the New York Geologic Survey in 1839. He named the formation for exposures in Onondaga County, New York (Dennison, 1961). In 1858, H. D. Rogers reported a similar formation in Pennsylvania and named it based on Latin nomenclature, but this terminology was not used by the First Pennsylvania Survey (Epstein, 1984). Instead, I. C. White and H. M. Chance used the names Caudi-galli grit and Corniferous limestone, based on similar exposures in New York, to name this formation in Pennsylvania in 1882 (Epstein, 1984). C. R. Boyd was the first to recognize similar strata in Virginia in 1881 and named the units Corniferous and Upper Helderberg (Dennison, 1961). It was not until 1912 that E. M. Kindle published a paper correlating the Onondaga fauna from New York State into southwest Virginia (Kindle, 1912). In his paper, Kindle mapped the fauna seen from the formation in New York into New Jersey, Pennsylvania, Maryland, West Virginia, and Virginia. He even suggested the formation extended west under Lake Erie into Ohio, and as far as southwestern Illinois (Kindle, 1912).

J. V. Lewis and H. B. Kummel (1915) used this information to map the Onondaga and surrounding formations in northern New Jersey. During a preliminary study on the formation, Bradford Willard (1936) recognized that the Onondaga Formation is composed of four distinct members in eastern Pennsylvania and thins into shale in central Pennsylvania and Maryland. In 1939, he named the shale to the southwest the Needmore (Dennison, 1961). He later decided to rename the Onondaga Formation the Buttermilk Falls Limestone and raised it to group rank (Epstein, 1984). This name was adopted in New Jersey for the limestone, but over the years the formation has been called both the Onondaga and Buttermilk Falls, depending on the author. In

1940, H. B. Kummel published an updated version of *The Geology of New Jersey* which included a slightly more detailed description of the previously mapped Onondaga Formation.

In the southern states around the same time, Charles Butts was outlining the general stratigraphy and paleontology of the Onondaga in Virginia (Dennison, 1961) while Edgar E. Rehn was working on a Master's thesis in 1942 on its formation under the supervision of Herbert P. Woodward. Rehn's thesis consisted of a detailed study of Onondaga stratigraphy in West Virginia and Virginia (Dennison, 1961). Later, "Woodward (1943) prepared a summary of West Virginia Devonian stratigraphy" (Dennison, 1961). In that summary, Woodward correlated the Needmore Shale and Huntersville Chert as equivalent facies to the Onondaga Formation and put them all in the Onondaga Group. He also correlated the Onondaga of Virginia and West Virginia with the formation in New York and the Columbus Limestone in Ohio (Dennison, 1961).

In 1954 and 1956, William A. Oliver Jr. conducted a detailed study of the Onondaga Formation in New York and published a series of papers. He subdivided the formation into four members based on the fauna and lithology, and determined the age and depositional environment for each (Oliver, 1956). These members are, from oldest to youngest, Edgecliff, Nedrow, Moorehouse, and Seneca (Figure 4). The name Seneca was recycled from Vanuxem (1839), who originally named the limestone in that area (Oliver, 1956). Oliver also mentions the presence of the Tioga bentonite, an ash deposit named in an earlier paper by C. R. Fettke in 1949 (Dennison, 1961), as a distinct-time boundary between the Moorehouse and Seneca members (Oliver, 1956). Later in the 1960s, Oliver continued his research on the Onondaga and decided, along with M. A. Ozol, to designate the cherty layers of the upper Edgecliff a separate member, the Clarence Member (Ver Straeten and Brett, 2006).

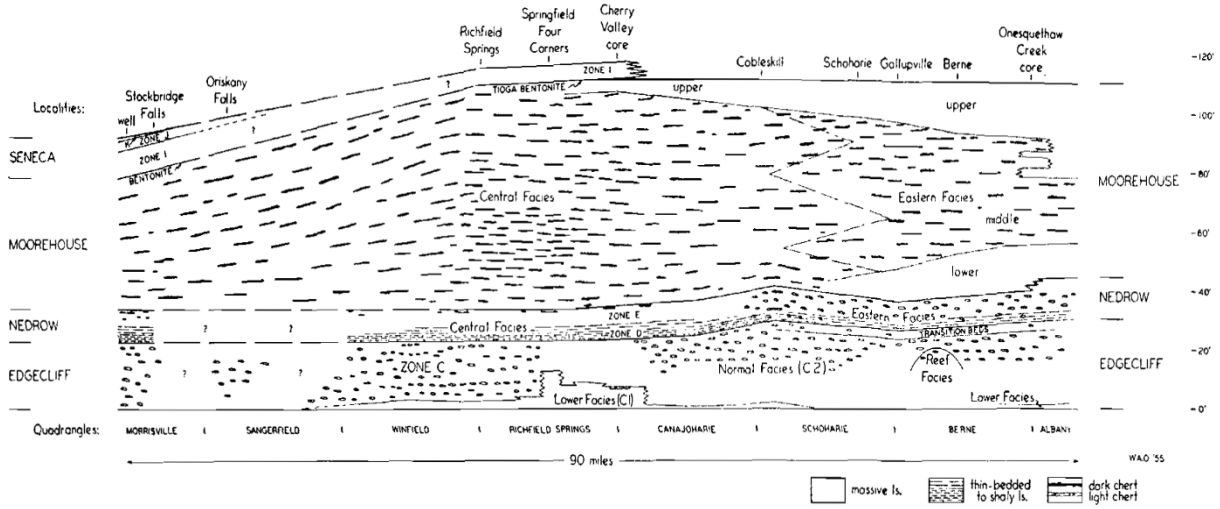

Figure 4: East-West Cross Section of the Onondaga Formation in Eastern New York showing relationships of the members, zones, and facies. (Oliver, 1956).

In 1961, J. M. Dennison published his comprehensive study on Onesquethaw Stage stratigraphy. This study was designed "to present a stratigraphic analysis of the sediments comprising the Onesquethaw stage in West Virginia, Virginia, and Maryland" (Dennison, 1961). The Onesquethaw stage is a Devonian-time unit that consists of the Esopus, Schoharie, and Onondaga formations.

By 1971, Jack B. Epstein had informally divided the Buttermilk Falls Formation in Pennsylvania into three members. The Foxtown Member was at the base of the formation overlain by the McMichael Member with the Stroudsburg Member at the top. Later, in a detailed stratigraphic study on the entire Onesquethaw Stage in Pennsylvania and surrounding states, J. D. Inners (1975) designated a fourth member of the Buttermilk Falls Formation, the Echo Lake Member (Epstein, 1984; Ver Straeten, 1996). This member is the youngest in the sequence and lies above the Tioga bentonite ash deposit and below the Marcellus Shale. Epstein (1984) also published a paper on the Onesquethaw stratigraphy focusing on northeastern Pennsylvania. In this paper, he published the names of the members stated above, their descriptions, which

member they correspond to in the Onondaga Formation in New York, regional correlations between the Buttermilk Falls Formation and other units, and the type of environment in which the units were deposited (Epstein, 1984).

Numerous other studies on the Onondaga of New York and Buttermilk Falls of Pennsylvania were conducted throughout the late 1980s and the 1990s. These studies include detailed work on the stratigraphy, paleontology, tectonics, depositional environment, bentonite layers, basinal development of the Appalachian basin, sequence stratigraphy, stratigraphic synthesis of the carbonates and shales, and correlation of units in the Middle-Devonian Onondaga and surrounding formations in New York, Pennsylvania, and Maryland (Figures 5A and B) (Ver Straeten, 1996; Brett and Ver Straeten, 1994; Ver Straeten and Brett, 2006).

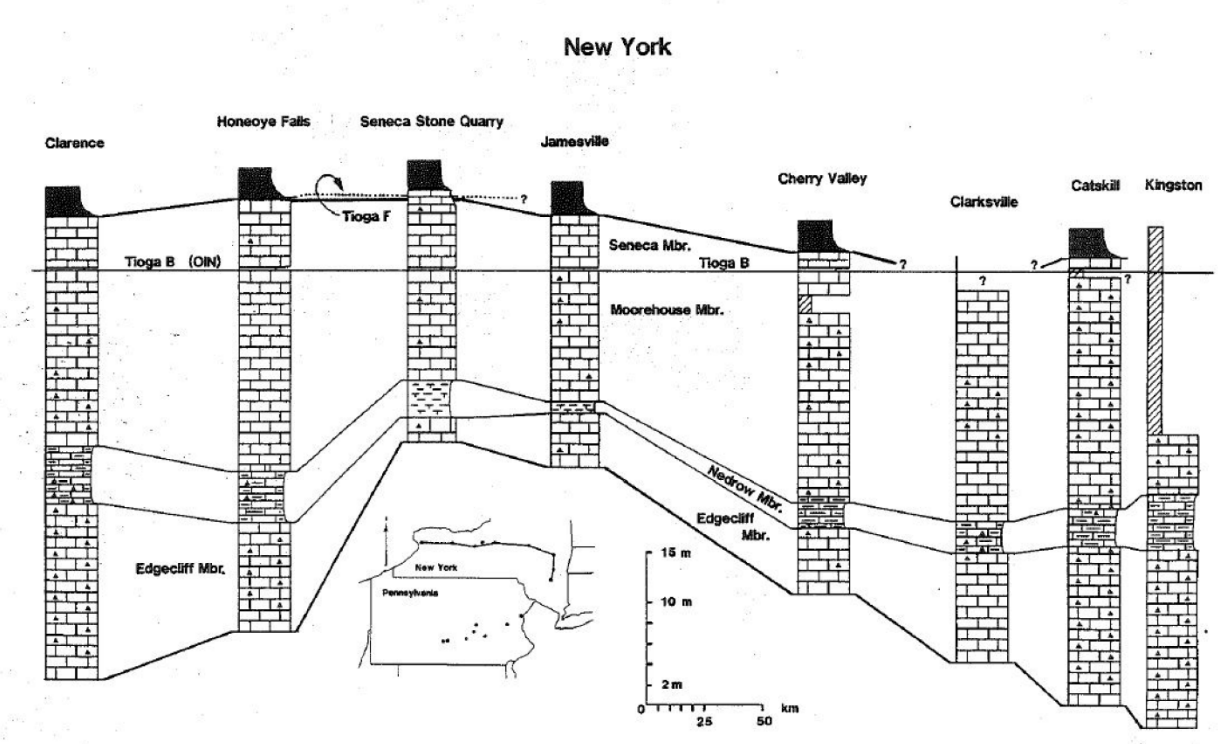

Figure 5A: Correlation of the New York members of the Onondaga Formation. (Brett and Ver Straeten, 1994)

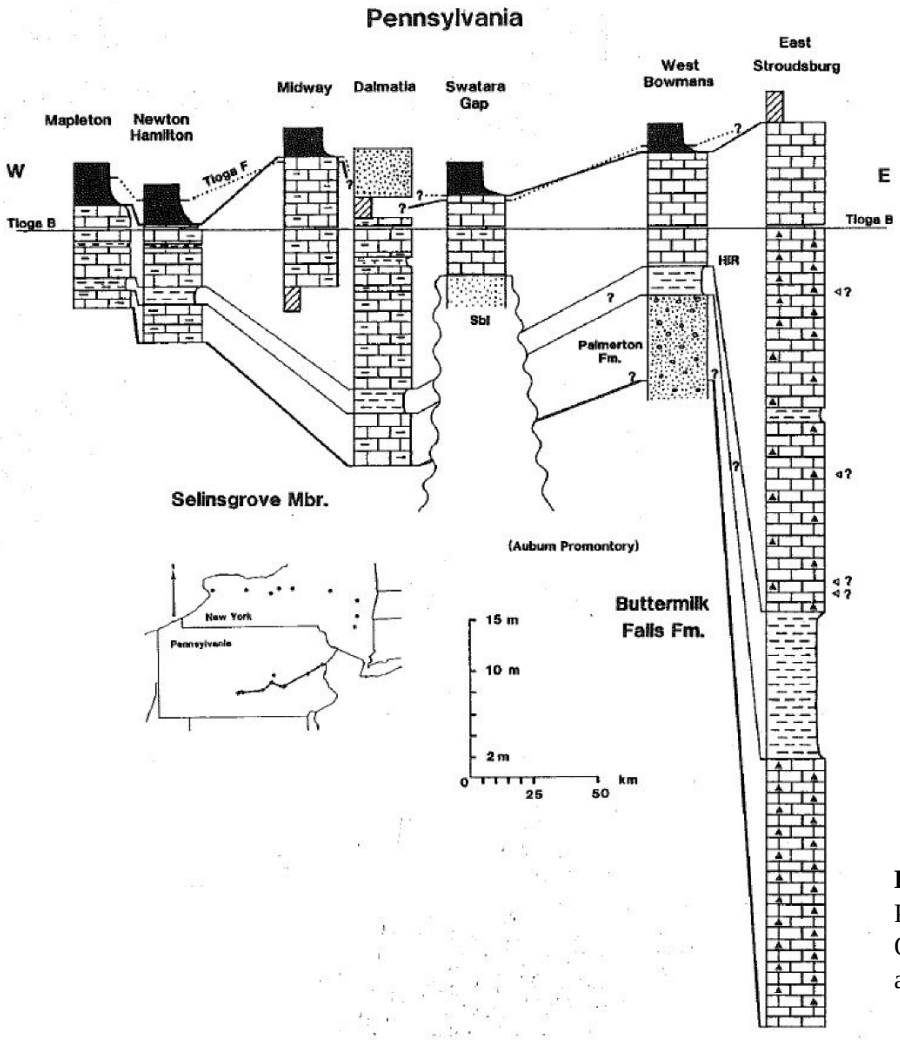

Figure 5B: Correlation of the Pennsylvania members of the Onondaga Formation. (Brett and Ver Straeten, 1994)

In 2001, Ver Straeten described the sequence stratigraphy of the Onondaga and surrounding units. He suggested the Buttermilk Falls Formation is lithologically the same and a "lateral equivalent" to the Onondaga Formation, and thus the name Buttermilk Falls and its members should be abandoned (Figures 6A and 6B). This became official in 2006, when he formally wrote of the abandonment of the Buttermilk Falls name, along with other nomenclature changes in units from the Pragian to Eifelian (Figure 6C). At this time, the Clarence Member in the Onondaga Formation was also abandoned (Ver Straeten and Brett, 2006).

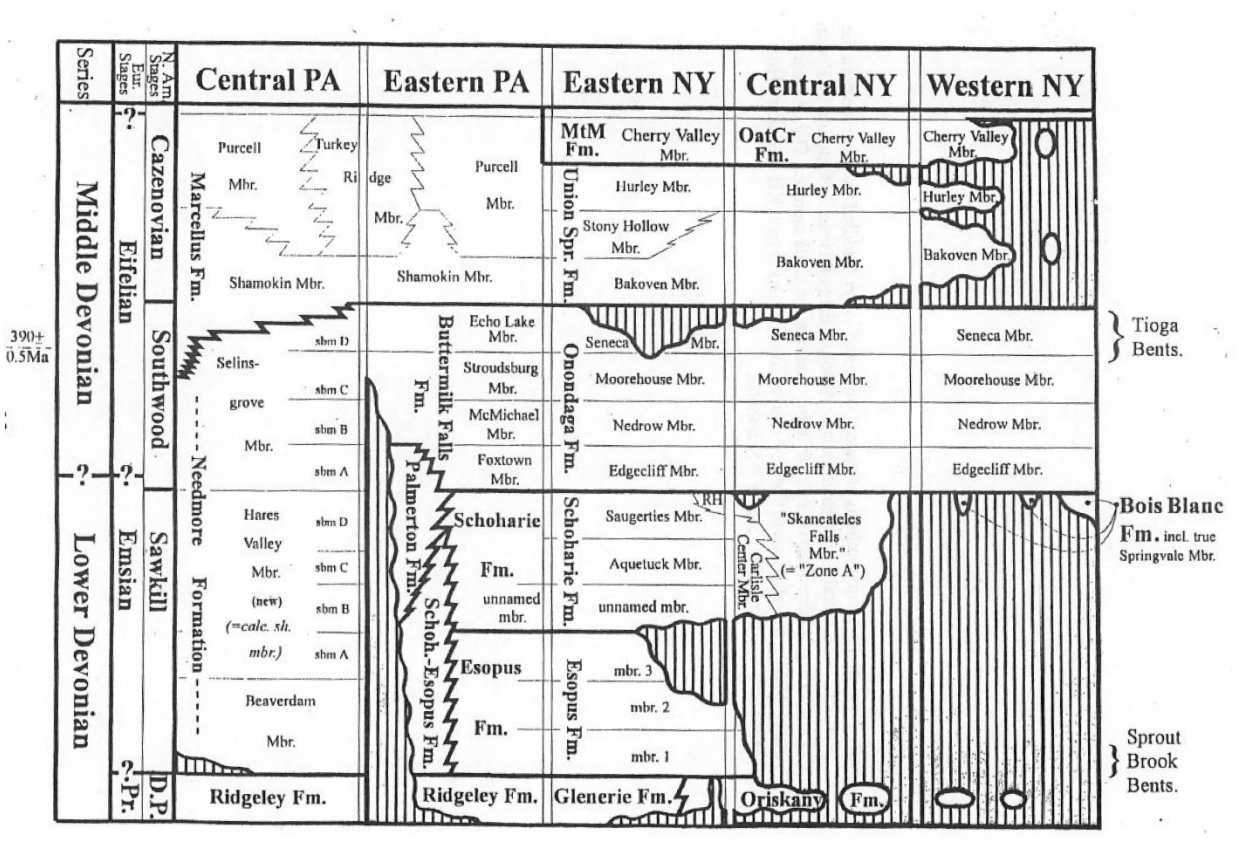

Figure 6A: Stratigraphic synthesis of upper Lower and lower Middle Devonian rocks in the Northern and Central Appalachian Basin before nomenclature change. Absolute date of Tioga B Bentonite by Roden et al. (1990). Abbreviations: calc. sh. mbr. = calcareous shale member; D.P. = Deer Park; MtM = Mount Marion; OatCr = Oatka Creek; Pr= Pragian; RH = Rickard Hill Mbr.; sbm = sub member; Schoh. = Schoharie. (Ver Straeten, 1996).

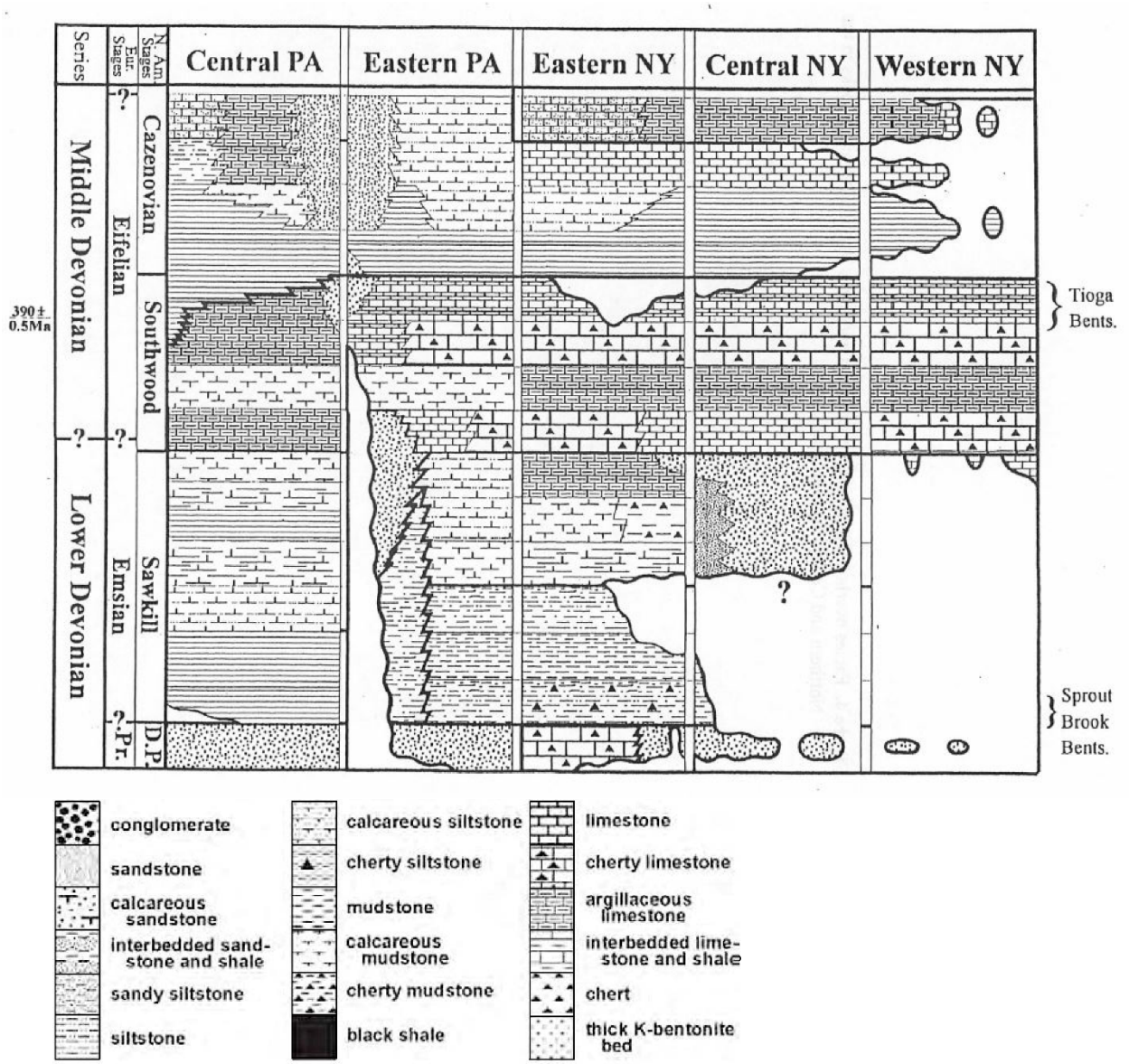

Figure 6B: Facies overlay of upper Lower and lower Middle Devonian rocks in the Northern and Central Appalachian Basin. (Ver Straeten, 1996)

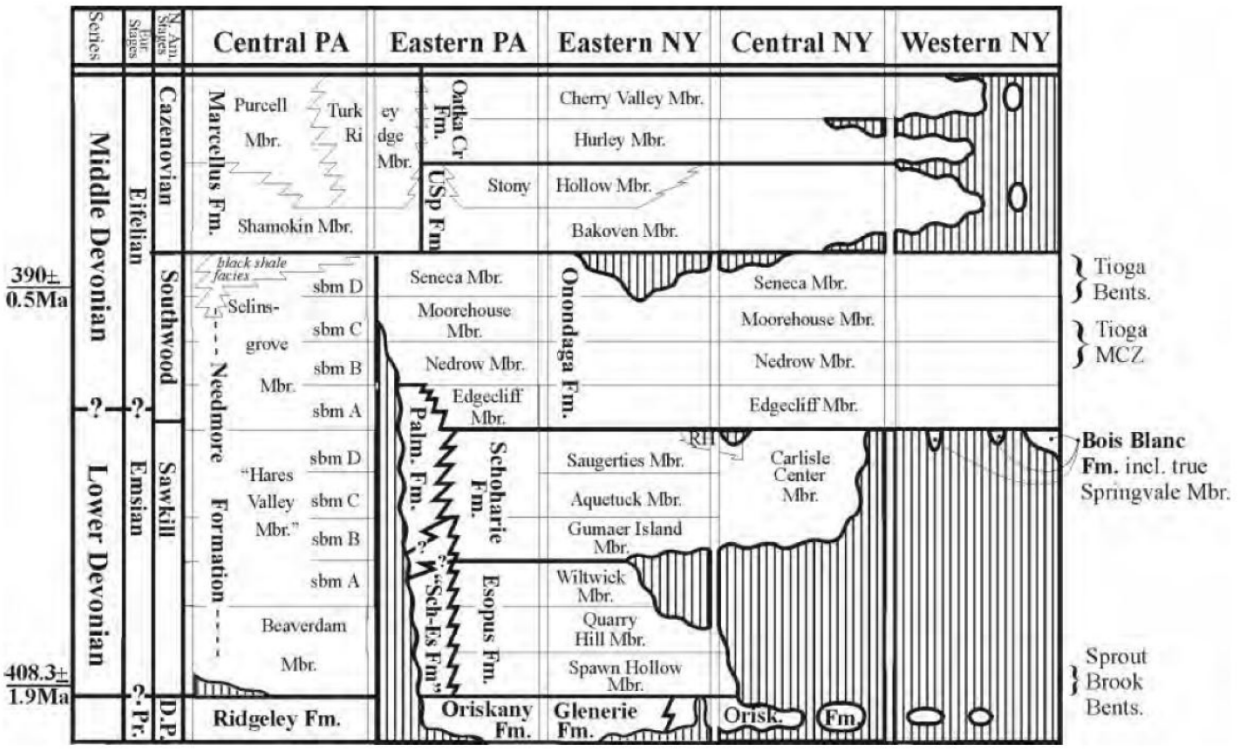

Figure 6C: Stratigraphic revision of upper Lower to lower Middle Devonian nomenclature, Pennsylvania and New York. Overlay showing revisions of upper Pragian to Eifelian strata in New York and eastern Pennsylvania. (Ver Straeten, 2001)

Within the last 10 years, Donald H. Monteverde and Ron W. Witte, geologists with the New Jersey Division of Water Supply and Geoscience, Geological and Water Survey, have been thoroughly mapping and examining the karst topography of the Onondaga Formation. In New Jersey, the formation is only exposed in a few outcrops, and none show a complete section of the formation. Bits and pieces of information have accumulated over the years through this mapping effort, but still more field work must be done.

Chert in the Onondaga Formation

Lately, chert in the Onondaga Formation has been of interest to both geologists and archeologists. Jarvis (1988) correlated specific chert artifacts with specific site locations in the Onondaga Formation in western New York. Using Instrumental Neutron Activation Analysis (INAA) along with microscopic petrology, optical emission spectrography, atomic absorption

spectrometry, and X-ray fluorescence (XRF) he established a "chemical blueprint" for chert artifact-to-source identification by defining elemental signatures for the seemingly homogeneous chert. This signature showed an increase in minor and trace elements from west to east. Jarvis related this to facies changes and proposed that particular elements could reflect the depositional environment of the chert (Jarvis, 1988).

Clark (2003) replicated Jarvis's study on INAA in southern Ontario near Lake Erie. As an archaeologist, his focus was on the potential accuracy of Jarvis's approach when applied to sites further west in the Onondaga Formation. His results were similar to Jarvis's, but he was unable to determine if the signature of the chert, as defined by Jarvis, was specific to different facies from one horizon in the Onondaga, or if it was tied to different members. Clark deduced that further investigation was needed to see if the geochemical signature changed vertically in chert from different members of the Onondaga, or if it changed horizontally in one bed from facies to facies (Clark, 2003).

In 1989, Maliva and Siever attempted to evaluate various models for nodular chert formation in Mesozoic and Paleozoic chert-bearing strata and managed to develop/refine a model for chertification (formation of chert) that is generally applicable to Phanerozoic strata containing nodular chert. Their evaluation focused on what the petrology of the chert and limestone reveals about the geochemical environment of chertification, the mechanism by which silica replaces carbonate, the nature of their contact, and the growth and nucleation of chert nodules. They looked at the Onondaga Formation in New York, along with five other Paleozoic and Mesozoic limestone formations containing chert nodules. From each formation, at least six exposures were studied which allowed an examination of the diagenetic history of silica and carbonate (Maliva and Siever, 1989). Sixty-five thin sections from the Onondaga Formation

were made for petrographic analysis, followed by cathodoluminescence, electron microprobe, insoluble residue, light stable isotope, and scanning electron microscopic examinations (Maliva and Siever, 1989).

Maliva and Siever (1989) first examined the dissolution of calcium carbonate and the precipitation of silica during nodular chert formation. Petrographic analysis revealed sponge spicules concentrated in areas where chert was present along with evidence showing the nature of the silica-carbonate contact. Pressure solutions in the grains were also preserved in the chert nodules. From their analyses, the depositional environment for the limestone and chert was determined. Their study also concluded a range of depths at which the chert could have formed.

After evaluating available models for chertification, they decided that none of the models accurately explained their results. In light of this, the authors developed their own model to explain how chert nodules formed in their samples. Their model, called the Force of Crystallization-Controlled Replacement Model, calls on the "solution-transfer" deformation mechanism of Durney (1972). This process involves dissolution of the carbonate and precipitation of silica along solution films in response to stress heterogeneities. Maliva and Siever's model accurately described chert formation in different types of limestones.

III. Methodology

The methodology of this research is based on standard procedures and the petrologic study conducted on chert in limestone by Maliva and Siever (1989).

Field Sampling

Samples of limestone and chert were collected from northern New Jersey along the Delaware River beginning at the New Jersey-New York border. A total of 13 sampled outcrops were located southwest along River Road and Old Mine Road which run parallel to the Onondaga outcrops (Figures 7A, B, C, and D). Sites were chosen to 1) get the best vertical representation of the entire Onondaga, and 2) show a lateral representation of the Onondaga across the state. Because a complete section of the Onondaga Formation in New Jersey does not exist in a single outcrop, samples containing chert are assigned to specific members based on thickness of the formation, member thicknesses, and the location of chert zones within each member. Determination of the thickness of the formation at each site, and where that site was located in the formation as a whole, was calculated as well (Appendix A).

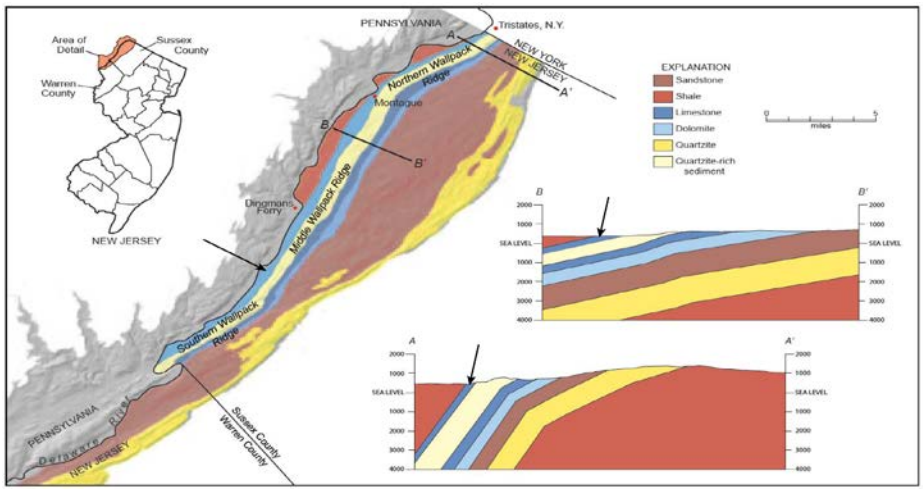

Figure 7A: Bedrock geology of Wallpack Ridge and surrounding area. Black arrows point to the Onondaga Formation on the map and cross-sections. Modified from original map by Ron Witte and Don Monteverde (2006).

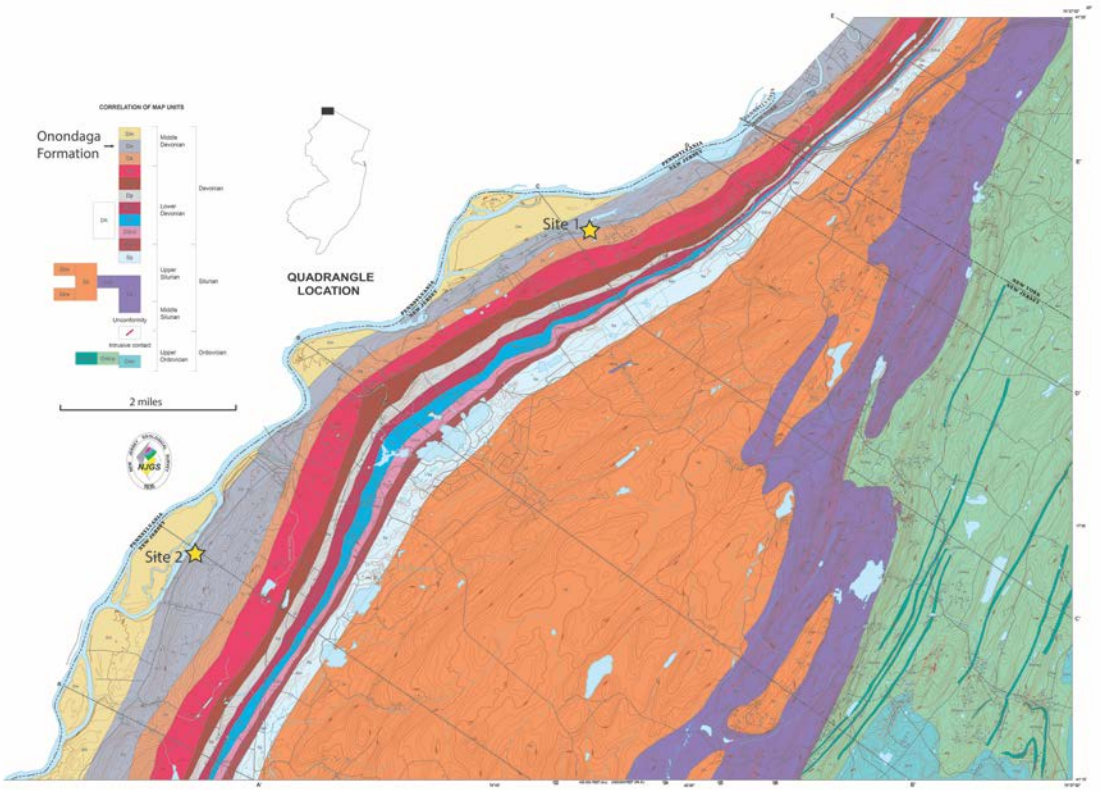

Figure 7B: Site locations on the Milford-Port Jervis Quadrangles. Modified from the geologic map by Don Monteverde and Jack Epstein (2015).

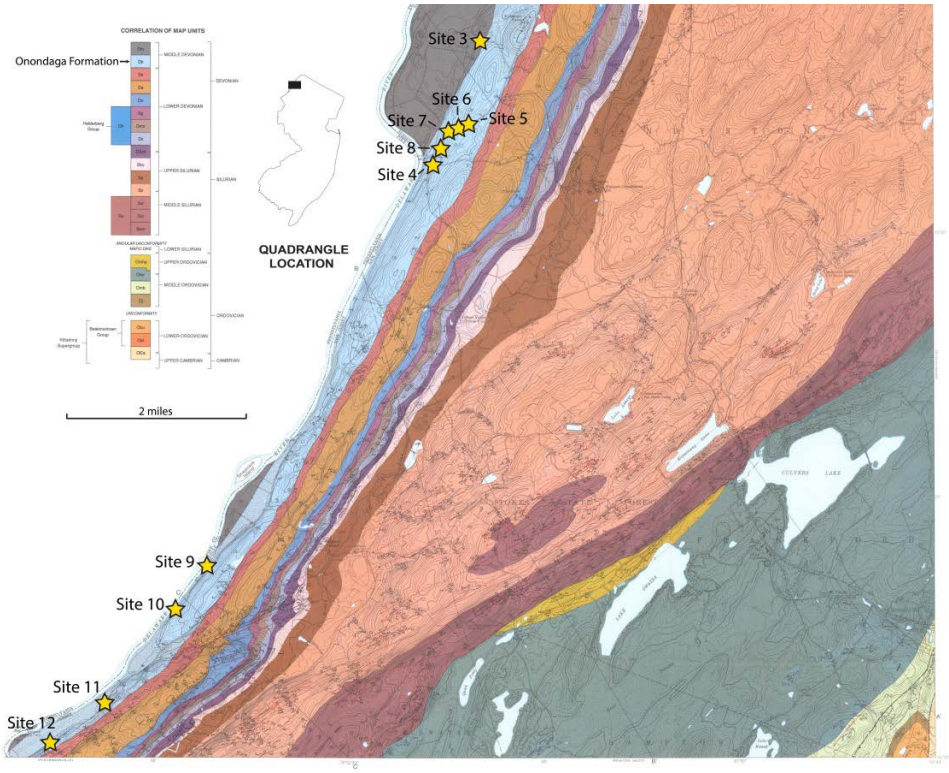

Figure 7C: Site locations on the Culvers Gap and Lake Maskenozha Quadrangles. Modified from the geologic map by Don Monteverde (1992).

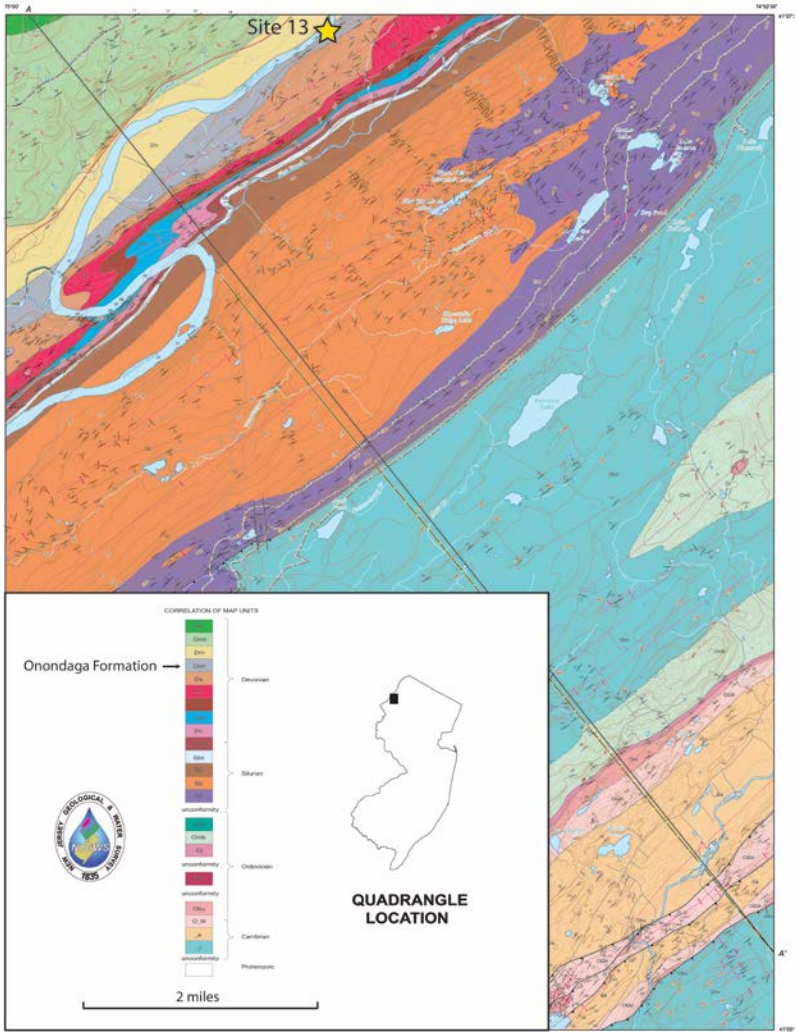

Figure 7D: Site locations on the Flatbrookville Quadrangle. Modified from the geologic map by Don Monteverde, Jack Epstein, Gregory Herman, and Ron Witte (2015).

Samples of the rock formation were collected from each site along with detailed stratigraphic and mineralogical descriptions noting the locations, orientation and size of chert nodules, prominent bedding features, fossils visible in hand specimen, etc. Some pictures were taken to document the appearance of outcrops and for scale (Appendix B). The number of samples varies per site due to a lack of outcrops and exposures in New Jersey. Samples at cherty outcrops include a nodule of chert embedded in the limestone matrix. These samples were used to study the limestone-chert contact and provide insight into the relationship of chert to the limestone. Samples were also taken at locations where no chert is present to see how the

limestone differs from locations where chert is present. These samples provide data on the formation in New Jersey depicting the chert and limestone contact in moderate detail as well as examining the constituents that make up the limestone matrix.

Thin Sections

Thin sections of each rock sample from the 13 sites were prepared in the Rock Saw laboratory at East Carolina University. A total of 29 thin sections were made. Multiple samples were collected at some sites and the number of thin sections made from each sample varies depending on what features were observed in hand specimen. These features could include a limestone-chert contact, burrows, fossils, or other notable features in hand sample.

Staining

The 29 thin sections were stained with Alizarin Red S and Potassium Ferricyanide to aid in mineral differentiation using methods described by Dickson (1965). Alizarin Red S is used to differentiate calcite, which will stain very pale pink to red, from dolomite, which will not stain at all. Potassium Ferricyanide is used to differentiate ferroan calcite and dolomite from non-ferroan varieties. Ferroan dolomite will take on a pale to deep turquoise hue depending on iron content, whereas non-ferroan dolomite will remain unstained. Ferroan calcite will be stained pale to dark blue on top of the Alizarin Red S stain giving it a mauve, purple, or royal blue hue. The chert and other non-carbonate grains will remain unstained as well. (Dickson, 1965)

Point Counting

Point counting thin sections is a means to determine the volumetric percentages of constituents in a rock sample. This is based on the Delesse method, which relates areal proportions of components in thin section to their volumetric proportions in rocks (Chayes, 1956). Each of the 29 thin sections was point counted to determine the abundance of ten

different constituents (Table 1). A total of 300 points per slide were tallied and the raw data and percentages of the ten constituents are reported in Appendices C and D.

Constituents
Micrite
Ferroan Sparite
Non-Ferroan Sparite
Non-Carbonate Mud
Fossils
Ferroan Dolomite
Non-Ferroan Dolomite
Microcrystalline Silica
Pores
Other

Table 1: Summary of Constituents.

Insoluble Residue Analysis

To determine the percentage of material that was not carbonate and in preparation for the X-ray diffraction analysis, an insoluble residue analysis was performed (Appendix E). The following procedure was modified from Minnesota Department of Transportation (2000). This was conducted by taking 100-150 grams of sample from each of the 13 sites, running it through a series of grinders to get the sample to about fine-sand size, then putting the sample through a ball mill machine to get into powder form. The sample needed to be a powder to run through the X-Ray Diffraction machine.

Once the samples from the 13 sites were a powder, they were then split in half. Half of the sample was put in a bag and labeled with the site name for archive/reserve purposes and to be used later in the X-Ray Diffraction Analysis. The other half was weighed, put into 1000 ml beakers, and covered with deionized water. Each sample was then digested with 6N hydrochloric acid in small increments, so the bubbling would not overflow the top of the beaker.

The samples were stirred and agitated to help bring the reaction to completion. This process was repeated until all effervescing had ceased. Then an additional 100 ml of acid was added to ensure that all the carbonate was dissolved. Each beaker was then transferred to a hot plate to be heated for 10 minutes to make sure the reaction had gone to completion and no more effervescing had occurred, then removed and left to cool.

While each of the samples were cooling, a piece of Whatman #1 filter paper was weighed and pressed into a funnel mounted on a vacuum pump as preparation to separate the insoluble residue from the solution in the beakers. After each sample had cooled, it was then poured through the vacuum pump and washed thoroughly with deionized water to make sure all the solution was removed from the residue. Occasionally the filter paper would rip while the solution was being poured so a second filter paper needed to be used. The filter paper and residue was then put in an oven at 80°C to dry overnight and then weighed again once completely dry.

X-Ray Diffraction Analysis (XRD)

In order to determine the mineralogy of the non-carbonate material from the insoluble residue analysis, an X-Ray Diffraction Analysis (XRD) was run using a PANalytical X'Pert Pro MPD unit with a copper tube. The samples used in this analysis were the same powdered samples from the 13 sites used in the insoluble residue analysis. Samples were analyzed from the powders of both before and after the insoluble analysis were done. This was to ensure no new material was created during the process (Appendix F).

XRD Procedure

A small amount of each powdered sample was placed on a no background Si-plate and the computer program, X'Pert Data Collector, was used for the analyses. The current was set to 45 mAmp and the tension to 40kV. Two scans of the sample were run from 3°-73° 2Θ. X'Pert

Highscore Plus was then used to analyze the X-Ray patterns and determine the sample mineralogy. X'Pert Highscore Plus uses reference patterns in its database to search and match the peaks in patterns of the unknown minerals. Peaks that X'Pert Highscore Plus could not identify were then matched by hand using reference patterns for minerals suspected to be in the samples as well as the suggested minerals the program recommended. To verify the minerals identified by XRD, a Scanning Electron Microscopy/Energy Dispersive X-ray microanalysis was used.

Scanning Electron Microscopy/Energy Dispersive X-Ray Microanalysis (SEM-EDS)

Six sample sites were chosen for examination by Scanning Electron Microscopy/Energy Dispersive X-Ray Microanalysis (SEM-EDS). These sites were chosen based on the insoluble residue percentages. Two sites were picked with a high percentage of insoluble residue, two were picked with an intermediate percentage, and two with a low percentage.

Sample Preparation

A solid sample, approximately the size of a quarter, was chosen from six sites for this analysis. This sample was then ground to the size of about fine-sand. These rock chips were put in 400 ml beakers and 10% HCl was added gradually until no more effervescing occurred when stirred or agitated. The samples were put through a vacuum pump to remove the solid from the solution, rinsed with deionized water, and put in the oven to dry overnight. Once dry, the samples were sorted through 180 µm and 150 µm sieves to break the non-carbonate mud down and isolate any possible mineral grains present. Chert from the 180 µm sieve was picked out and stored for analysis in the SEM-EDS. Any remaining material in the 180 and 150 µm sieves was then put in a weigh boat, and the larger loose grains were gently broken down by hand. This process of acid solution, drying, sorting, and picking was repeated until no more grains could be easily broken.

Once all the grains from each sample site were separated and any known minerals, such as the chert were picked out, they were analyzed by SEM-EDS. Samples were mounted on aluminum stubs using double-sided carbon tape. Each sample site had a stub with >180 µm, 180-150 µm, and <150µm grain sizes as well as the chert that had been separated out previously. A total of 26 samples were examined by SEM-EDS.

SEM-EDS Procedure

The samples were analyzed with a FEI Quanta 200 Scanning Electron Microscope with Oxford INCA X-act EDS elemental detector using copper for optimization. The SEM was run in Low Vacuum mode (0.45 Torr), with a spot size of 7.2, a voltage of 20.00 kV, and a working distance of 11.486 mm. Spectra were analyzed with the INCA analysis software (Appendix G). INCA cannot detect elements lighter than boron. Occasionally a high-resolution SEM image (spot size of 4.5, voltage of 15.00kV) of a particular grain was acquired to examine crystal morphology as a guide to mineral identification.

IV. Results

Petrology

The petrology of this formation is based on point counting 29 thin sections. The ten different constituents that were point counted will be discussed in further detail below (Table 2). Raw data from the point counts can be found in Appendix C.

Micrite

Micrite is microcrystalline calcite and is considered a carbonate mud. It was identified as small, transparent, sometimes cloudy crystals usually 4 μm or less in size in thin section (Folk, 1959). These crystals sometimes had a light pink, red, or purple hue in plane-polarized light due to staining and orientation of the c-axis of the crystal (Dickson, 1965). Very minor amounts of a royal blue hue were observed in some of the micrite indicating some iron content as well. Also from staining the thin sections, the micrite exhibited a lower relief than the non-carbonate matrix since the HCl-based stain dissolved a little of the carbonate material away. When viewed under crossed-polarized light, micrite usually displayed upper 2nd to 3rd order interference colors. (Figure 8)

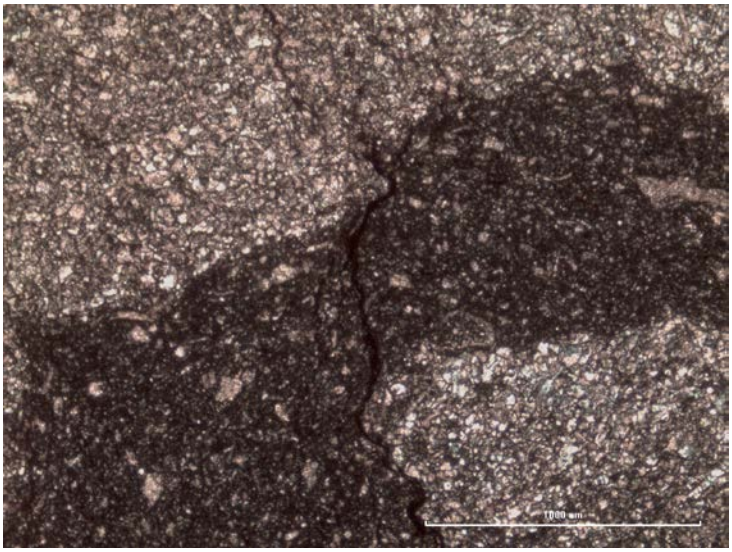

Figure 8: Limestone matrix consisting of micrite and non-carbonate mud. Darker material is more condensed non-carbonate mud. Plane-polarized light, 50X magnification.

Micrite was present at all sites and ranged from 84.3% to 2.3% with an average of 31.3%. It was most abundant in sites 1 and 12 and least abundant in sites 9 and 10.

Sparite

Sparite refers to a crystalline, sparry-calcite cement that is usually chemically precipitated. In thin section it was identified as transparent crystals (>4 μm size) with numerous twins present under crossed-polarized light and 3rd order interference colors. The sparite also exhibited a lower relief due to staining. The staining did, however, break the sparite into two categories: ferroan sparite and non-ferroan sparite (Figure 9 and 15). Ferroan sparite usually had a royal blue, purple, or mauve color depending on iron content. Non-ferroan sparite showed colors from very pale pink to red. In both instances of sparite, the color intensity of the grains from staining was affected by the orientation of the c-axis of the crystal (Dickson, 1965).

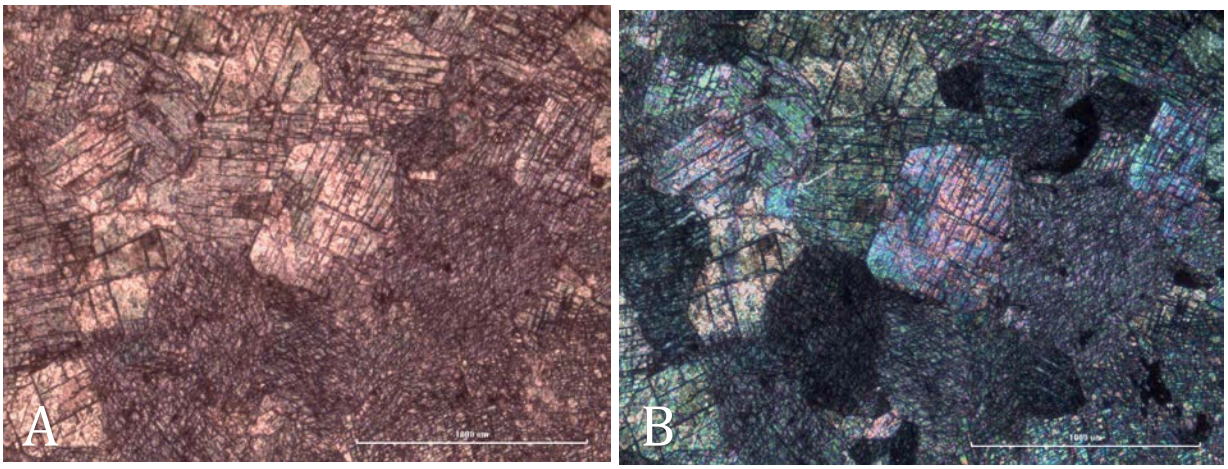

Figure 9: A) Non-Ferroan Sparite in slide 3-a-4, plane-polarized light, 50X magnification. B) Same thin section image, crossed-polarized light, 50X magnification.

Ferroan sparite ranged from 9.7% to 0.0% with an average of 0.8%. It was present in sites 1, 2, 3, 8, 9, 10, and 13. It was most abundant in sites 9 and 10. Non-ferroan sparite ranged from 9.3% to 0.0% with an average of 0.7%. It was present in sites 1, 3, 8, 9, 10, and 12. It was most abundant in sites 3 and 9.

Non-Carbonate Mud

Non-carbonate mud was identified in the matrix as well and showed higher relief, was brown and cloudy, translucent in appearance, took on no stain, and showed 1st to 2nd order interference colors in crossed-polarized light (Figure 8). This material was not affected by the HCl and is what makes up most of the insoluble residue. Further discussion of this material will be in the XRD and SEM-EDS results section.

Non-carbonate mud was present at all sites and ranged from 78.0% to 6.7% with an average of 34.7%. It was most abundant in sites 13 and 10, and least abundant in sites 1 and 3.

Fossils

Fossils were present in almost all thin sections observed. The only thin section that did not contain fossils was 4-a-1. In some cases, fossils were present in the slide but were not accounted for during the point count. Fossils ranged from 6.3% to 0.0% with an average of 1.1%. They were most abundant in sites 6 and 3.

Fossils observed in the 29 thin sections consisted of mollusks, echinoderms, sponge spicules, brachiopods, ostracods, and bryozoans (Figure 10). Mollusks were broken down into three main types: pelecypods (bivalves), cephalopods, and gastropods. Two types of echinoderms were found as well: echinoids and crinoids. Of these fossils, pelecypods were the most abundant. Sponge spicules were the second most abundant fossil found.

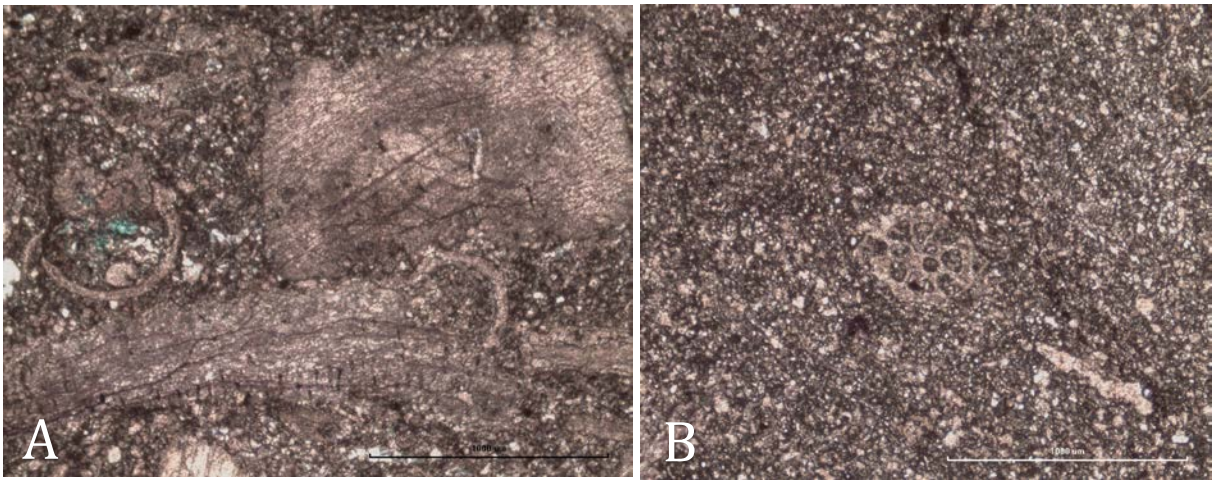

Figure 10: A) Mollusks, echinoderms, and brachiopods. B) Bryozoan. Plane-polarized light, 50X magnification.

Most of the fossils counted were either replaced with silica or sparite. Occasionally some were filled in with micrite or sparite but had a silica-based rim. The sparite could be of both the ferroan and non-ferroan variety. The silica could either be chalcedony, mosaic quartz crystals, dog-tooth quartz spar, microcrystalline quartz, or a mix of the four. In some fossils, usually the brachiopods, the silica replaced the calcite shell but kept the same texture of the shell (Figure 11).

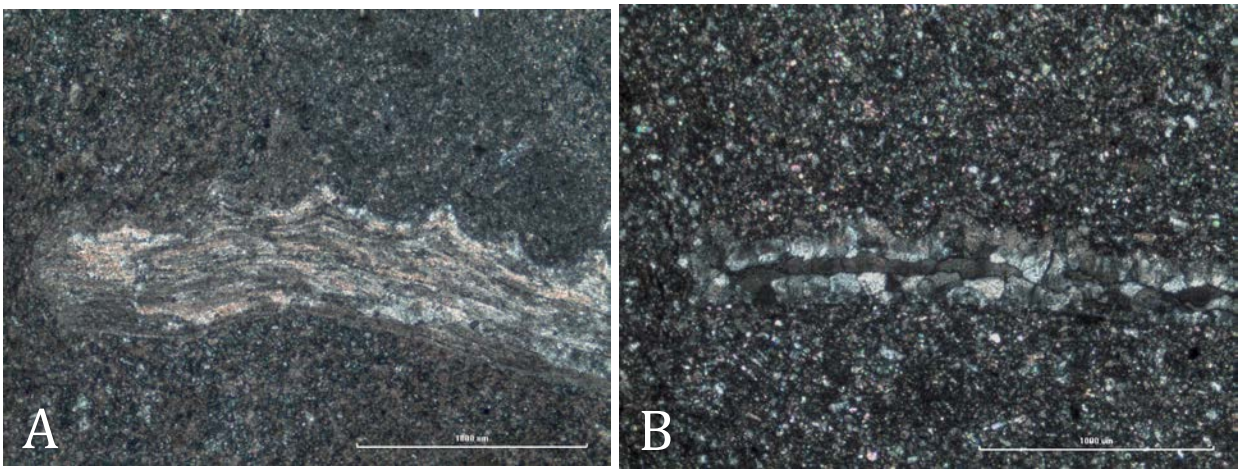

Figure 11: A) Silica-replaced brachiopod showing original shell texture. B) Silica-replaced brachiopod showing mosaic quartz rim with micrite center. Crossed-polarized light, 50X magnification.

Sponge spicules that were found were either composed of silica or replaced by calcite and of the monaxon variety (Figure 12). The calcite-filled spicules indicate that the spicule

underwent dissolution and was filled with calcite. Most of the time sponge spicules were observed in thin sections containing chert nodules, but sometimes slides without chert nodules had spicules as well. All fossils found in the matrix, regardless of what they were filled in with, were counted as fossils in the point count. A complete list of the fossils found in each thin section can be found in Appendix D.

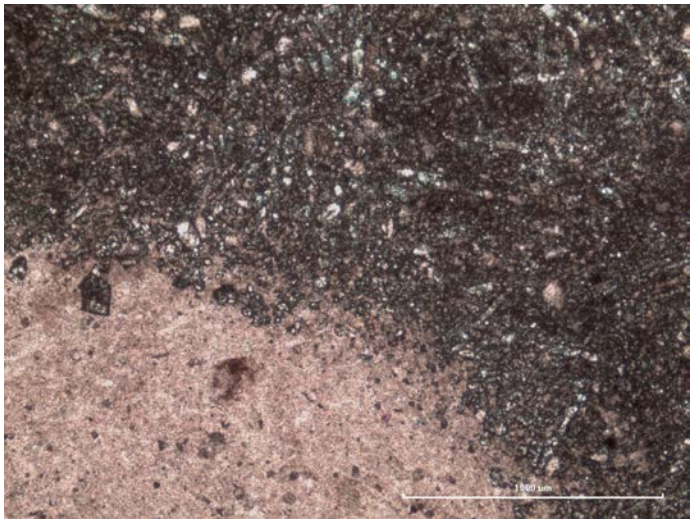

Figure 12: Sponge spicules at the limestone/chert boundary. Plane-polarized light, 50X magnification.

Dolomite

Dolomite, $CaMg(CO_3)_2$, is usually formed during diagenesis and found in carbonate sedimentary rocks. In thin section, this mineral formed transparent, rhombohedral crystals with 3rd order interference colors under crossed-polarized light. Due to staining, the relief was slightly lower than the non-carbonate material. Also from staining, the dolomite was broken into two categories: ferroan dolomite and non-ferroan dolomite. Non-ferroan dolomite did not take on any stain whereas ferroan dolomite took on a pale to dark turquoise color (Dickson, 1965). The dolomite rhombs were usually found in the chert nodules and on the contact between the chert nodules and matrix. Both varieties of dolomite were common in these areas. Occasionally there were areas where the ferroan sparite appeared to be altering to ferroan dolomite. Dolomite

was almost always found in thin sections containing chert nodules. The only time dolomite appeared in a thin section without chert was in slide 10-b-1. (Figure 13)

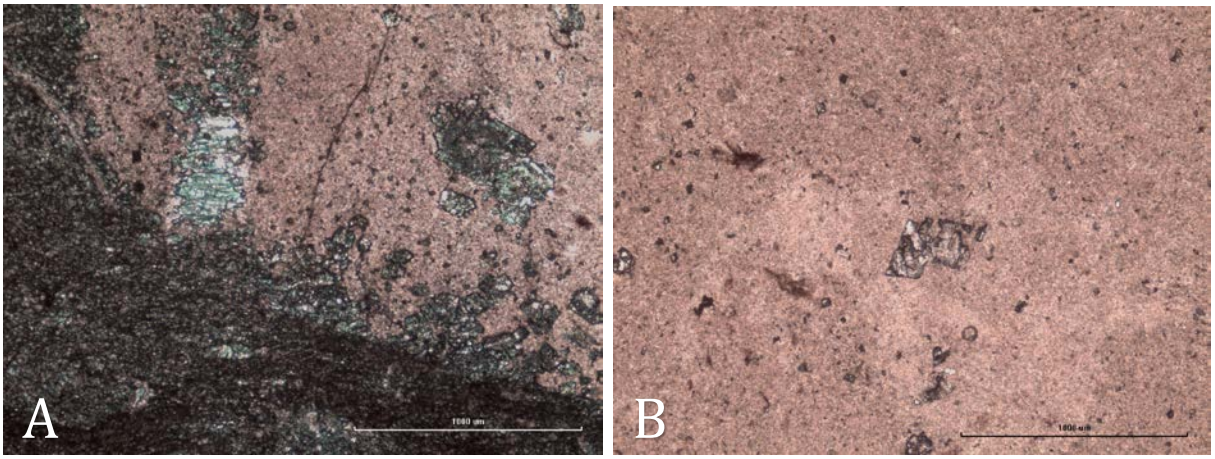

Figure 13: A) Ferroan dolomite rhombs on the chert/limestone contact and within the chert nodule. B) Non-Ferroan dolomite rhomb in chert nodule. Plane-polarized light, 50X magnification.

Ferroan dolomite ranged from 2.7% to 0.0% with an average of 0.3%. It was present in sites 1, 2, 3, 7, and 9. It was most abundant in sites 7 and 9. Non-ferroan dolomite ranged from 2.7% to 0.0% with an average of 0.9%. It was present in sites 1, 2, 3, 5, 7, 8, 9, and 10. It was most abundant in sites 1, 8, and 9.

Microcrystalline Silica

Microcrystalline silica typically refers to the chert nodules. Some occurrences of chert did not appear as a distinct nodule either in hand specimen or thin section. These were counted in the microcrystalline silica category. Chert was identified as having a microcrystalline texture (crystals that are not large enough to distinguish under the microscope) and exhibited 1st order gray to black interference colors. The chert had a higher relief than the carbonate minerals because it did not react with the HCl during the staining process. (Figure 14)

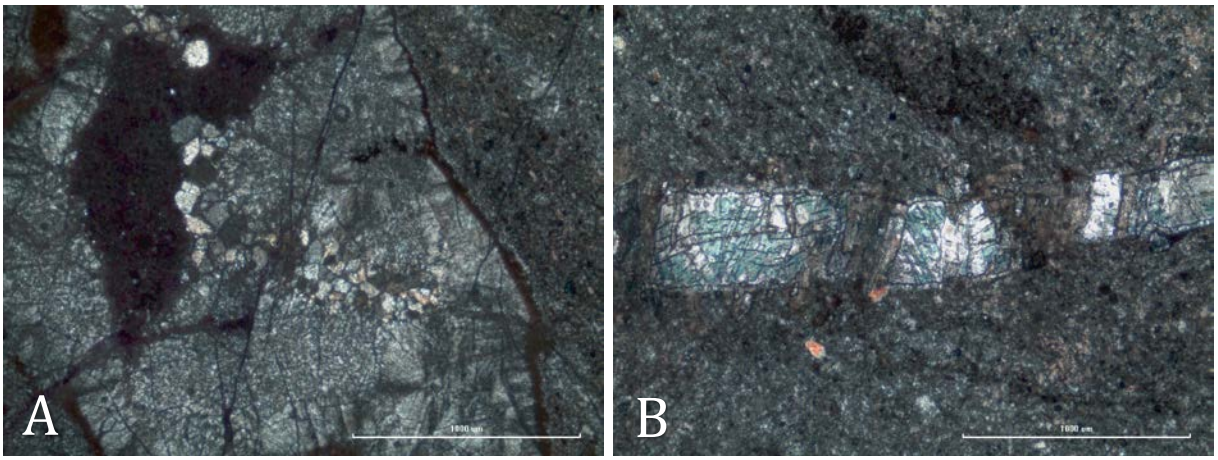

Figure 14: A) Macro quartz and chalcedony in chert nodule. Black feature is a pore within the nodule and iron stained fractures are seen cutting through the chert. B) Ferroan sparite filled fossil preserved in chert nodule. Fossil appears fractured and shows silica isopacheous rim cement. Chert has filled in and healed the fractures. Crossed-polarized light, 50X magnification.

In the chert nodules, ghosts of fossils and other grains were present that the chert had incorporated into its structure. Some of the recrystallized fossils in the nodules consisted of macro-quartz crystals in either a sparry or mosaic pattern. Most of the fossil ghosts, however, were simply recrystallized with the microcrystalline silica. There was one instance of mosaic quartz grains and chalcedony as radiating fibers in slide 3-a-1 (Figure 14A). All of these structures were counted as microcrystalline silica in the point count since they were the same chemical composition as the chert nodule. If a fossil appeared in the chert nodule but had not been recrystallized, then it was counted as a fossil (Figure 14B). The same goes for any of the other constituents that had not been recrystallized by the chert.

In hand specimen, the chert appears as dark gray to black nodules ranging from 0.25-4 inches in diameter. Some of the nodules were spherical whereas some were oblong with an indistinct shape. At site 1 the nodules appear to line up along a bedding plane, but at site 8 they occur randomly throughout the limestone. The majority of the chert nodules have a sharp contact with the lighter gray limestone around it. A few of the nodules observed, have black

lines branching off of them that appear to be made of the same material. In both the hand specimens and thin sections, the nodules appear homogeneous in nature.

Microcrystalline silica was present at all sites except for three: sites 6, 11, and 12. It ranged from 78.0% to 0.0% with an average of 26.4%. It was most abundant in sites 5 and 9.

Pores

Pores counted in thin section were void spaces in both the matrix and chert nodules (Figure 14A). Cement-filled pores were not counted in this section. If a fracture created pore space, then it was counted as a fracture and noted that the fracture contained pore space.

Pores were present in sites 2, 3, 5, 6, 8, 9, and 10. They ranged from 1.7% to 0.0% with an average of 0.4%. Porosity was most abundant in sites 5 and 9.

Other

There were several other minor constituents that were noted in thin section and lumped together into the "other" category. These were fractures, opaque grains, stylolites, intraclasts, iron staining, authigenic feldspar, and a burrow (Figures 15, 16, 17, and 18).

The fractures found in the thin sections were either filled in with ferroan sparite, non-ferroan sparite, microcrystalline silica, ferroan dolomite, or pore space. Ferroan sparite-filled fractures could sometimes have ferroan dolomite mixed in (Figure 15A). It appeared one variety may have been altering to the other, but it is unclear as to which one was being altered. Occasionally, the grains that filled in the fractures were iron stained. In a few slides, fractures were present but had not yet opened up to allow for space inside the fracture to significantly be filled in.

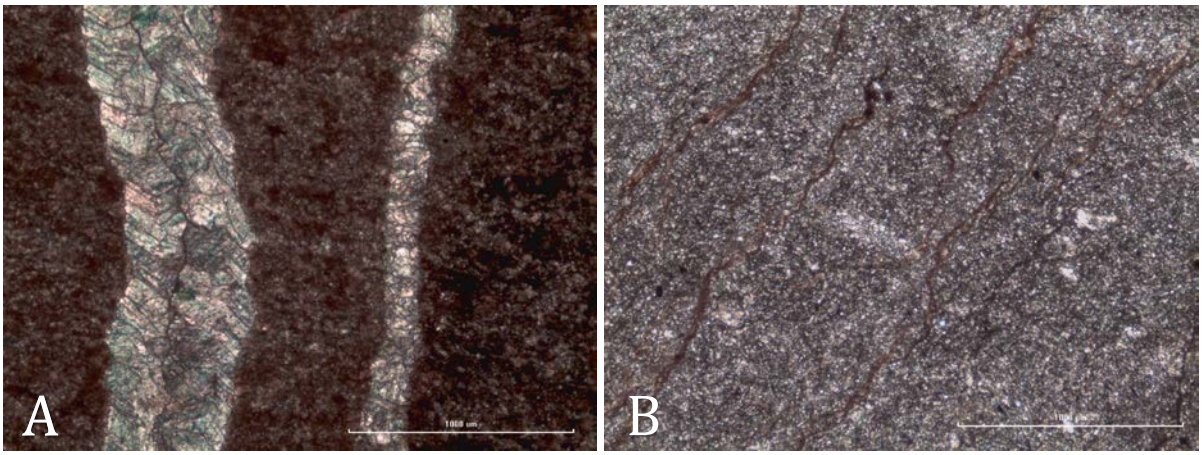

Figure 15: A) Fractures through limestone matrix refilled in with ferroan sparite. B) Stylolites running through limestone matrix. Plane-polarized light, 50X magnification.

Intraclasts were present in two thin sections: 4-a-1 and 9-b-2. In both cases they seemed to be almost entirely made up of a terrigenous mud. In 4-a-1, the clasts appeared elliptical in shape, and in 9-b-2 the clasts were squarer with apparent solution seams at their base. (Figure 16)

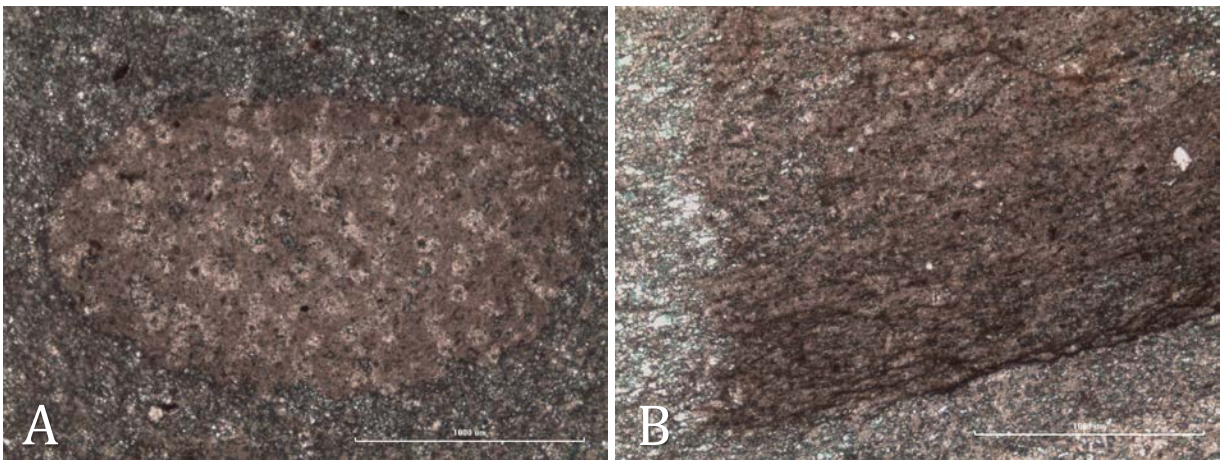

Figure 16: A) Intraclast from slide 4-a-1. B) Intraclast from slide 9-b-2. Plane-polarized light, 50X magnification.

Feldspar grains were observed in a few slides. These grains were observed only in 200X magnification and showed subhedral to euhedral crystal growth suggesting an authigenic origin. In crossed-polarized light, the feldspars displayed 1st order interference colors, contained two or

three twins characteristic of albite twinning, remained unstained, and showed higher relief than the surrounding carbonate. (Figure 17)

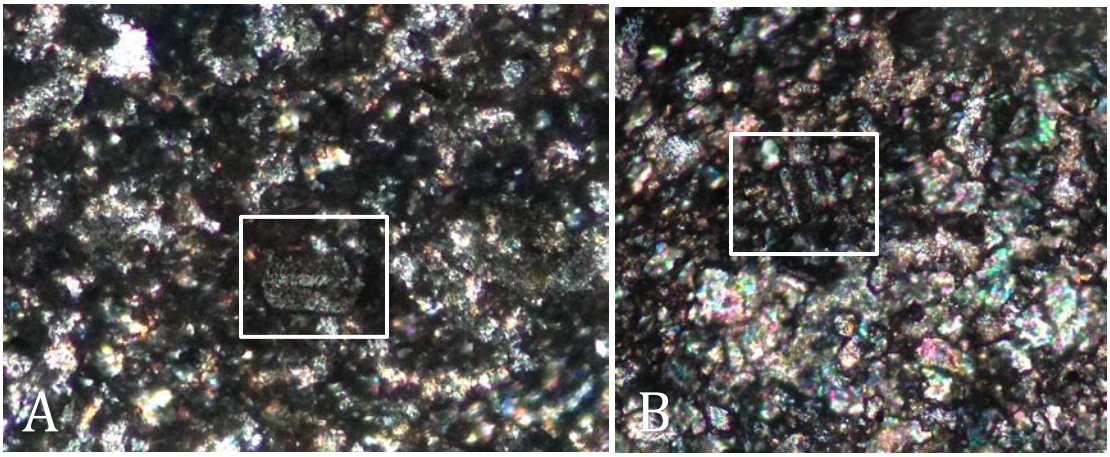

Figure 17: Both images show authigenic feldspar grains in the white boxes. Crossed-polarized light, 200X magnification.

The only burrow visible in thin section was in slide 7-a-1 (Figure 18). This burrow appears about 5 mm in length and is filled in with ferroan sparite, ferroan saddle dolomite, non-ferroan sparite, non-ferroan dolomite, macro crystalline quartz, and chalcedony. The four varieties of carbonate were intergrown. Some grains had areas where one part of the grain was ferroan whereas the rest was not. Chalcedony was found only at the top of the burrow.

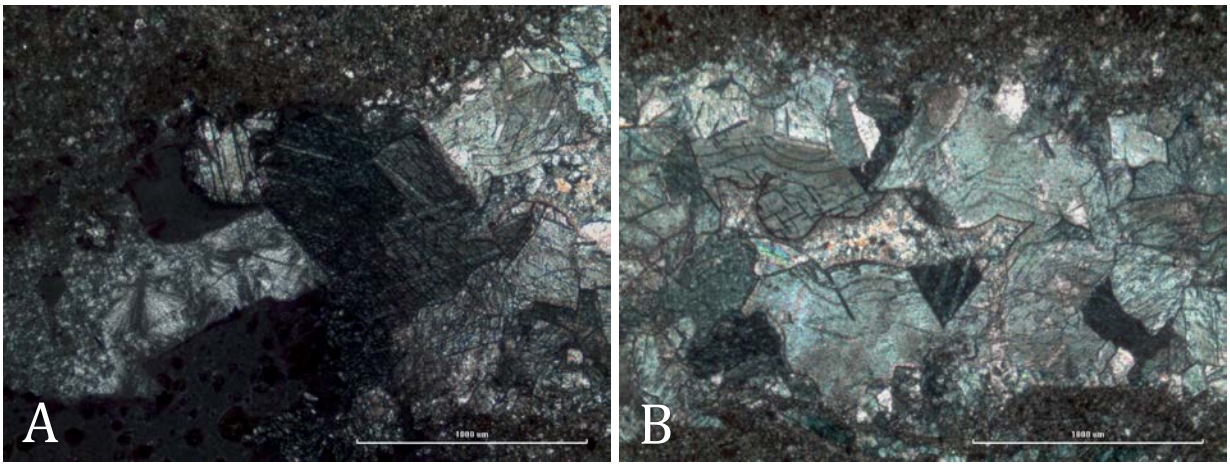

Figure 18: A) Chalcedony located at the top of a burrow in slide 7-a-1. B) Macro quartz intergrown with ferroan saddled dolomite in a burrow in slide 7-a-1. Crossed-polarized light, 50X magnification.

The "others" category ranged from 28.0% to 0.0% with an average of 3.4%. The most abundant contributor to this category were intraclasts in slide 4-a-1 (Figure 16). As with the fossils, a complete list of the "other" constituents found in each thin section can be found in Appendix D.

Lithofacies

Lithofacies were assigned to the different sites based on the point count and insoluble residue analyses using Dunham's classification scheme (Dunham, 1962). The results for these analyses can be found in Tables 2, 3, and 4. The raw data can be found in Appendix C and E.

Site #	Micrite	Ferroan Sparite	Non-ferroan Sparite	Non-Carbonate Mud	Fossils	Ferroan Dolomite	Non-ferroan Dolomite	Microcrystalline Silica	Pores	Other	Total
1	69.7%	0.3%	1.2%	9.3%	0.7%	0.5%	1.5%	16.8%	0.0%	0.0%	100.0%
2	36.1%	0.1%	0.0%	32.4%	0.5%	0.3%	0.7%	25.6%	0.5%	3.8%	100.0%
3	54.4%	0.4%	2.5%	15.3%	2.3%	0.1%	0.4%	22.8%	0.2%	1.5%	100.0%
4	27.3%	0.0%	0.0%	43.0%	0.0%	0.0%	0.0%	1.7%	0.0%	28.0%	100.0%
5	10.3%	0.0%	0.0%	36.7%	0.7%	0.0%	1.0%	48.3%	1.7%	1.3%	100.0%
6	41.3%	0.0%	0.0%	51.3%	6.3%	0.0%	0.0%	0.0%	0.3%	0.7%	100.0%
7	20.0%	0.0%	0.0%	50.7%	1.3%	1.0%	0.7%	22.7%	0.0%	3.7%	100.0%
8	20.3%	0.1%	0.4%	36.6%	0.3%	0.0%	1.5%	39.0%	0.1%	1.8%	100.0%
9	4.4%	5.3%	1.6%	29.3%	1.6%	2.0%	1.8%	46.7%	1.3%	6.0%	100.0%
10	7.7%	3.7%	0.7%	73.3%	1.3%	0.0%	0.7%	7.3%	1.0%	4.3%	100.0%
11	54.7%	0.0%	0.0%	41.0%	0.3%	0.0%	0.0%	0.0%	0.0%	4.0%	100.0%
12	56.0%	0.0%	0.3%	42.0%	1.7%	0.0%	0.0%	0.0%	0.0%	0.0%	100.0%
13	12.3%	0.7%	0.0%	78.0%	0.7%	0.0%	0.0%	5.7%	0.0%	2.7%	100.0%

Table 2: Point count results. Slides from each site were averaged together to find the percentage of each constituent at each site as a whole.

Site #	Percent Insoluble Residue (%)
1	17.9
2	62.2
3	10.2
4	76.7
5	92.4
6	45.4
7	46.0
8	62.3
9	75.7
10	75.1
11	30.2
12	42.9
13	52.6

Table 3: Insoluble residue analysis results. Sites 1, 2, 3, 5, 7, 8, and 9 had chert nodules present. This may have skewed the percent insoluble residue.

Site #	Lithofacies
1	Siliceous Mudstone with Nodular Chert
2	Siliceous Mudstone with Nodular Chert
3	Siliceous Mudstone with Nodular Chert
4	Calcareous Mudrock
5	Calcareous Mudrock with Nodular Chert
6	Calcareous Mudrock
7	Calcareous Mudrock with Nodular Chert
8	Calcareous Mudrock with Nodular Chert
9	Calcareous Mudrock with Nodular Chert
10	Cherty Calcareous Mudrock
11	Siliceous Mudstone
12	Siliceous Mudstone
13	Cherty Calcareous Mudrock

Table 4: Summary of Lithofacies at each site.

Siliceous Mudstone

A mudstone is a limestone that is composed of less than 10% grains in the matrix (Dunham, 1962). These grains could be sparites, dolomites, or fossils. Less than 10% of these grains were found in the samples. A siliceous mudstone consists of this limestone matrix with

the non-carbonate mud component. For this lithofacies, the non-carbonate mud percentage was always less than the micrite percentage in the matrix. There was also no microcrystalline silica present in these samples. Sites 11 and 12 were assigned to this category.

Siliceous Mudstone with Nodular Chert

This lithofacies contained visible chert nodules in hand specimen and thin section. To determine the lithofacies of the matrix without the chert nodules, the percentages of the other constituents were recalculated without the percentage of microcrystalline silica. They were then named based on the criteria described under "Siliceous Mudstone". Sites 1, 2, and 3 were part of this category.

Calcareous Mudrock

This lithofacies contained greater than 50% non-carbonate mud. In order for a sample to be classified as a limestone, it must contain at least 50% carbonate material. Sites classified under this category contained carbonate material, but it was under the 50% limit. For these reasons, the lithofacies was called a calcareous mudrock instead of mudstone which is used for the carbonates. There was also no microcrystalline silica present in these samples. Site 6 was classified under this category.

Calcareous Mudrock with Nodular Chert

Chert nodules were present in both hand specimen and thin section for the samples in this lithofacies. Similar calculations were performed as with the samples in the "Siliceous Mudstone with Nodular Chert" section to determine the matrix of the rocks. The rock samples were then named based on the criteria described under "Calcareous Mudrock". Sites 5, 7, 8, and 9 were part of this category.

Cherty Calcareous Mudrock

Samples categorized in this lithofacies contained small amounts of microcrystalline silica not present as chert nodules. There was also a very large non-carbonate mud percentage and relatively low abundance of carbonate material. For these reasons, these samples were also categorized as a "Calcareous Mudrock" with a Cherty component. Sites 10 and 13 were part of this category.

XRD Analysis

Results from the XRD analysis are based on minerals identified by the X'Pert Highscore Plus program. Any mineral peaks not identified by the program were identified by hand as stated in the "XRD Procedure". Calcite and quartz were identified as present in the powdered samples of all 13 sites prior to insoluble residue analysis. The only mineral identified by the program in all samples following the insoluble residue analysis was quartz. This left many unidentified peaks in the spectra that needed to be determined by hand. Due to the overabundance of silica present in the insoluble residue, the intensity of the quartz peaks masks any other mineral peaks in the spectrum. Determination of specific minerals is difficult from these low-intensity peaks, but determination of mineral groups can be made with a moderate degree of confidence. The additional mineral groups were alkali feldspars and phyllosilicates. These two groups, along with the quartz, are believed to make up the non-carbonate mud component of the point count analysis.

Some peaks were not identified. These peaks did not match up with any known minerals found in carbonate rocks and may have resulted from mineral contamination during sample preparation. This contamination most likely resulted from the grinding wheels the sample went

through. The pulverizer wheels may have also contaminated the sample as bits of the iron alloy wheels were found in samples prepared for the SEM-EDS.

Alkali Feldspars

The presence of three alkali feldspars were indicated by X'Pert Highscore Plus: orthoclase, anorthoclase, and albite. Within the feldspar group, there is a significant overlap in mineral signatures, making identification of specific minerals difficult based on spectra alone. Orthoclase was the most easily identifiable of the three and appears to be the second most abundant mineral after quartz (Figure 19). Albite was present, as well, but to a lesser extent than orthoclase. Anorthoclase cannot be distinguished with confidence and is unlikely to appear in a carbonate setting. Alkali feldspars were found in all 13 sites.

Phyllosilicates

Two main phyllosilicates were indicated by X'Pert Highscore Plus: illite and muscovite. Major peaks for both these minerals are present in the spectra and the majority of their peaks overlap (Figure 19). Due to major peak overlap between these two minerals, it is difficult to determine which mineral is actually present. No other phyllosilicates were observed and phyllosilicates were found in all 13 sites.

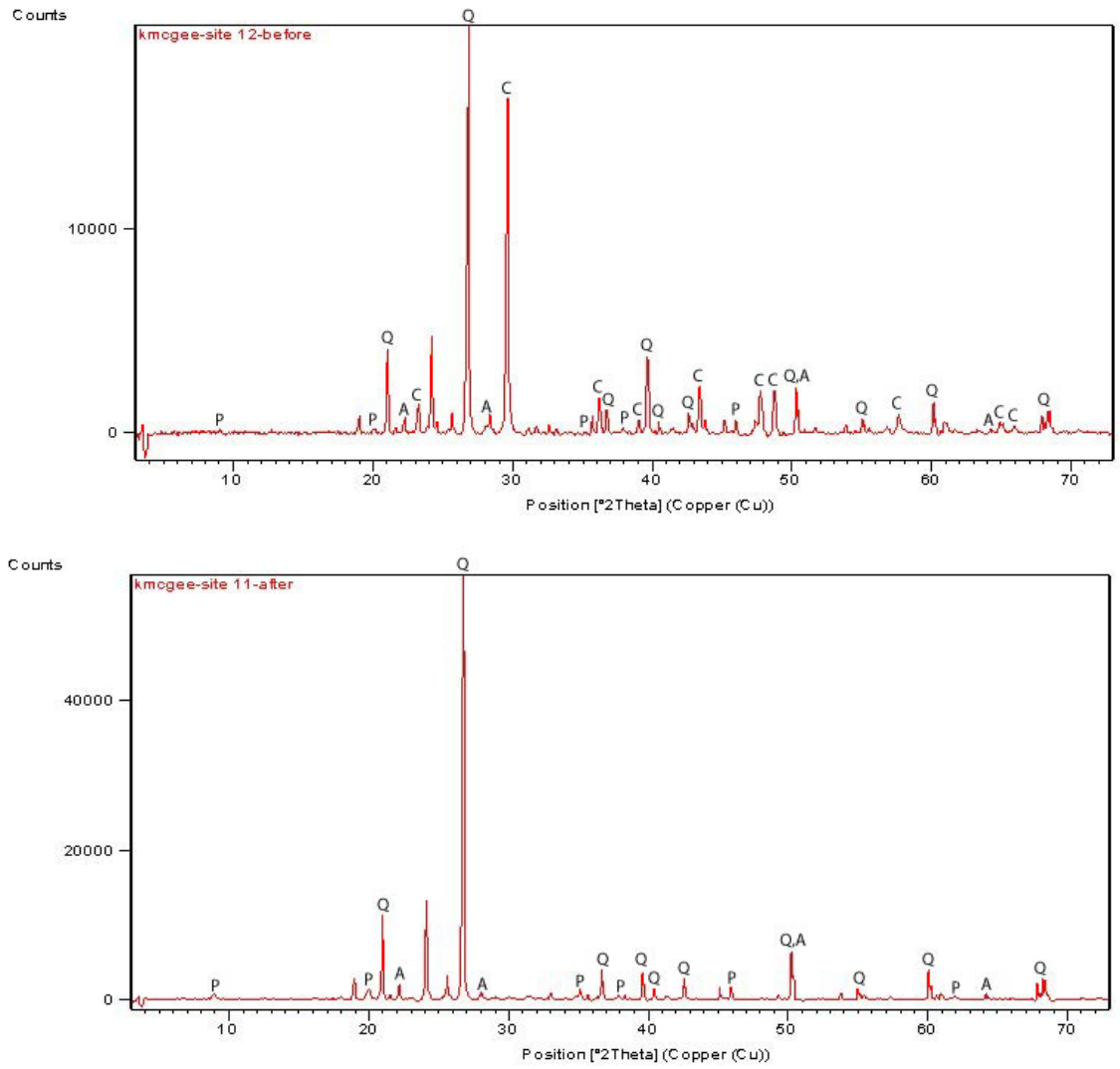

Figure 19: Typical XRD spectrum before (upper) and after (lower) insoluble residue analysis. C-Calcite, Q-Quartz, A-Alkali feldspar, and P-Phyllosilicate.

SEM-EDS Analysis

Results from the semi-quantitative analysis on the SEM-EDS were compared to spectra in Welton's SEM Petrology Atlas (1984) and mineral standards analyzed by Akland (2017). These analyses indicated the presence of silica, alkali feldspars, phyllosilicates, pyrite, and a few other minerals. A further in-depth analysis was performed on the alkali feldspars and phyllosilicates whereas the silica, pyrite, and other minerals were identified based solely on the

elements observed in their spectra. Data tables for the alkali feldspars and phyllosilicates can be found in Appendix G.

Several factors related to sample preparation and mounting contributed to ambiguity with respect to mineral identifications. First, analyses were conducted on loose grains mounted on carbon tape, rather than on polished thin sections. Secondly, many grains were covered with coatings of other minerals to varying extents. Third, iron contaminates were present. The carbon tape on which the grains were mounted sometimes resulted in a false peak for C. Mineral coatings often resulted in two mineral spectra being overlain, complicating mineral identification. Iron contaminates may have been present and could have skewed Fe weight percent (wt. %) concentration on any of the samples observed. Iron filings were removed after HCl dissolution during the mineral separation process. These filings were analyzed in the EDS and have major elemental peaks of Fe and O, and minor peaks of Mn, Ni, and Cl. They may have come from the pulverizer wheels which were comprised of an iron alloy and were introduced into the samples during the grinding process.

Silica

Silica refers to any material that yielded silicon and oxygen as its major elemental components in the EDS (Figures 20 and 21). This could refer to chert nodules observed in thin section and hand specimen and quartz crystals detected in the SEM-EDS (Figures 21A and C). Silica pseudomorphs were also found replacing dolomite rhombs, other minerals, and voids in the SEM-EDS (Figure 21B). Minor elements found in the silica spectrum included K, C, Ca, Fe, Mg, Al, Na, S, Cl, Ti, Ni, and Zr. These elements may be trace elements found within the silica, but it is more likely that they are from very minor amounts of different minerals within and coating the silica grains. These elements are present in silica in varying amounts throughout all

six sites. The few exceptions are: site 8 lacks Na and Ti, site 9 lacks S, site 12 lacks Ca and Cl, and site 13 lacks Na in any of the silica spectra. Ni was found in only one spectrum from site 9 and Zr was found in only one spectrum from site 12. There is no lateral or vertical trend found in the minor elements within the silica spectra between the sites. The silica appears to be relatively homogenous in nature with minor elemental differences within the sites.

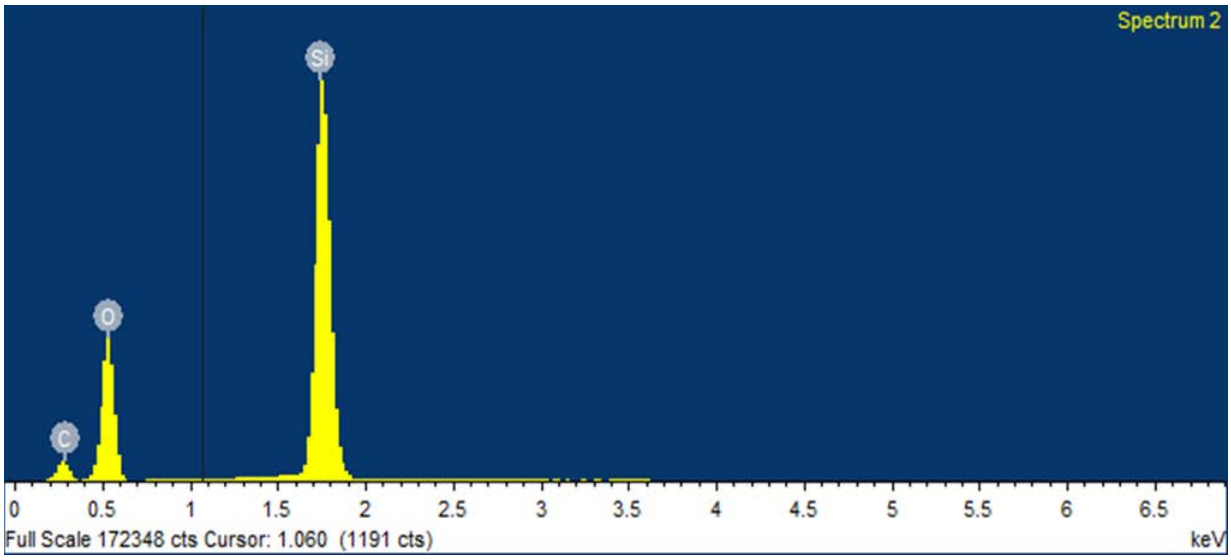

Figure 20: Typical EDS spectrum of silica.

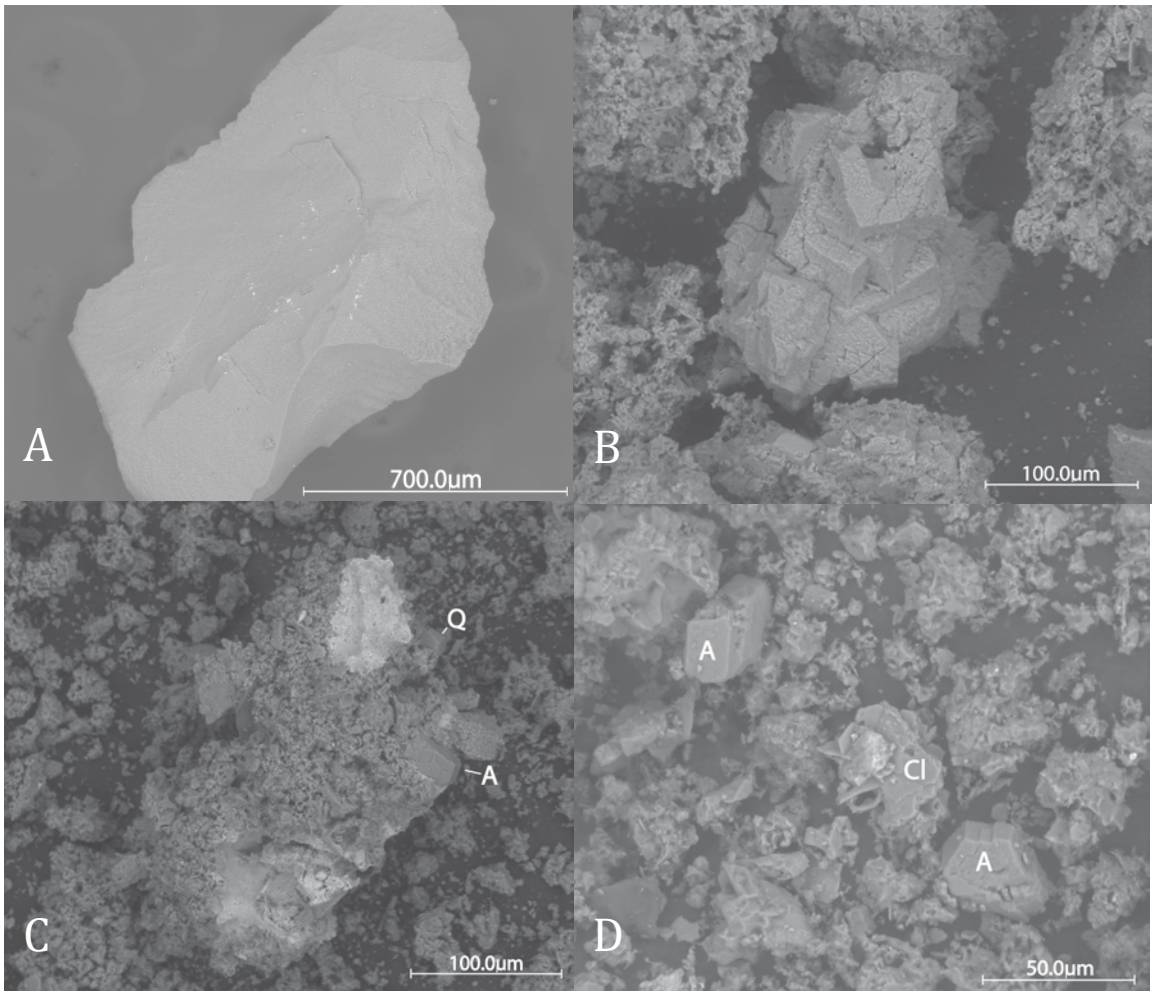

Figure 21: SEM images of A) fragment of a chert nodule, B) silica pseudomorphs replacing dolomite, C) authigenic quartz and albite crystals, and D) albite and chlorite crystals. Q-quartz, A-Albite, and Cl-Chlorite.

Alkali Feldspars

The main alkali feldspar identified was albite which yielded a spectrum showing Na, Al, Si, and O as the major elements (Figures 21C, D, 22A, and 23). The weight percentages of the elements calculated for these minerals were consistent with those determined by Alkland (2017) for the albite standard. Albite was also identified in thin section (Figure 17). The main difference between albite and the other alkali feldspars is its Na to K ratio. Albite shows a range in Na wt. % of 2%-8%, whereas the wt. % of K is less than 1% (Figure 22A). One albite grain contained ~2 wt. % of K, but this may have been an albite grain in close contact with another

feldspar grain or an alteration of an albite to another alkali-feldspar. Albite spectra were recognized at sites 1, 3, 12, and 13.

The other alkali-feldspar group is called K-feldspars because they contain significantly more K than Na (Figures 22A, 24, and 25A). The wt. % of K and Na were similar to those of albite except that the K values ranged from 1%-9% and the Na values ranged from 0%-3%. A few of the K-feldspar values plotted lower on the graph in Figure 22 because the K-feldspar grains may have been coating a chert grain providing higher wt. % for Si and O and lower wt. % for K, Al, and Na. K-feldspar spectra were recognized at sites 3, 8, 12, and 13.

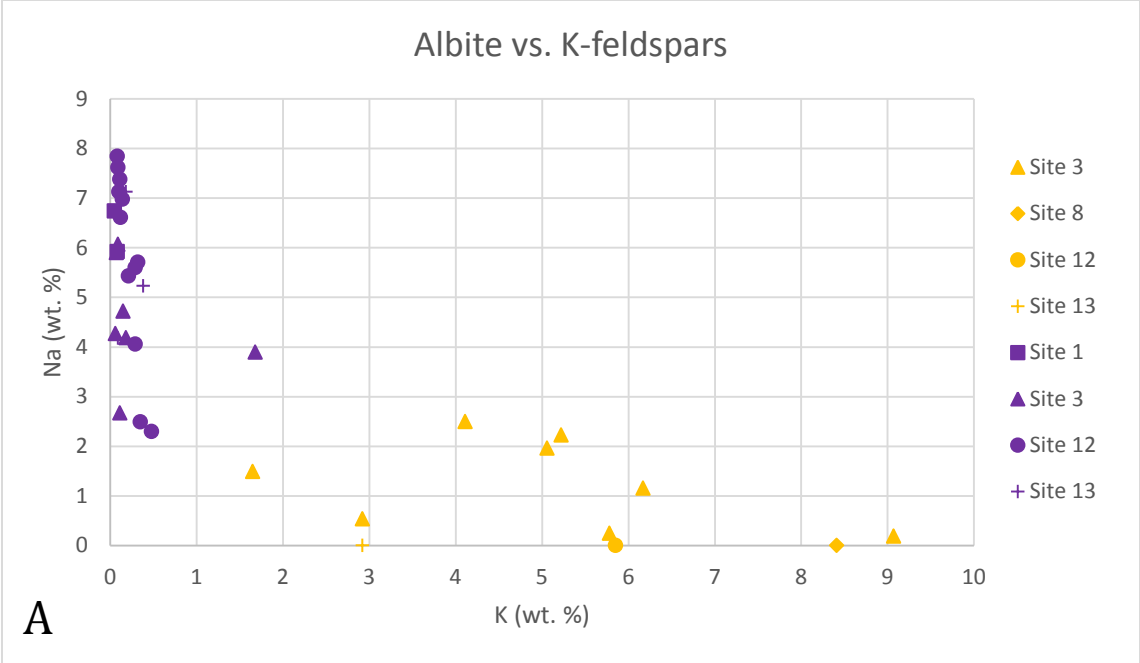

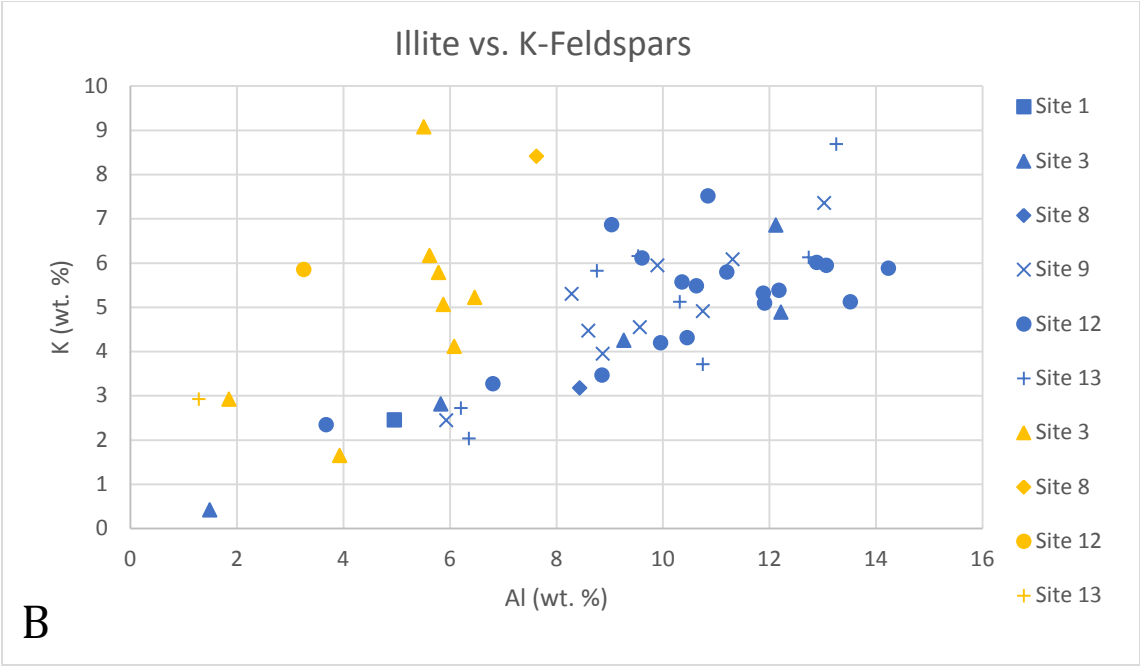

Figure 22: A) Wt. % comparison of the alkali feldspars. B) Wt. % comparison of K-feldspar to illite. Purple=Albite, Gold=K-feldspar, and Blue=Illite.

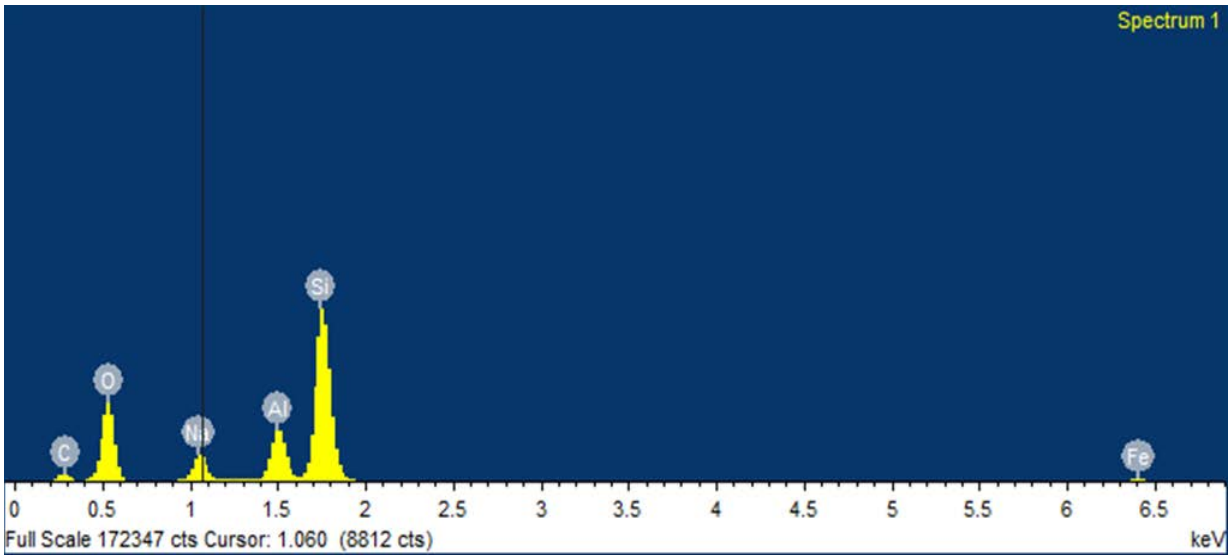

Figure 23: Typical EDS spectrum of albite.

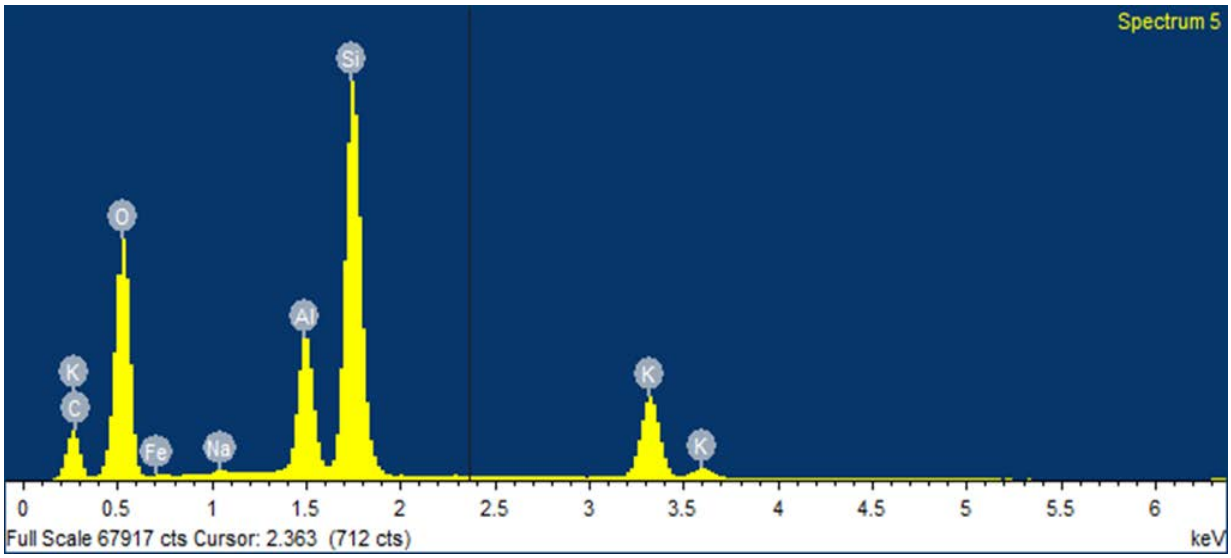

Figure 24: Typical EDS spectrum of K-feldspar.

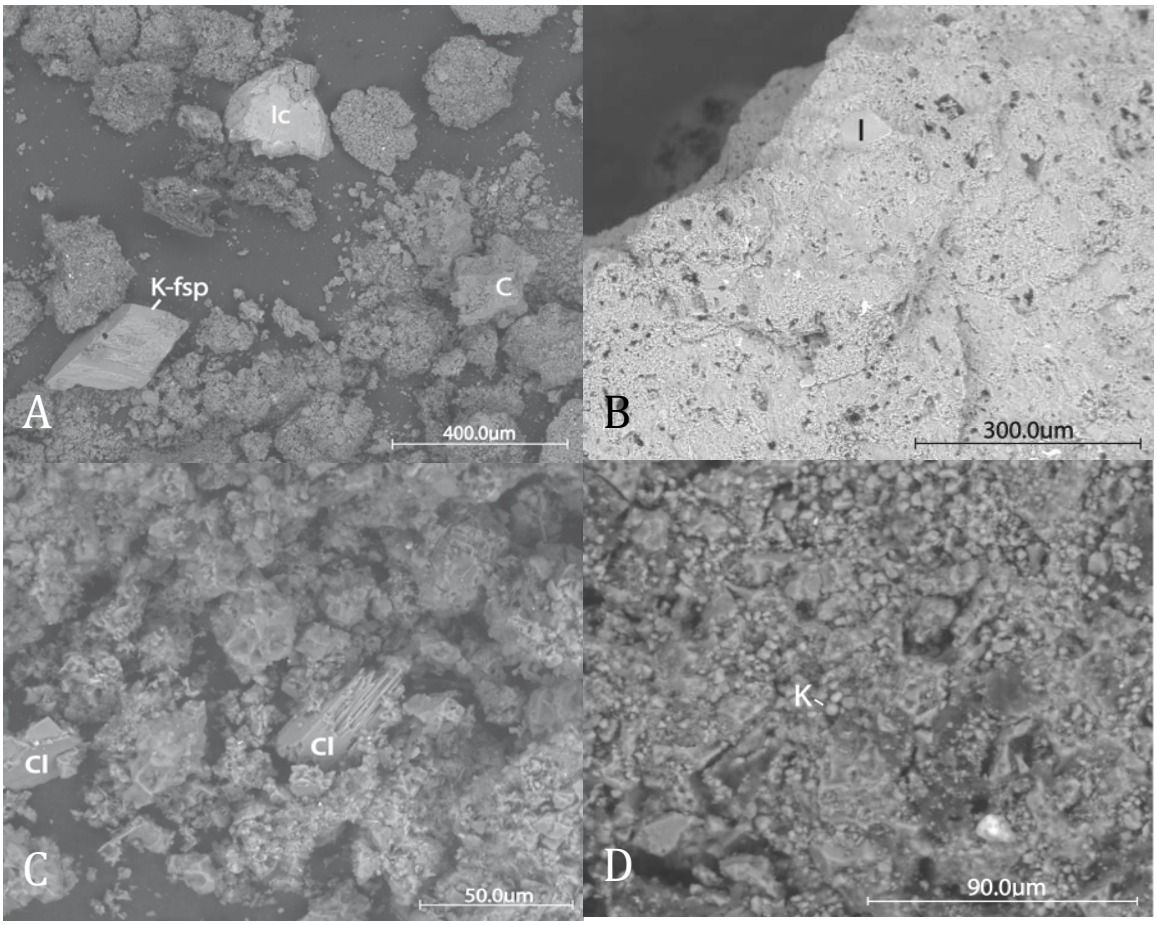

Figure 25: SEM images of A) K-feldspar grain, B) illite grain on chert, C) chlorite crystals, and D) kaolinite grain. K-fsp-K-feldspar, C-Chert, Ic-Iron coating, I-Illite, Cl-Chlorite, and K-Kaolinite.

Phyllosilicates

The phyllosilicates were broken down into three main groups: illite, chlorite, and kaolinite (Figure 25B, C, and D). These were distinguished based on the main cations observed in their spectra: K, Mg, Fe, and Al. The cations K, Mg, and Fe were plotted against Al to explore compositional trends for these three groups. The wt. % of Si and O remained relatively constant between these three groups and are therefore not plotted.

Illite was distinguished from the other phyllosilicates by its generally higher K content and a lower Mg and Fe content (Figure 26). The K values ranged from 0%-9%, whereas Mg ranged from 0%-3% and Fe ranged from 0%-11%. A few of the outliers may be illite partially coating chert giving it a higher Si and O values and lowering the other values, or it was near

another grain of different composition and the EDS was picking up some chemistry from the other grain as well.

Illite can generally be differentiated from K-feldspar based on its lower ratio of K to Al (Figures 27 and 22B). K-feldspar had a K range from 1%-9% and an Al range from 1%-8%. Illite, on the other hand, had a K range from 0%-9% and an Al range from 1%-14%. Outliers on the low end of the graph in Figure 22B may be due to these minerals covering chert grains and thus showing higher wt. % of Si and O and low wt. % of K and Al. Illite grains were identified at all six sites observed.

Chlorite was distinguished by having a higher Mg and Fe content and a lower K content than the other two groups. The wt. % values of K ranged from 0%-1%, Mg ranged from 4%-12%, and Fe ranged from 2%-12% (Figure 26). Chlorite usually consisted of only Mg, Fe, Al, Si, and O (Figure 28) and was found at sites 3 and 12.

Only two spectra tentatively identified as kaolinite were found. These were distinguished by having very large Al peaks and very minor K, Mg, and Fe peaks (Figure 29). The wt. % values of Al ranged from 11%-18%, K ranged from 0%-1%, Mg ranged from 0%-1%, and Fe ranged from 1%-4% (Figure 26). Figure 25D shows a very small kaolinite grain that was part of a larger mass of material. Because of this, the kaolinite spectra do not show pure kaolinite, but are probably reflecting the chemistry of surrounding minerals as well. For example, the kaolinite grains plot with a larger amount of Fe than expected. This may be because of nearby iron coatings on other grains. Kaolinite spectra were recognized in sites 3 and 8.

There were five spectra that exhibited a pattern like the other phyllosilicates, but did not seem to fit in any of the three groups. These are labeled unknown and were plotted with the other phyllosilicates to show their correlation with these other minerals (Figure 26). Four of the

spectra come from site 12 and are similar to chlorite, but with higher wt. % of K and Al. The K value for the unknowns from site 12 ranged from 1%-6% and the Al value ranged from 10%-11%. The last unknown spectrum was from site 3 and did not fit in with any pattern. The wt. % of this unknown spectrum were Si at 22%, O at 28%, Al at 6%, K at 1%, Mg at 3%, and Fe at 23%. In this case, Fe, Si, and O had roughly the same weight percentages, which were not typical of other phyllosilicates.

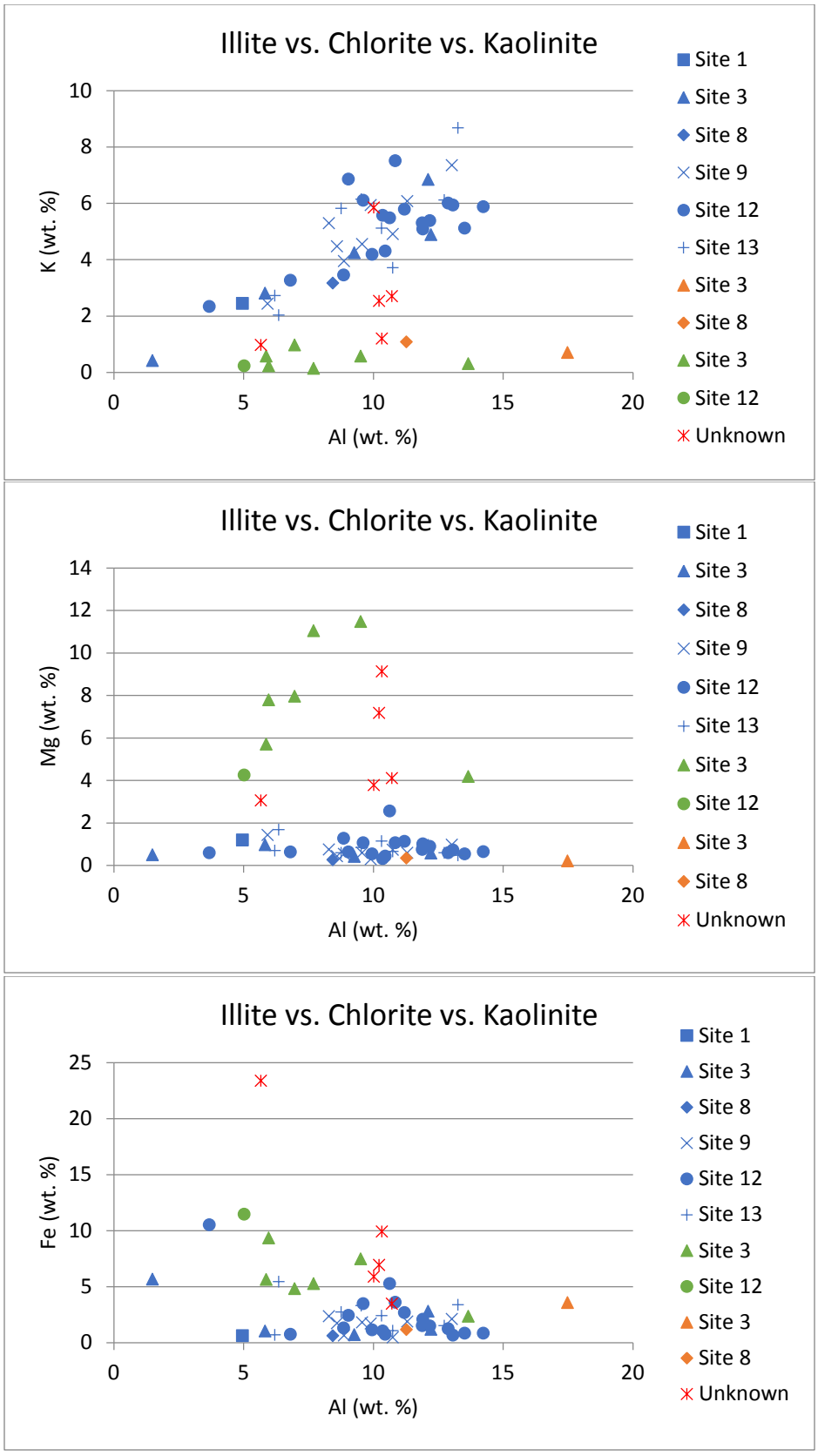

Figure 26: Wt. % comparison of the phyllosilicates. Blue=Illite, Green=Chlorite, Orange=Kaolinite, and Red=Unknowns.

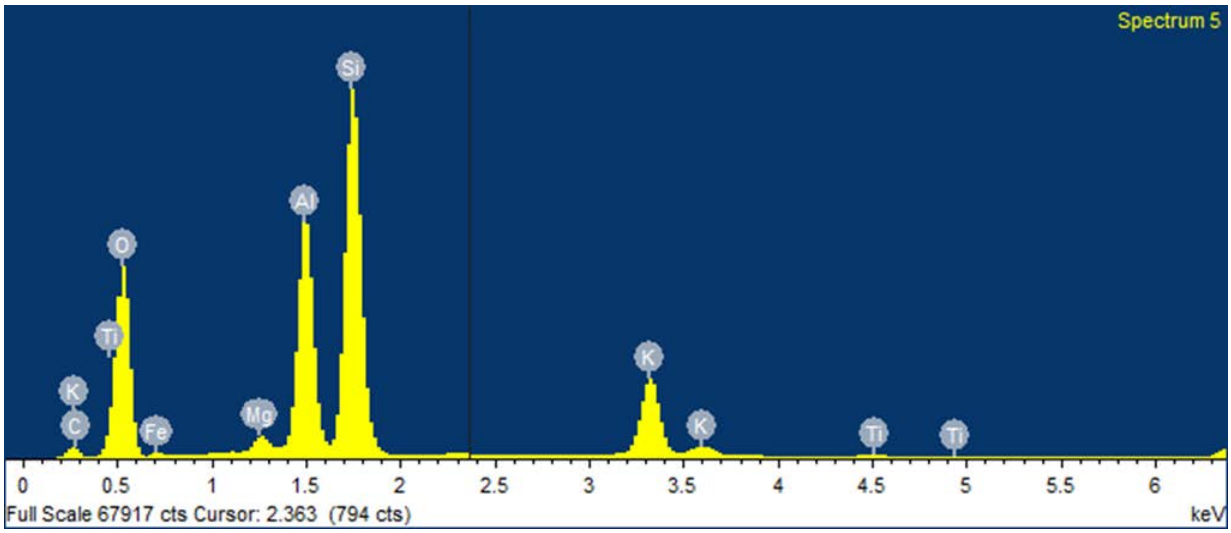

Figure 27: Typical EDS spectrum of illite.

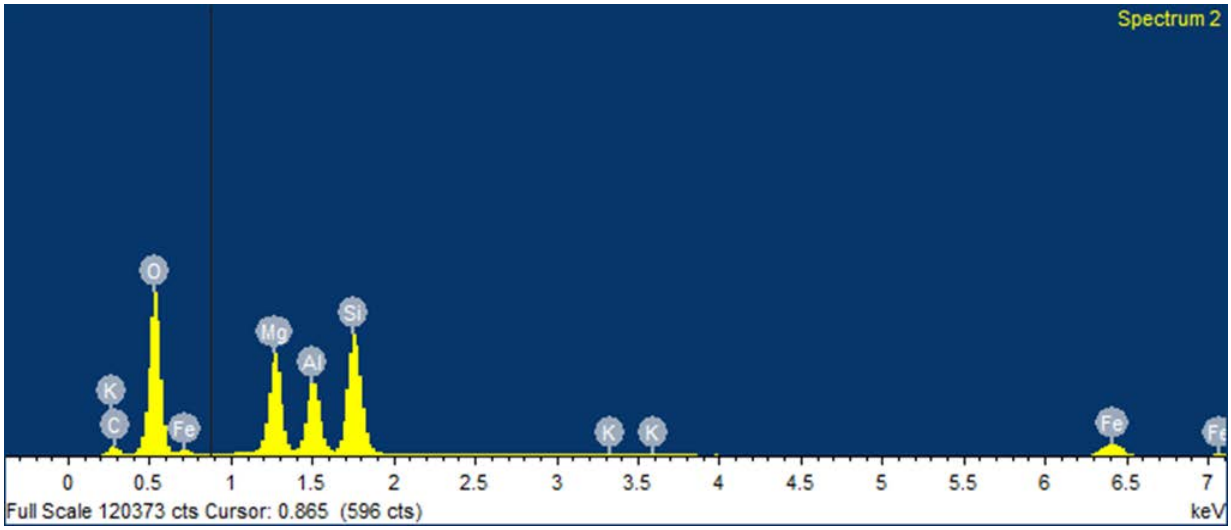

Figure 28: Typical EDS spectrum of chlorite.

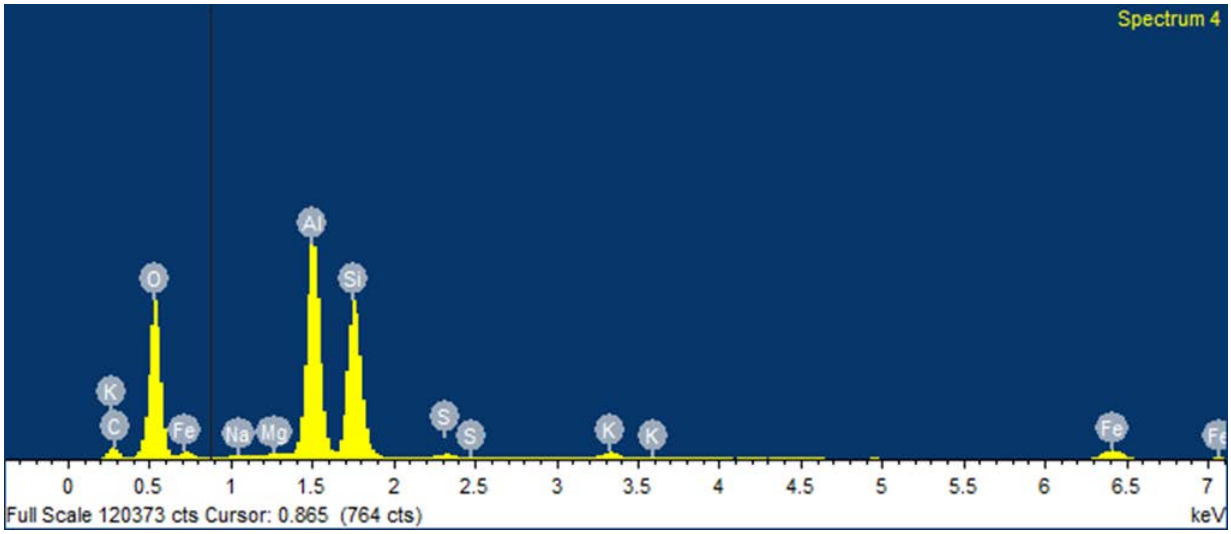

Figure 29: Typical EDS spectrum of kaolinite.

Pyrite

Pyrite was identified in the EDS by major peaks of Fe and S. It usually occurred as bright nodules on a larger grain and, therefore, the other grain's signature was often picked up as well (Figure 30 and 31A). Pyrite was found in sites 3, 12, and 13.

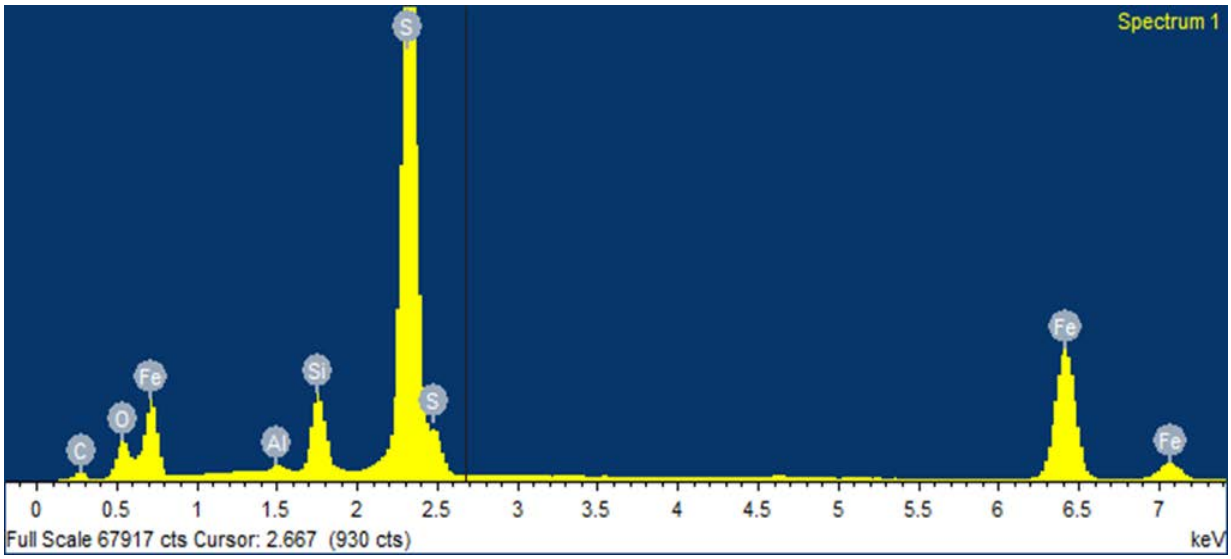

Figure 30: Typical EDS spectrum of pyrite.

Other

Other spectra identified by the EDS consisted of 3 iron oxides, 2 rutiles, and 1 zircon. The iron oxide grains appeared as bright, tabular crystals with Fe and O as the major elements detected (Figure 31B and 32). Iron oxides were found at sites 3 and 8. Rutile occurred as small grains embedded in a larger chert grain. The major elements detected by the EDS were Ti, Si, and O (Figure 31C and 33). Rutiles were found at sites 12 and 13. Site 13 contained the only zircon grain that was identified. This appeared as a small, bright grain on a larger grain. The EDS picked up major elements of Zr, Si, and O (Figure 31D and 34).

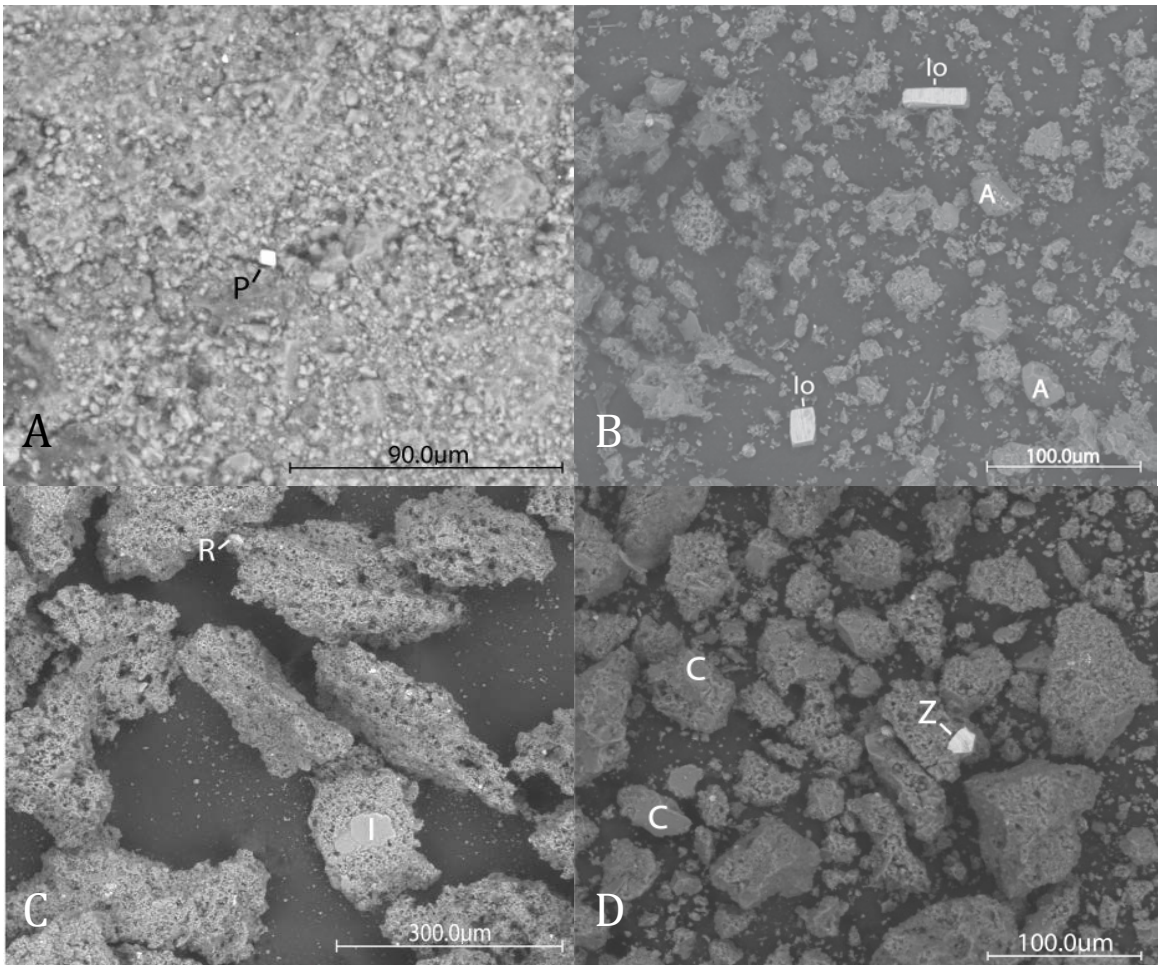

Figure 31: SEM images of A) pyrite grain, B) iron oxide and albite grains, C) rutile and illite grains, and D) zircon grain. P-Pyrite, Io-Iron oxide, A-Albite, R-Rutile, I-Illite, C-Chert, and Z-Zircon.

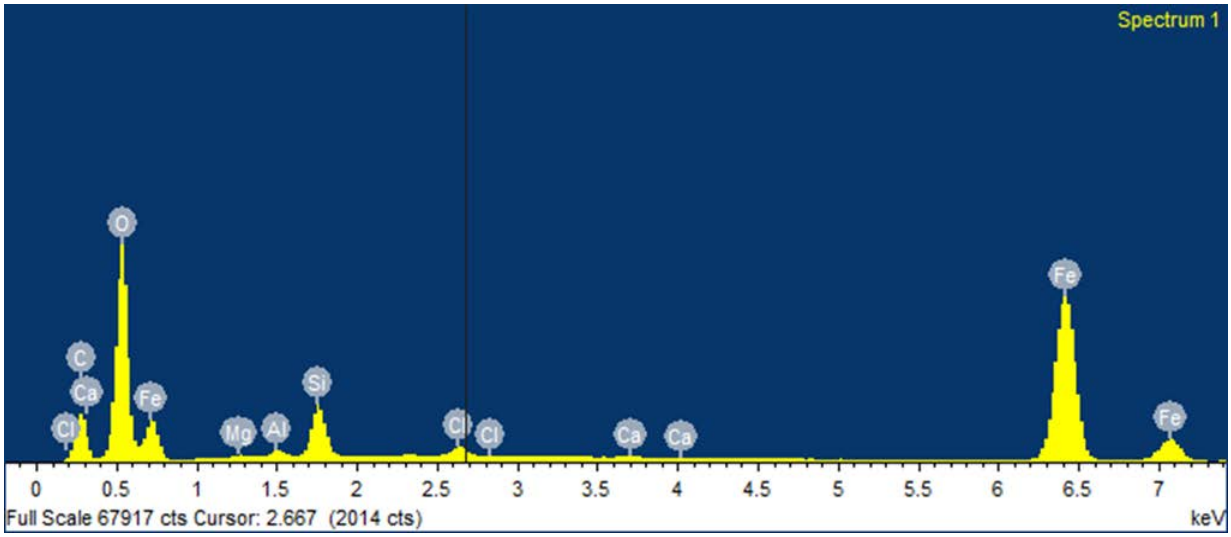

Figure 32: Typical EDS spectrum of iron oxide.

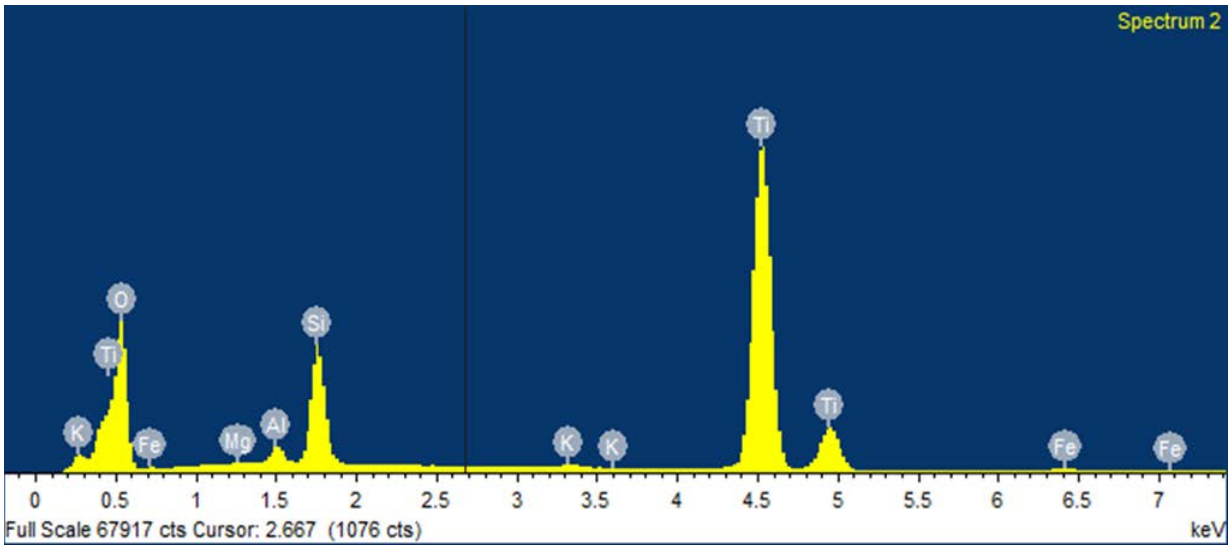

Figure 33: Typical EDS spectrum of rutile.

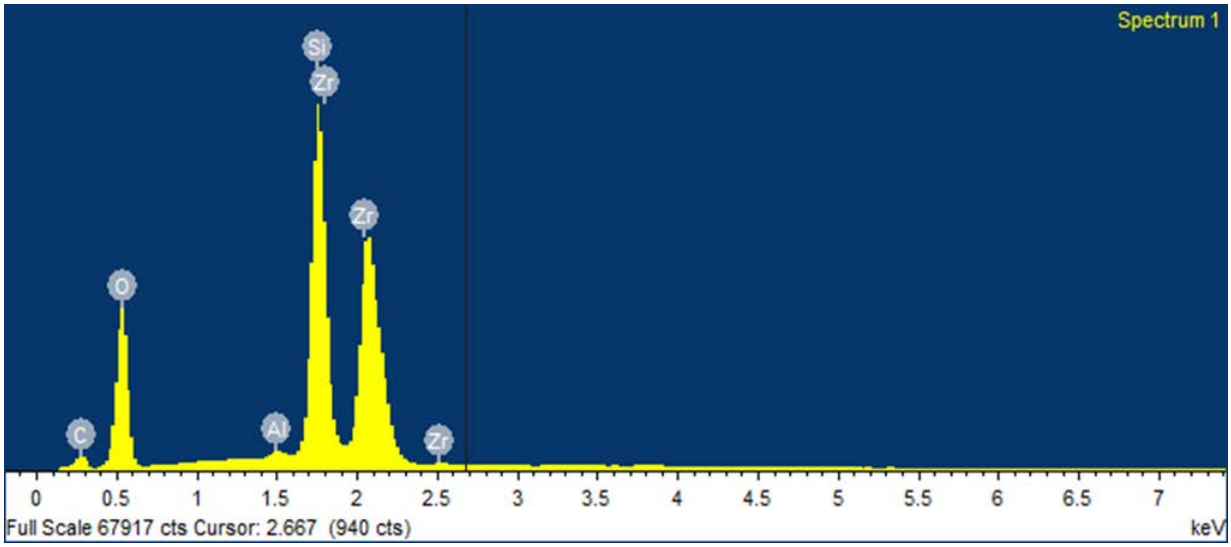

Figure 34: Typical EDS spectrum of zircon.

V. Discussion

Diagenesis

The first step in the formation of the Onondaga was the deposition of the carbonate mud and fossils with an influx of terrigenous sediment. Some of this terrigenous sediment consolidated and later formed darker areas of non-carbonate mud observed in thin section. As this material was being deposited, some of the semi-consolidated mud was ripped up and redeposited within the unconsolidated sediment forming intraclasts (Figure 16). This could be from storm events or other turbulent flows in the basin. The initial deposition of sediment was then buried as more sediment accumulated on top and underwent early stage compaction and cementation (Figure 35). These processes lead to the initial intergrowth and cementation of the micrite and non-carbonate mud observed during the point count analysis. Cementation is also present in the form of sparry-calcite-isopachous-rim cement on some fossils which later altered to silica in chert nodules. Compaction is shown on these same fossils to have fractured the fossil and rim cement as well (Figure 14B). Silica later filled in these fractures.

As burial and compaction continued, dissolution of carbonate mud and some fossils began (Figure 35). This can be seen as fossils (that should have initially been composed of calcite or magnesium calcite) were replaced with silica material in thin section (Figure 11). Sponge spicules also likely underwent dissolution at this time, since some spicules found in thin sections exhibit moldic porosity which was later refilled with ferroan sparite. Other spicules still retain their original silica structure.

Around the time of dissolution, formation of chert nodules started (Figure 35). Nodules may have originated in areas of high spicule concentration or close to another silica source, i.e. volcanics or wind-blown dust as a nucleation point. The force of crystallization-controlled

replacement model of Maliva and Siever (1989) best explains chert nodule growth from this point. In this model, chert nodule formation occurs resulting from the dissolution of carbonate and precipitation of chert along solution films in response to stress heterogeneities. Along these films, calcite would not show evidence of dissolution related to chertification (Maliva and Siever, 1989). The model also states, "The volumetric rate of calcite dissolution is inherently equal to the silica precipitation rate in force of crystallization-controlled replacement because the silica phase must always be in contact with the host carbonate phase in order for replacement to occur" (Maliva and Siever, 1989). In all the thin sections in this study where a chert/limestone contact occurs, the carbonate matrix is always in contact with the chert. At this contact, the carbonate shows little evidence of dissolution and the chert shows little evidence of precipitation. This is directly observed in Figures 12 and 13A.

The source of silica for nodular chert growth is partially from sponge spicules (as indicated from dissolution of spicules observed in thin section), but there do not appear to be enough spicules present to account for all the chert. In this case, the silica source was possibly from dissolution of the non-carbonate mud along the solution films, as well as from freshwater input into the groundwater system. Evidence of fluid flow through the system around the time of chert nodule formation is also suggested by the presence of preserved parallel lines of chert branching off of the main nodule in one direction in a few hand specimens at Site 8. A third possible source of silica could be volcanism. Ver Straten (1996) mentions the presence of numerous minor Tioga bentonite beds within various members of the Onondaga in Pennsylvania. This indicates volcanism likely deposited ash into the sediment during deposition. This ash could be a source of silica for chert nodule growth in the Onondaga Formation.

Dolomite formation most likely occurred during chert nodule growth. As dissolution of the carbonate occurred, magnesium from any Mg-calcite would have been released into solution. This magnesium was now free to form dolomite. This explains why dolomite rhombs are predominately found at the chert/limestone contact. As chert nodule growth continued, some of the dolomite was incorporated and preserved within the nodules (Figure 13).

As the lithification process continued, further burial and compaction of the sediment occurred. This lead to the recrystallization of some of the micrite into microspar and silica replacing fossils (Figure 11). Fossils that were not replaced initially had isopachous rim cement overgrowths preserving them (Figure 14B). The solidified chert nodules also began to develop fractures due to the pressure associated with deposition of overlying sediments. The fractures are present cutting through the chert nodules and only the surrounding matrix. They do not extend very far into the matrix past the chert/limestone contact (Figures 13A and 14A). The matrix underwent continued intergrowth and cementation of the micrite and non-carbonate mud. The various opaque minerals observed in thin section (that were not detrital in origin) formed around this time and are present in the chert nodules as well as the surrounding matrix. These minerals have euhedral crystal structure which indicates an authigenic origin. Iron staining of minerals and fractures observed in thin section likely occurred around this time, as well.

Deeper burial of the sediment occurred resulting in the formation of stylolites and pressure seams as noted in some of the thin sections (Figure 15B). Continued dissolution of fossils and the final stages of cementation likely occurred during this time. Finally, more fractures developed throughout the lithified sediment and were later filled with ferroan sparite cement (Figure 15A). This cement also filled any voids and fossils exhibiting moldic porosity (Figure 14B).

The growth of authigenic feldspar grains likely occurred after lithification during tectonic uplift. As suggested by Hearn, Sutter, and Belkin (1987), "the migration of basinal brines in a gravity-driven flow system" is what likely caused the growth of feldspars. Their study on Cambrian carbonate rocks yields cooling temperatures of 100-200°C and salinities of 18-21 wt. % NaCl equivalents of the fluids in these brines. Their evidence points towards an event of basin-wide fluid migration during the Alleghanian Orogeny.

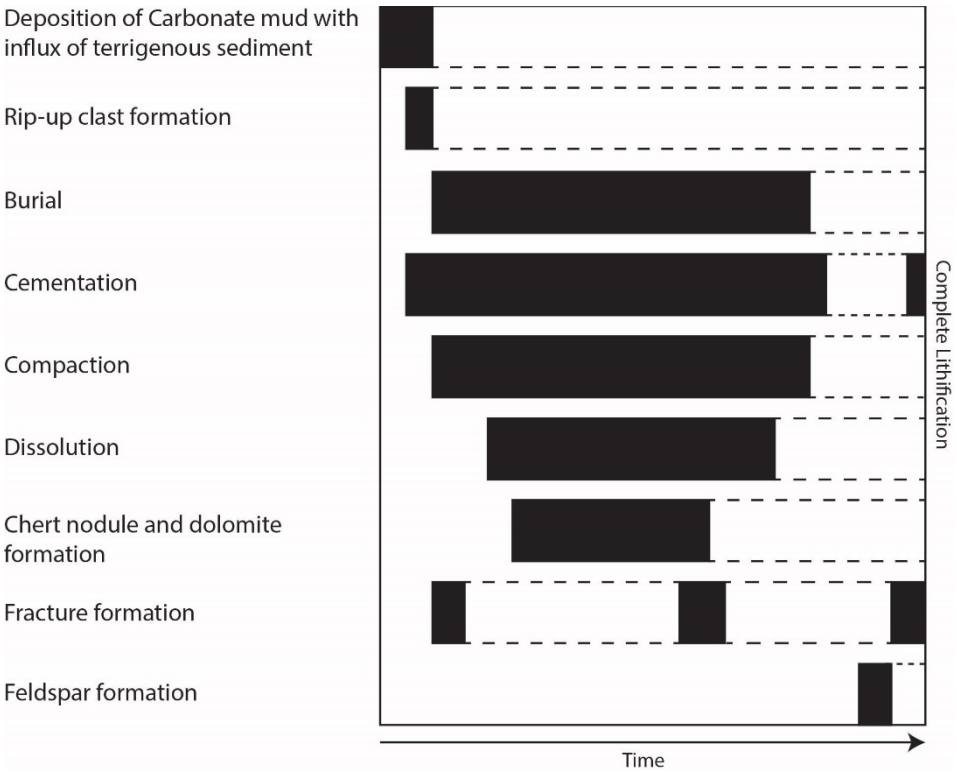

Figure 35: Summary of diagenetic sequence.

Depositional Environment

Based on the results of this study, the most likely depositional environment for the Onondaga Formation was a carbonate ramp. This environment coincides with observations made by Ver Straten (1996) on the Onondaga's depositional environment as "a carbonate ramp geometry". He states, "The sea floor appears to have featured gentle, low angle slopes from topographically higher areas into more basinal regions" (Ver Straten, 1996). Characteristic features of this type of environment include mudstone-dominant lithology, diverse shelly fauna, and lack of corals, which would indicate a more reef-like environment. Based on the petrologic results noted previously, the rocks observed in this study all consisted of a fine-grained matrix (Table 4). Mollusks were the main fossil group observed in thin sections, and corals were not present in any thin section or hand specimen.

Interpretations

The lithology of the Onondaga Formation in New Jersey is similar to the lithology of the Onondaga described just over the border in New York and Pennsylvania. In New York State, Oliver (1956) mentions the units of the Onondaga darken, become thicker, and the fauna changes to the south. In New Jersey, the formation is observed as a dark-gray limestone with black chert nodules locally. This is seen right over the border in Port Jervis, New York, but is not the case near Albany, New York. There the limestone and chert are lighter gray and there is an abundance of corals noted in the formation. The New Jersey Onondaga lacks these corals as well. This trend in the Onondaga is seen throughout New Jersey and into eastern Pennsylvania where descriptions of the formation by Ver Straten (1996) and Epstein (1984) are similar to what is observed in New Jersey.

Based on the lithofacies identified (Table 4), observations made in thin section and hand specimen, and where sites plotted relative to the full thickness of the formation, member identification can be determined with some confidence. Only two members of the Onondaga were identified in this study. These are the Edgecliff and Moorehouse members (Figure 36). Member identification was based on descriptions by Ver Straten (1996), Epstein (1984), and Oliver (1956). They describe the Edgecliff and Moorhouse members as limestones relatively similar both in lithologic composition and the fact that they contain dark-gray to black chert nodules. The main difference is the shaly Nedrow Member located between the two. No shaly hand specimens of Nedrow description were collected in this study; therefore the Nedrow is not thought to be present in the 13 sites.

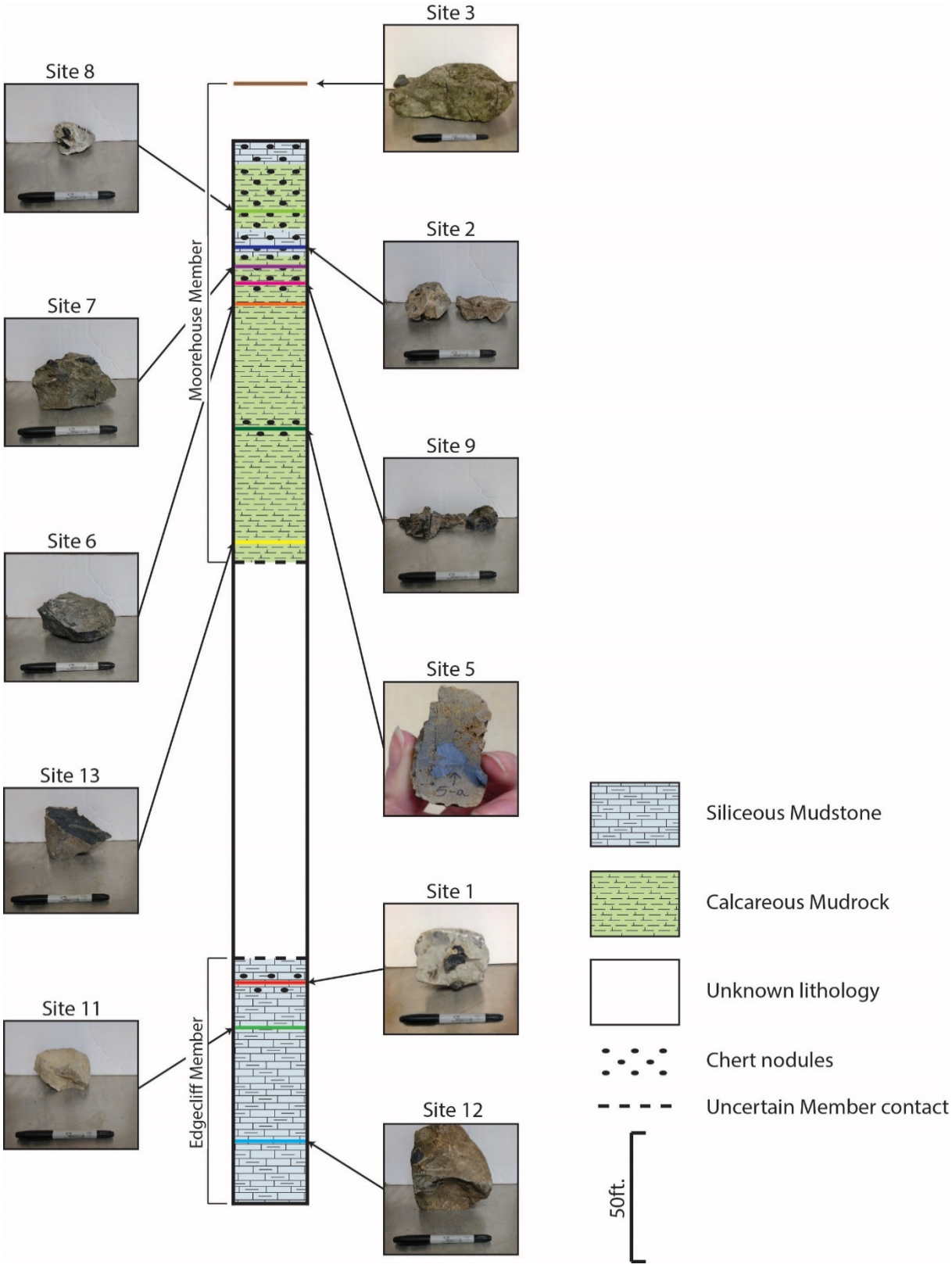

Figure 36: Vertical columnar section of the Onondaga Formation in New Jersey based on site locations and lithologies. Sites 4 and 10 were float samples and therefore cannot be accounted for in the location on the vertical columnar section.

Figure 36 shows the average thickness of the Onondaga Formation in New Jersey. Based on lithology and the proximity to the lower contact observed from geologic maps (Figures 7B, C, and D), sites 12, 11, and 1 are assumed to be part of the Edgecliff Member. Above these sites, a portion of the formation remains unaccounted for due to a lack of data. The remaining sites are lithologically similar to sites 12, 11, and 1. Due to these remaining sites' location above this unaccounted for segment and location above the lower contact, they are believed to be part of the Moorehouse Member. Because the Nedrow Member is located between the Edgecliff and Moorehouse members, it most likely lies within the unknown lithologic section on Figure 36.

Site 13 initially appears not indicative of the Moorehouse Member due to its lack of chert nodules. However, Oliver (1956) mentions the base of the Moorehouse is not so cherty, therefore this site is still believed to be part of the Moorehouse Member. Site 3 appears to plot above the top of the formation. It is a dark-gray cherty limestone which correlates to the Moorehouse Member. Its placement above the Onondaga thickness is due to the unknown locality of the upper contact in that area. On Figure 7C, site 3's location falls in the Marcellus Shale group, which is a hydrocarbon-rich black shale. Because site 3 is clearly is not a shale, that suggests the contact on the map is not accurate.

The lithofacies observed at each site indicate a deepening trend of the carbonate ramp environment in the foreland basin during the early Devonian (Table 4 and Figure 36). The Onondaga Formation consists of siliceous mudstones at its base grading upward to calcareous mudrocks toward its top. This was also observed by Kümmel (1940) who suggested the Onondaga in NJ shows a deepening trend of the basin through time and recession of the shoreline. Later, Ver Straten (2001) extended this observation to the Onondaga Formation in New York and Pennsylvania.

There are no noticeable mineralogical trends either laterally or vertically in this formation. Results from the SEM-EDS analysis show silica, alkali feldspars, phyllosilicates, and pyrite throughout most sites. Site 9 was the exception, being predominately silica and could be due to underrepresentation of other minerals in the observed sample or incomplete EDS readings of site 9 samples. The minor amounts of other minerals, such as rutile and zircon, suggest a detrital source for the terrigenous sediment.

The large percentages from the insoluble residue analysis suggests a high input of terrigenous material into the system. The majority of this material, however, was identified as silica in the XRD and SEM-EDS analyses. The alkali feldspars and phyllosilicates identified in these analyses were minor with respect to the silica (Figure 19). Alkali feldspars formed through authigenic means. The paucity of phyllosilicates in this material suggests that there was not a significant amount of weathering of the source material and that the sediment making up the Onondaga Formation must have been close to the source. This can also be inferred from trace grains of detrital rutile and zircon present in only two sites. Based on the timing of formation of the Onondaga, the petrology is greatly influenced by tectonic processes of the incipient Acadian orogeny. Low elevation of the mountains east of the basin and a more temperate climate (Brett and Ver Straten, 1994) would produce this minor amount of phyllosilicates found in the formation.

VI. Summary of Conclusions

Through careful analysis of the results of this study, the following conclusions were made about the petrology and diagenesis of the Onondaga Formation in New Jersey:

1. The trends observed laterally and vertically in the Onondaga Formation in New Jersey are the same trends seen in New York and Pennsylvania.
2. Only two members of the Onondaga Formation are identified in this study: the Edgecliff and Moorehouse.
3. Lithofacies observed in the formation indicate a deepening upward trend of the basin.
4. Presence of trace minerals such as zircon and rutile show a detrital origin for the siliciclastic mud component indicating Onondaga sediment formation was close to the source.
5. The paucity of phyllosilicates indicates that there was not significant weathering during sediment accumulation and the sediment also formed close to the source.

References

Akland, M. J., 2017, Origin and geochemical evolution of localized, high-ferrous-iron zones in the Upper Castle Hayne Aquifer, Beaufort County, North Carolina [Master's thesis]: East Carolina University, p. 219-226.

Blakey, R. C., 2009, Middle Devonian (385Ma): North American Paleogeographic Maps: http://jan.ucc.nau.edu/rcb7/nam.html.

Boyd, C. R., 1881, Resources of southwest Virginia: N. Y., John Wiley & Sons, 321 p.

Brett, C. E., and Ver Straeten, C. A., 1994, Stratigraphy and facies relationships of the Eifelian Onondaga Limestone (Middle Devonian) in western and west central New York State, *in* Brett C.E., and Scatterday J., eds., New York State Geological Association: 66th Annual Meeting Field Trip Guidebook, p. 221-269.

Chance, H. M., 1882, Special survey of the Lehigh water gap, *in* White, I. C., The geology of Pike and Monroe Counties: Pennsylvania Geol. Survey, 2d ser., Bull. G-6, p. 349-363.

Chayes, F., 1956, Petrographic modal analysis: An elementary statistical appraisal: N. Y., John Wiley & Sons, Inc., 113 p.

Clark, G. R., 2003, The chemical characterization of Onondaga chert from the Peace Bridge site (AfGr-9): Implications for the spatial movement of late Archaic lithics in southern Ontario [Master of Arts]: University of Manitoba.

Dennison, J. M., 1961, Stratigraphy of Onesquethaw Stage of Devonian in West Virginia and bordering states: West Virginia Geological Survey Bulletin, v. 22, p. 1-44.

Dickson, J. A. D., 1965, A modified staining technique for staining carbonates in thin section: Nature, v. 205, p. 587.

Dunham, R. J., 1962, Classification of carbonate rocks according to depositional textures, in Ham, W. E., ed., Classification of carbonate rocks: American Association of Petroleum Geologists Memoir 1, p. 108-121.

Dutrow, B. L., and Clark, C. M., 2015, X-ray powder diffraction (XRD): http://serc.carleton.edu/research_education/geochemsheets/techniques/XRD.html (accessed April 2016).

Epstein, J. B., 1971, Geology of the Stroudsburg quadrangle and adjacent areas, Pennsylvania-New Jersey: U.S. Geol. Survey Open-File Report no. 1508, 339 p.

Epstein, J. B., 1984, Onesquethawan stratigraphy (Lower and Middle Devonian) of northeastern Pennsylvania: U.S. Geological Survey Professional Paper 1337, 35 p.

Fettke, C. R., 1952, Tioga bentonite in Pennsylvania and adjacent States: American Association of Petroleum Geologists Bulletin, v. 36, p. 2038-2040.

Fichter, L.S., and Baedke, S.J., 2000, The Devonian Acadian Orogeny and Catskill clastic wedge: Middle to Late Devonian; 380 - 350 mya. The Geological Evolution of Virginia and the Mid-Atlantic Region: http://csmres.jmu.edu/geollab/vageol/vahist/J-MidlatD.html (accessed January, 2016).

Folk, R. L., 1959, Practical petrographic classification of limestones: American Association of Petroleum Geologists Bulletin, v. 43, p. 1-38.

Hall, J., 1839, Third annual report of the fourth geological district of the State of New York: N. Y. Geol. Survey, Third Rept., p. 287-339.

Hearn, P. P., Jr., Sutter, J. F., and Belkin, H. E., 1987, Evidence for Late-Paleozoic brine migration in Cambrian carbonate rocks of the central and southern Appalachians: Implications for Mississippi Valley-type sulfide mineralization: Geochimica et Cosmochimica Acta, v. 51, p. 1323-1334, doi: 10.1016/0016-70378790222-5.

Inners, J. D., 1975, The stratigraphy and paleontology of the Onesquethaw Stage in Pennsylvania and adjacent states [unpublished Ph. D. thesis]: University of Massachusetts, Amherst, Mass., 666 p.

Jarvis, H. W., 1988, INAA characterization of Onondaga chert: A preliminary study in western New York [Master of Arts]: SUNY Buffalo, 75 p.

Kindle, E. M., 1912, The Onondaga fauna of the Allegheny region: U.S. Geological Survey Bulletin, v. 508, 144 p.

Kümmel, H. B., 1940, The geology of New Jersey: Department of Conservation and Development State of New Jersey Geologic Series Bulletin, v. 50, 203 p.

Lewis, J. V., and Kümmel, H. B., 1915, The geology of New Jersey: Geological Survey of New Jersey Bulletin, v. 14, 146 p.

Maliva, R. G., and Siever, R., 1989, Nodular chert formation in carbonate rocks: Journal of Geology, v. 97, no. 4, p. 421-433.

Minnesota Department of Transportation, 2000, Determination of Acid Insoluble Residue in Limestone and Dolostone, Lab Manual 1221: http://www.dot.state.mn.us/materials/manuals/laboratory/1221.pdf (accessed January 2017).

Monteverde, D. H., 1992, Bedrock geologic map of the Sussex County, New Jersey portions of the Culvers Gap and Lake Maskenozha quadrangles: New Jersey Geologic Survey, scale 1:24,000.

Monteverde, D. H., and Epstein, J. B., 2015, Bedrock geologic map of the New Jersey and New York portions of the Milford, Pa-NJ and Port Jervis South, NJ-NY-Pa quadrangles, Sussex County NJ and Orange County NY: New Jersey Geologic Survey unpublished map, scale 1:24,000.

Monteverde, D. H., Epstein, J. B., Herman, G. C., and Witte, R. W., 2015, Bedrock geologic map of the Flatbrookville quadrangle, Sussex and Warren Counties, New Jersey: New Jersey Geologic Survey unpublished map, scale 1:24,000.

Oliver, W. A., Jr., 1954, Stratigraphy of the Onondaga limestone (Devonian) in central New York: Geological Society of America Bulletin, v. 65, p. 621-652.

Oliver, W. A., Jr., 1956, Stratigraphy of the Onondaga Limestone in eastern New York: Geological Society of America Bulletin, v. 67, p. 1441-1474.

Oliver, W. A., Jr., 1966, Clarence Member of the Onondaga Limestone, *in* Changes in Stratigraphic Nomenclature by the U.S. Geological Survey 1965: U.S. Geological Survey Bulletin 1244-A, p. A48-A49.

Ozol, M. A., 1964, Alkalai reactivity of cherts and stratigraphy and petrology of cherts and associated limestones of the Onondaga Formation of central and western New York [unpublished PhD thesis]: Rensselaer Polytechnic Institute, 228 p.

Rehn, E. E., 1942a, Onondaga group of parts of West Virginia and Virginia [unpublished master's thesis]: Ohio State University, 229 p.

Rogers, H. D., 1858, The geology of Pennsylvania: a government survey: Philadelphia, J. B. Lippincott & Co.

USGS., 2016, New Jersey geologic map data: http://mrdata.usgs.gov/geology/state/state.php?state=NJ (accessed February 2016).

USGS., 2016, Onondaga Limestone: http://mrdata.usgs.gov/geology/state/sgmc-unit.php?unit=NYDon;2 (accessed February 2016).

Vanuxem, J., 1839, Third annual report of the geological survey of the third district: New York Geol. Survey Annual Report 3, p. 241-285.

Ver Straeten, C. A., 1996, Upper Lower and lower Middle Devonian stratigraphic synthesis, central Appalachian Basin of Pennsylvania: Pennsylvania Topographic and Geological Survey Open File Report 96-47, 59 p.

Ver Straeten, C. A., 2001, Event and sequence stratigraphy and a new synthesis of the Lower to Middle Devonian, eastern Pennsylvania and adjacent areas, *in* J.D. Inners and G.M. Fleeger, eds., 66th Annual Field Conference of Pennsylvania Geologists: 2001: A Delaware River Odyssey, p. 35-53.

Ver Straeten, C. A., and Brett, C. E., 2006, Pragian to Eifelian strata (middle Lower to lower Middle Devonian), northern Appalachian Basin – Stratigraphic nomenclatural changes: Northeastern Geology & Environmental Sciences, v. 28, no. 1, p. 80-95.

Welton, J. E., 1984, SEM Petrology Atlas: Tulsa, Oklahoma, The American Association of Petroleum Geologists, Methods in Exploration Series, No. 4, 235 p.

Willard, B., 1936, The Onondaga Formation in Pennsylvania: The Journal of Geology, v. 44, no. 5, p. 578-603.

Wirth, K., and Barth, A., 2015, X-ray fluorescence (XRF): http://serc.carleton.edu/research_education/geochemsheets/techniques/XRF.html (accessed April 2016).

Witte, R. W., and Monteverde, D. H., 2006, Karst in the Delaware Water Gap National Recreation Area: Unearthing New Jersey, v. 2, no. 1, p. 1-6.

Woodward, H. P., 1943, Devonian system of West Virginia: West Virginia Geol. Survey, v. 15, 655 p.

Appendix A: Site Thickness Calculations

Site #	Dip of rocks	Elevation of base contact (ft.)	Elevation of upper contact (ft.)	Site elevation (ft.)	Site Distance from base of formation (ft.)	Site Distance from base after topography factored in (ft.)	True Site dist. from base of formation (ft.)
1	25° NNW	420	407	445	200	253.6	**107.2**
2	15° WNW	770	375	465	3350		**396.0**
3	11° NW	660	550	520	2400	1679.8	**320.5**
4	14° WNW	660	395				
5	16° W	650	418	560	1620	1306.1	**360.0**
6	16° W	650	418	540	1900	1516.4	**418.0**
7	16° W	640	415	520	2020	1601.5	**441.4**
8	14° W	650	408	550	1960	1558.9	**377.1**
9	16° NW	620	325	325	1620		**260.0**
10	13° NW	440	330				
11	30° NNW	600	330	380	520	138.9	**69.5**
12	25° NNW	532	335	385	380	64.8	**27.4**
13	35° NNW	540	355	350	580	308.7	**177.0**

Table A1: Calculations of the thickness of the Onondaga Formation at each site location along with where each site was located within that thickness. All site thicknesses were calculated from the lower contact. Sites 4 and 10 were float samples and their location could not be calculated within the thickness. Sites 2 and 9 had varying dips along the formation thickness and could not be calculated from a single dip. In this case, formation thickness and site location had to be calculated by hand on a geologic cross-section and entered separately. The average thickness and where each site plotted on that thickness with reference to each other was then calculated to construct a vertical cross-section to show site location with respect to one another.

Map thickness of formation (ft.)	Map thickness after topography factored in (ft.)	True thickness of formation (ft.)	Site location in average thickness (ft.)
1240	1212.1	**512.3**	86.46
3960		**440.0**	371.91
2160	1594.1	**304.2**	435.44
2840	1777.1	**429.9**	
2600	1790.9	**493.6**	301.38
2600	1790.9	**493.6**	349.89
2600	1815.3	**500.4**	364.56
2640	1669.4	**403.9**	385.89
1800		**300.0**	358.14
1980	1503.5	**338.2**	
1300	832.3	**416.2**	68.98
1500	1077.5	**455.4**	24.83
760	495.8	**284.4**	257.26
	Average thickness:	**413.2**	

Table A1: Continued...

Appendix B: Outcrop and Hand Specimen Descriptions from each Site Location

Site 1- (41°20’24.69” N, 74°43’47.16” W) A dark gray limestone, fine grained, medium to light gray weathering, black chert nodules present in limestone ~1-1.5 in. wide by 1 in. thick with some chert nodules up to 2 in. wide. Bedding planes in limestone ranging from 4-8 in. thick. Chert nodules seem to follow bedding planes. Outcrop at least 4 ft. thick. One hand specimen collected. (Figure B1-A)

Site 2- (41°17’13.93” N, 74°48’56.35” W) A dark gray limestone, fine grained, medium olive-gray to brown-gray weathering, black chert nodules present ~0.5 to 2 in. wide. Outcrop is ~2 ft. thick, but mostly covered by moss. Four hand specimens collected. (Figure B1-B)

Site 3- (41°14’21.57” N, 74°50’48.15” W) Dark gray limestone, fine to medium grained, light gray, olive-gray to brown-gray weathering, black chert nodules as large as ~3-4 in. across. Chert shows no orientation. Massive bedding is ~2 ft. thick and outcrop is ~10 ft. thick. One hand specimen collected. (Figure B1-C)

Figure B1: A) Site 1 outcrop. B) Site 2 outcrop. C) Site 3 outcrop.

Site 4- (41°13’13.97” N, 74°51’21.68” W) Float samples collected from stream bed. A dark gray limestone, fine grained, light gray to brown-gray weathering, with possible black chert lenses. Transitional contact between the chert and limestone. One hand specimen collected.

Site 5- (41°13’31.14” N, 74°51’00.93” W) A light orange-brown-gray limestone, fine grained, gray-orange-brown weathering, with black chert nodules ~1 in. across. Outcrop is ~3 ft. thick. One hand specimen collected.

Site 6- (41°13’29.64” N, 74°51’06.74” W) A dark gray limestone, fine grained, medium olive-gray weathering, with no visible chert present. Mollusk shell found in hand specimen ~5 mm long and most likely a bivalve. Outcrop is ~3 ft. thick. One hand specimen collected.

Site 7- (41°13’28.25” N, 74°51’10.69” W) A dark gray limestone, fine grained, medium olive-gray weathering, black chert nodules present ~0.5-1 in. across, and a few thin, wavy mud-like layers visible. Outcrop is ~3 ft. thick. One hand specimen collected.

(The trend from Sites 5-7 shows an increase in very thin limestone and mud-like beds.)

Figure B2: A) Site 8 outcrop. B) Site 9 outcrop. C) Site 11 outcrop.

Site 8- (41°13’19.27” N, 74°51’17.43” W) A dark gray limestone, fine grained, light gray weathering. Large black chert nodules up to ~3 in. across and showing no orientation. Some chert lenses as well. Most of the chert nodules show a sharp contact with the surrounding limestone, but a few exhibit a sharp contact toward the base of the nodule with a gradational contact toward the top. Some chert nodules also have black lines branching off of them and appearing to be the same composition as the chert. Both a crinoid and bivalve shell found in hand specimen ~4 mm and ~5 mm across. Bedding

layers are ~5-10 in. thick and outcrop is ~13 ft. thick. Seven hand specimens collected. (Figure B2-A)

Site 9- (41°09'13.13" N, 74°54'23.47" W) A dark gray limestone, fine grained, light to medium gray weathering with large lighter gray limestone nodules eroding away faster. Light gray limestone nodules as long as 1 ft. by 5 in. Residue rims of darker material on the edge of lighter limestone nodules. Black chert nodules present in the darker limestone host rock ~1 in. long. Burrows found in lighter limestone nodules and some brachiopod shells visible at outcrop. Outcrop thickness could not be measured along the river's edge. Two hand specimens collected. (Figure B2-B)

Site 10- (41°08'52.62" N, 74°54'43.76" W) Float samples collected on hillside. A medium gray limestone, fine grained, light brown-gray weathering, with possible black chert lenses. Transitional contact between the chert and limestone. Three hand specimens collected.

Site 11- (41°07'57.71" N, 74°55'40.31" W) A medium gray limestone, fine grained, light gray to brown-gray weathering. No chert visible in outcrop. Massive beds present from 0.5-1.5 ft. thick. Outcrop is ~10-15 ft. thick which increases to ~20 ft. thick towards the South. One hand specimen collected. (Figure B2-C)

Site 12- (41°07'40.85" N, 74°56'13.70" W) A medium-dark gray limestone, fine grained, light brown-gray weathering. No chert visible in outcrop. One hand specimen collected.

Site 13- (41°07'23.67" N, 74°56'50.55" W) A dark gray limestone, fine grained, medium brown-gray to gray weathering. No visible chert. A pyrite filled burrow present in hand specimen ~3 in. long. Outcrop thickness could not be measured along the river's edge. One hand specimen collected.

Appendix C: Raw Point Count Data and Percentages

Sample #	Micrite	Ferroan Sparite	Non-ferroan Sparite	Non-Carbonate Mud	Fossils	Ferroan Dolomite	Non-ferroan Dolomite	Microcrystalline Silica	Pores	Other	Total
1-a-1	165	0	3	36	2	3	2	89	0	0	300
1-a-2	253	2	4	20	2	0	7	12	0	0	300
2-a-1	85	0	0	102	0	2	2	82	0	27	300
2-b-1	110	1	0	92	3	1	4	77	3	9	300
2-c-1	164	0	0	101	3	0	1	24	3	4	300
2-d-1	74	0	0	94	0	1	1	124	0	6	300
3-a-1	84	1	1	26	2	1	4	175	0	6	300
3-a-2	180	1	0	50	10	0	0	55	0	4	300
3-a-3	162	0	1	84	4	0	1	44	0	4	300
3-a-4	227	3	28	24	12	0	0	0	2	4	300
4-a-1	82	0	0	129	0	0	0	5	0	84	300
5-a-1	31	0	0	110	2	0	3	145	5	4	300
6-a-1	124	0	0	154	19	0	0	0	1	2	300
7-a-1	60	0	0	152	4	3	2	68	0	11	300
8-a-1	60	0	0	105	0	0	4	125	1	5	300
8-b-1	85	1	0	84	1	0	6	120	1	2	300
8-c-1	86	1	2	102	1	0	7	98	0	3	300
8-d-1	107	0	3	161	0	0	1	9	0	19	300
8-e-1	30	0	4	150	2	0	5	107	0	2	300
8-e-2	74	0	0	89	0	0	4	131	0	2	300
8-f-1	10	0	0	43	2	0	5	234	1	5	300
8-g-1	36	0	0	145	0	0	3	112	0	4	300
9-a-1	15	29	5	99	2	8	8	128	5	1	300
9-b-1	7	11	6	52	8	3	1	203	2	7	300
9-b-2	18	8	3	113	4	7	7	89	5	46	300
10-b-1	23	11	2	220	4	0	2	22	3	13	300
11-a-1	164	0	0	123	1	0	0	0	0	12	300
12-a-1	168	0	1	126	5	0	0	0	0	0	300
13-a-1	37	2	0	234	2	0	0	17	0	8	300

Table C1: Raw Point Count Data.

Sample #	Micrite	Ferroan Sparite	Non-ferroan Sparite	Non-Carbonate Mud	Fossils	Ferroan Dolomite	Non-ferroan Dolomite	Microcrystalline Silica	Pores	Other	Total
1-a-1	55.0%	0.0%	1.0%	12.0%	0.7%	1.0%	0.7%	29.7%	0.0%	0.0%	100%
1-a-2	84.3%	0.7%	1.3%	6.7%	0.7%	0.0%	2.3%	4.0%	0.0%	0.0%	100%
2-a-1	28.3%	0.0%	0.0%	34.0%	0.0%	0.7%	0.7%	27.3%	0.0%	9.0%	100%
2-b-1	36.7%	0.3%	0.0%	30.7%	1.0%	0.3%	1.3%	25.7%	1.0%	3.0%	100%
2-c-1	54.7%	0.0%	0.0%	33.7%	1.0%	0.0%	0.3%	8.0%	1.0%	1.3%	100%
2-d-1	24.7%	0.0%	0.0%	31.3%	0.0%	0.3%	0.3%	41.3%	0.0%	2.0%	100%
3-a-1	28.0%	0.3%	0.3%	8.7%	0.7%	0.3%	1.3%	58.3%	0.0%	2.0%	100%
3-a-2	60.0%	0.3%	0.0%	16.7%	3.3%	0.0%	0.0%	18.3%	0.0%	1.3%	100%
3-a-3	54.0%	0.0%	0.3%	28.0%	1.3%	0.0%	0.3%	14.7%	0.0%	1.3%	100%
3-a-4	75.7%	1.0%	9.3%	8.0%	4.0%	0.0%	0.0%	0.0%	0.7%	1.3%	100%
4-a-1	27.3%	0.0%	0.0%	43.0%	0.0%	0.0%	0.0%	1.7%	0.0%	28.0%	100%
5-a-1	10.3%	0.0%	0.0%	36.7%	0.7%	0.0%	1.0%	48.3%	1.7%	1.3%	100%
6-a-1	41.3%	0.0%	0.0%	51.3%	6.3%	0.0%	0.0%	0.0%	0.3%	0.7%	100%
7-a-1	20.0%	0.0%	0.0%	50.7%	1.3%	1.0%	0.7%	22.7%	0.0%	3.7%	100%
8-a-1	20.0%	0.0%	0.0%	35.0%	0.0%	0.0%	1.3%	41.7%	0.3%	1.7%	100%
8-b-1	28.3%	0.3%	0.0%	28.0%	0.3%	0.0%	2.0%	40.0%	0.3%	0.7%	100%
8-c-1	28.7%	0.3%	0.7%	34.0%	0.3%	0.0%	2.3%	32.7%	0.0%	1.0%	100%
8-d-1	35.7%	0.0%	1.0%	53.7%	0.0%	0.0%	0.3%	3.0%	0.0%	6.3%	100%
8-e-1	10.0%	0.0%	1.3%	50.0%	0.7%	0.0%	1.7%	35.7%	0.0%	0.7%	100%
8-e-2	24.7%	0.0%	0.0%	29.7%	0.0%	0.0%	1.3%	43.7%	0.0%	0.7%	100%
8-f-1	3.3%	0.0%	0.0%	14.3%	0.7%	0.0%	1.7%	78.0%	0.3%	1.7%	100%
8-g-1	12.0%	0.0%	0.0%	48.3%	0.0%	0.0%	1.0%	37.3%	0.0%	1.3%	100%
9-a-1	5.0%	9.7%	1.7%	33.0%	0.7%	2.7%	2.7%	42.7%	1.7%	0.3%	100%
9-b-1	2.3%	3.7%	2.0%	17.3%	2.7%	1.0%	0.3%	67.7%	0.7%	2.3%	100%
9-b-2	6.0%	2.7%	1.0%	37.7%	1.3%	2.3%	2.3%	29.7%	1.7%	15.3%	100%
10-b-1	7.7%	3.7%	0.7%	73.3%	1.3%	0.0%	0.7%	7.3%	1.0%	4.3%	100%
11-a-1	54.7%	0.0%	0.0%	41.0%	0.3%	0.0%	0.0%	0.0%	0.0%	4.0%	100%
12-a-1	56.0%	0.0%	0.3%	42.0%	1.7%	0.0%	0.0%	0.0%	0.0%	0.0%	100%
13-a-1	12.3%	0.7%	0.0%	78.0%	0.7%	0.0%	0.0%	5.7%	0.0%	2.7%	100%

Table C2: Percentages of constituents.

Appendix D: List of Fossils and Other Constituents

Sample #	Sponge Spicules	Mollusks	Brachiopods	Bryozoans	Echinoderms	Ostracods
1-a-1		I			I	
1-a-2	?	I			I	
2-a-1		I				?
2-b-1		I				I
2-c-1	I	I				?
2-d-1	?	I				
3-a-1	?	I				
3-a-2	?	I				
3-a-3	?	I				
3-a-4	I	I				
5-a-1	?	?				
6-a-1		I	I	I	I	
7-a-1	I	I				
8-a-1		I				?
8-b-1		I			I	
8-c-1		I	I		I	
8-d-1	?	?				
8-e-1	I	I			I	
8-e-2	?	I			I	
8-f-1		I				
8-g-1		I	I			
9-a-1		I	I	I	?	
9-b-1	I	I			?	?
9-b-2	I	I				
10-b-1	I	I		?		
11-a-1		I			I	I
12-a-1	I	I				
13-a-1	I	I				

Table D1: List of fossils in each thin section.

Sample #	Fractures filled in with							Opaque grains	Intraclasts	Styolites	Iron staining	Authigenic feldspar	Burrow
	Silica	Fe-Sparite	Non-Fe Sparite	Iron staining	Pore space	Fe-Dolomite	None						
2-a-1		I		I				I					
2-b-1	I				I			I					
2-c-1								I			I		
2-d-1				I				I					
3-a-1	I			I				I			I		
3-a-2							I	I			I		
3-a-3							I	I		I			
3-a-4								I			I		
4-a-1							I	I	I				
5-a-1	I						I						
6-a-1								I		I	I	I	
7-a-1						I							I
8-a-1			I					I					
8-b-1							I	I					
8-c-1								I					
8-d-1			I		I								
8-e-1											I		
8-e-2			I		I			I					
8-f-1								I					
8-g-1							I	I					
9-a-1								I					
9-b-1							I	I					
9-b-2								I	I	I	I		
10-b-1								I		I	I		
11-a-1								I		I	I		
13-a-1								I					

Table D2: List of other constituents in each thin section.

Appendix E: Insoluble Residue Analysis Results

Site #	Weight Initial (g) (sample + weighboat)	Sample Weight Initial (g)	Weight Weighboat (g)	Weight Filter Paper (g)	Weight Final (g) (sample + filter paper + weighboat)	Sample Weight Final (g)	Percent Insoluble Residue (%)	
1	76.74	71.05	5.69	0.77	19.19	12.73	17.9	√
2	71.07	65.30	5.77	1.03	47.39	40.59	62.2	√
3	65.59	59.95	5.64	1.04	7.56	6.09	10.2	√
3a*			5.73	1.05	11.99			
4	59.98	54.32	5.66	1.02	48.32	41.64	76.7	
5	35.18	29.50	5.68	1.04	33.99	27.27	92.4	√
6	52.97	47.23	5.74	1.07	28.24	21.43	45.4	
7	54.93	49.16	5.77	1.02	29.40	22.61	46.0	√
8	58.80	52.93	5.87	1.07	7.25	32.95	62.3	√
8a*			5.72	1.10	39.46			
9	49.21	43.39	5.82	1.04	39.71	32.85	75.7	√
10	76.69	70.79	5.90	1.06	7.62	53.15	75.1	
10a*			5.68	1.06	59.23			
11	69.78	63.92	5.86	1.05	26.23	19.32	30.2	
12	49.85	44.07	5.78	1.04	25.73	18.91	42.9	
13	54.48	48.73	5.75	1.01	32.41	25.65	52.6	

*2nd weighboat and filter paper was needed because 1st filter paper ripped

Check marks indicated samples where chert nodules were present in hand specimen.

Table E1: Insoluble Residue Analysis Results.

Appendix F: X-Ray Diffraction Analysis (XRD) Results

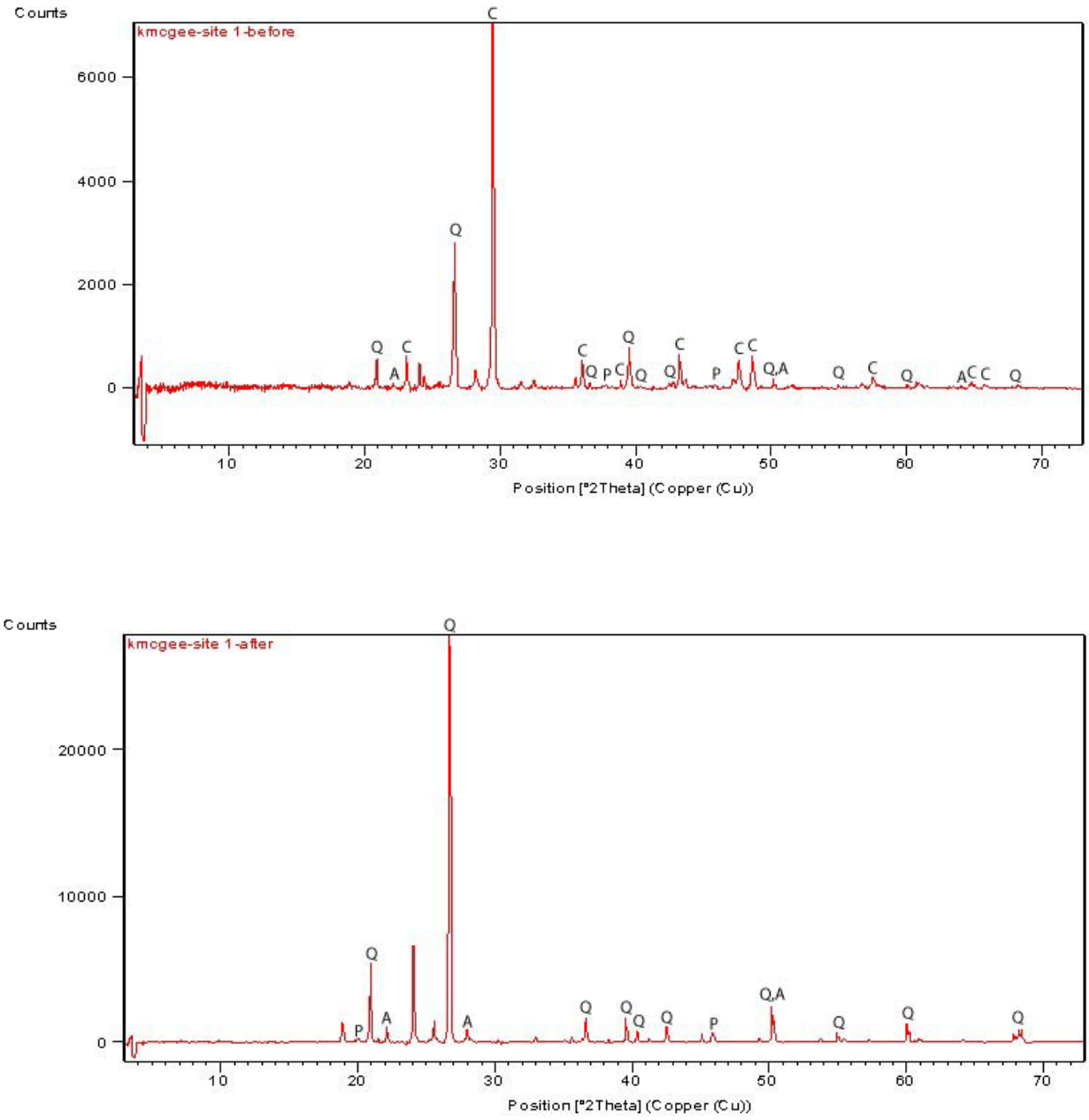

Figure F1: XRD analysis of site 1 before and after insoluble residue analysis. C-Calcite, Q-Quartz, A-Alkali feldspar, and P-Phyllosilicate.

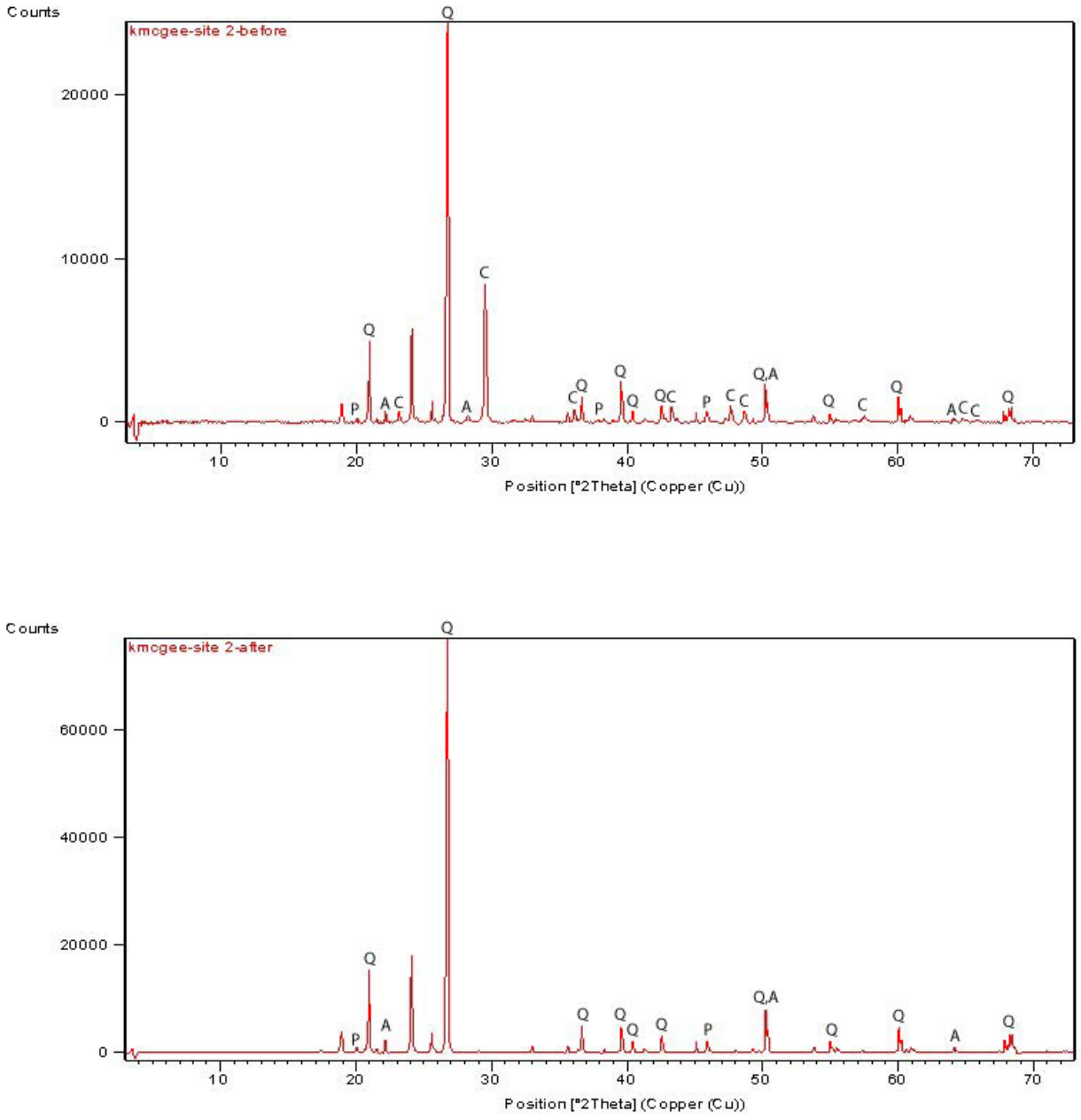

Figure F2: XRD analysis of site 2 before and after insoluble residue analysis. C-Calcite, Q-Quartz, A-Alkali feldspar, and P-Phyllosilicate.

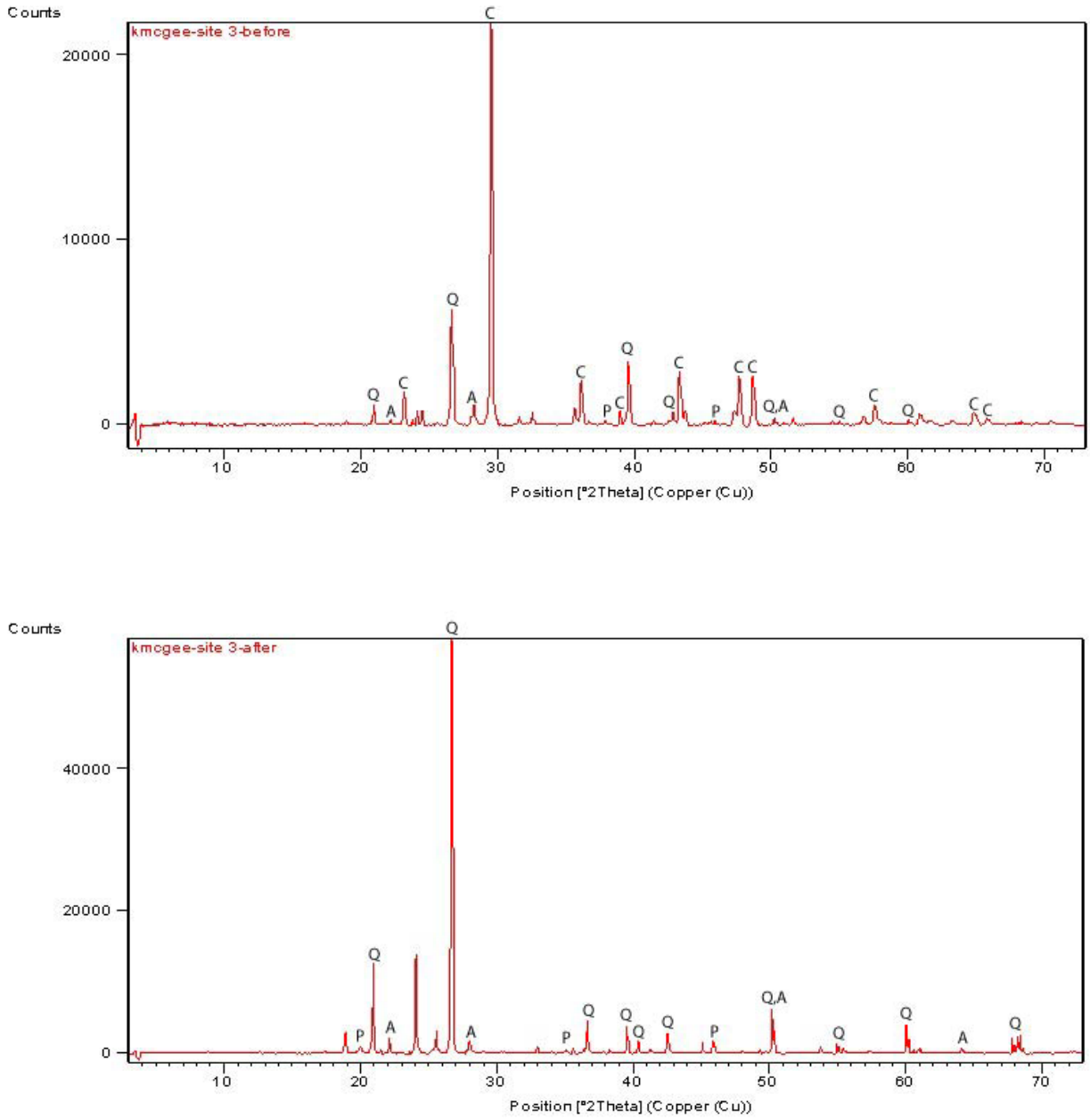

Figure F3: XRD analysis of site 3 before and after insoluble residue analysis. C-Calcite, Q-Quartz, A-Alkali feldspar, and P-Phyllosilicate.

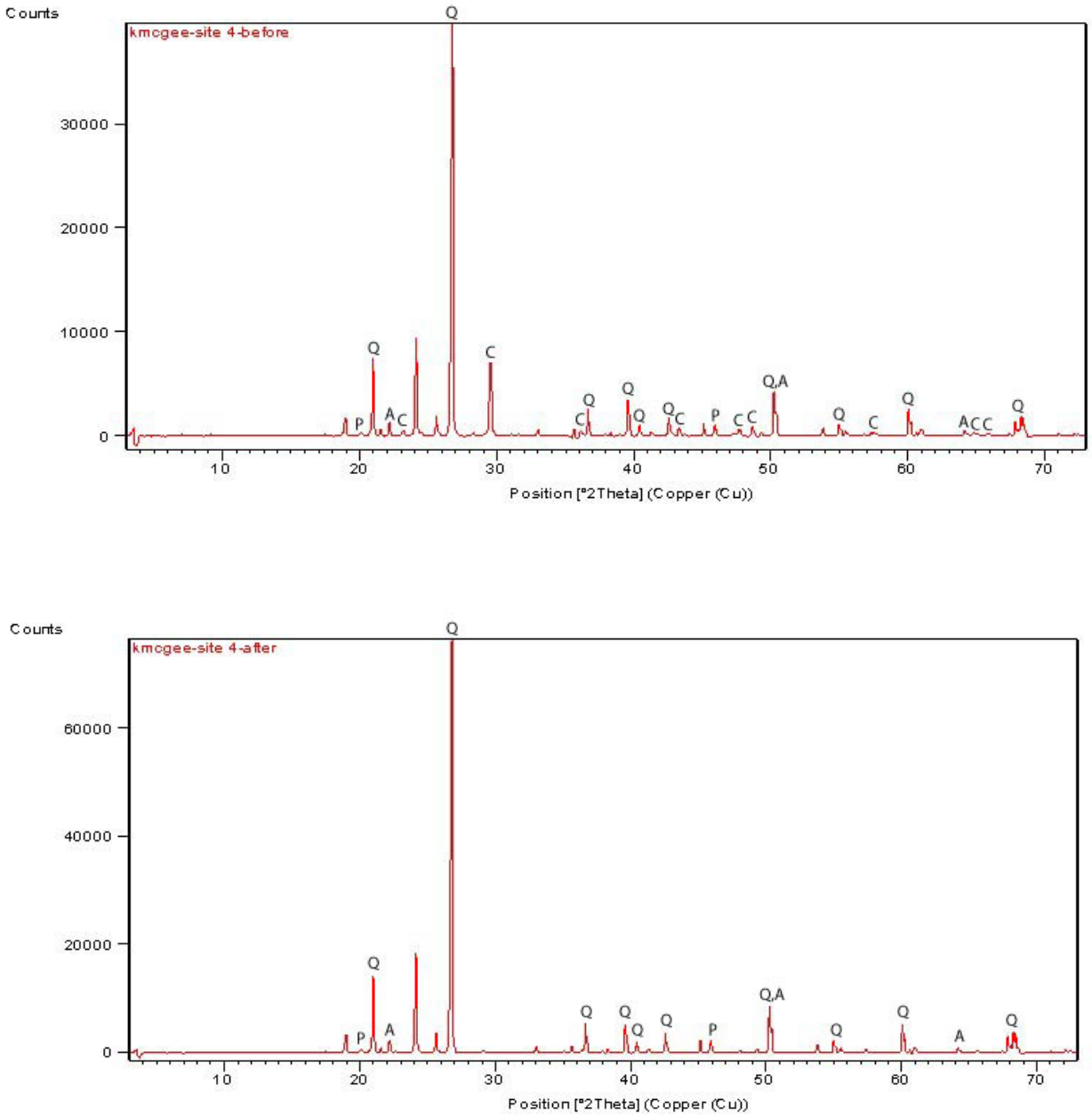

Figure F4: XRD analysis of site 4 before and after insoluble residue analysis. C-Calcite, Q-Quartz, A-Alkali feldspar, and P-Phyllosilicate.

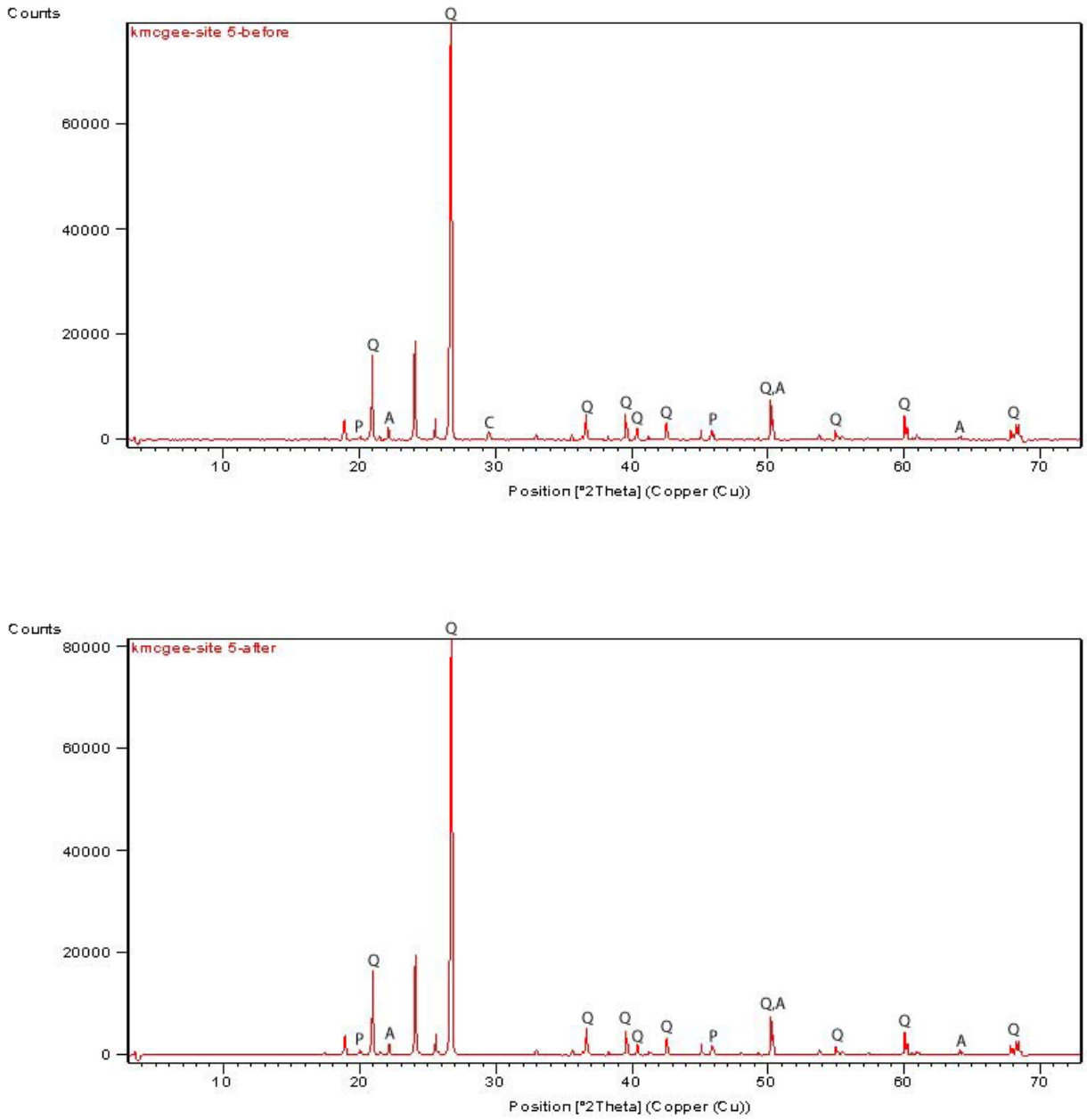

Figure F5: XRD analysis of site 5 before and after insoluble residue analysis. C-Calcite, Q-Quartz, A-Alkali feldspar, and P-Phyllosilicate.

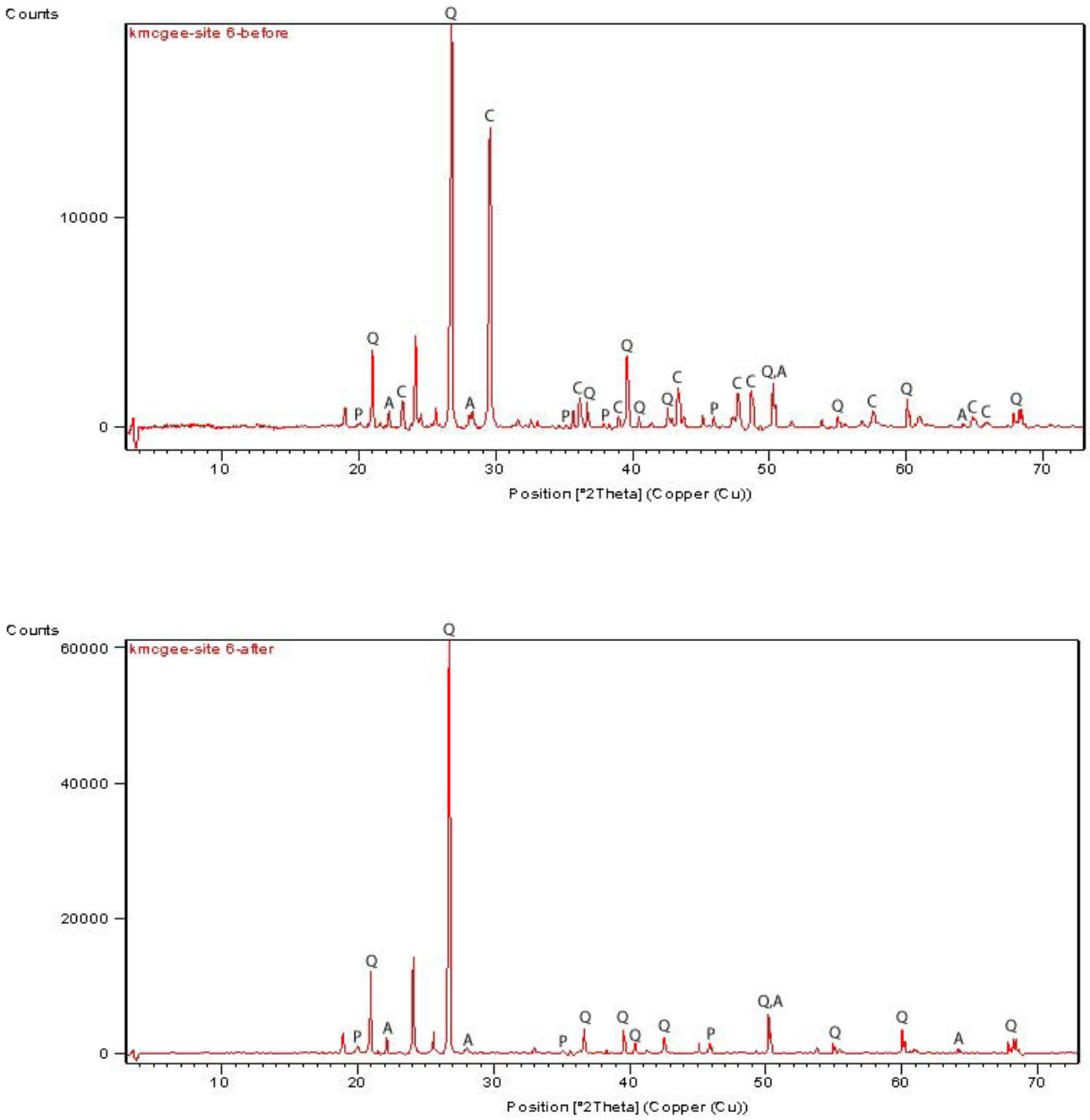

Figure F6: XRD analysis of site 6 before and after insoluble residue analysis. C-Calcite, Q-Quartz, A-Alkali feldspar, and P-Phyllosilicate.

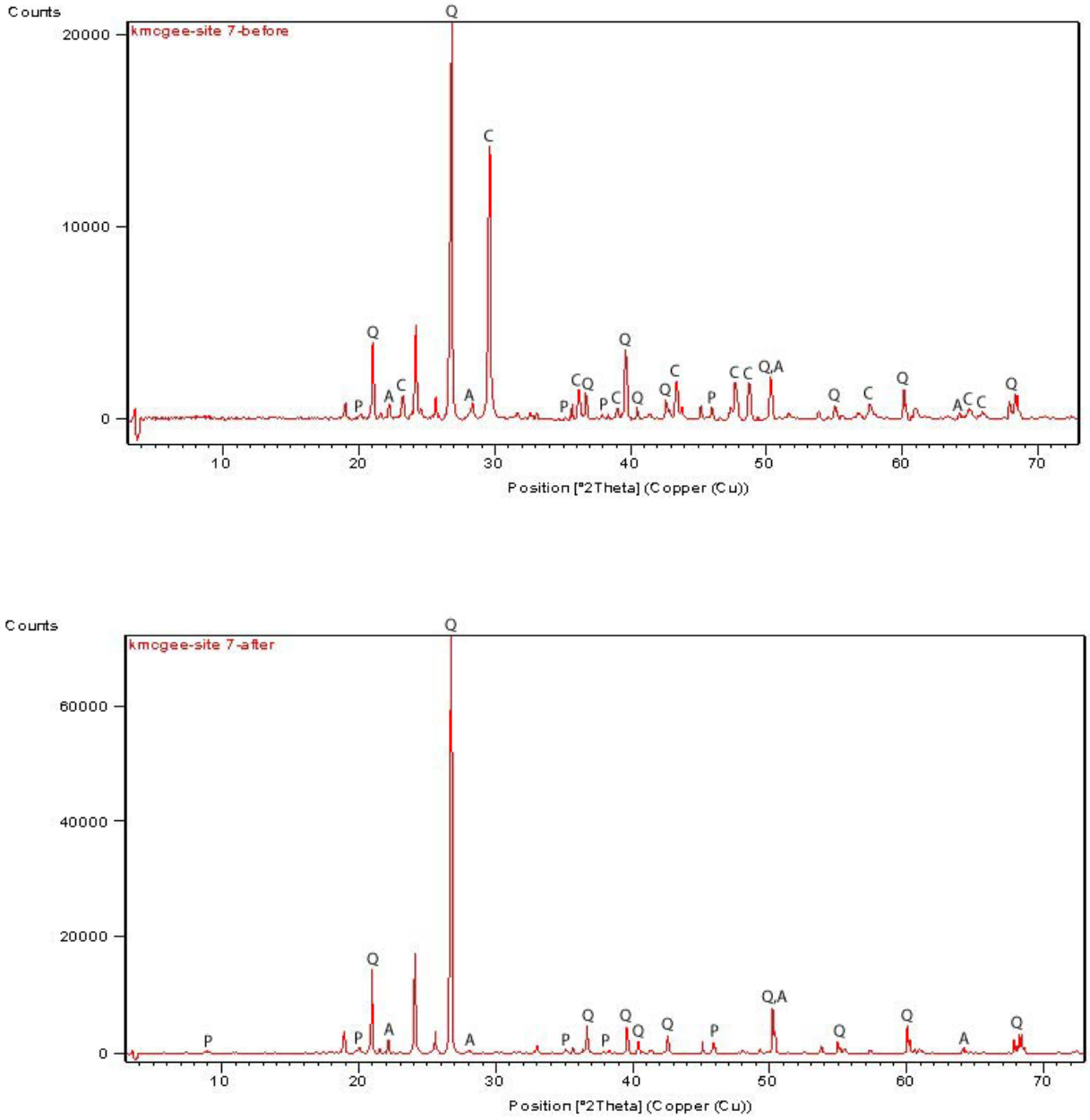

Figure F7: XRD analysis of site 7 before and after insoluble residue analysis. C-Calcite, Q-Quartz, A-Alkali feldspar, and P-Phyllosilicate.

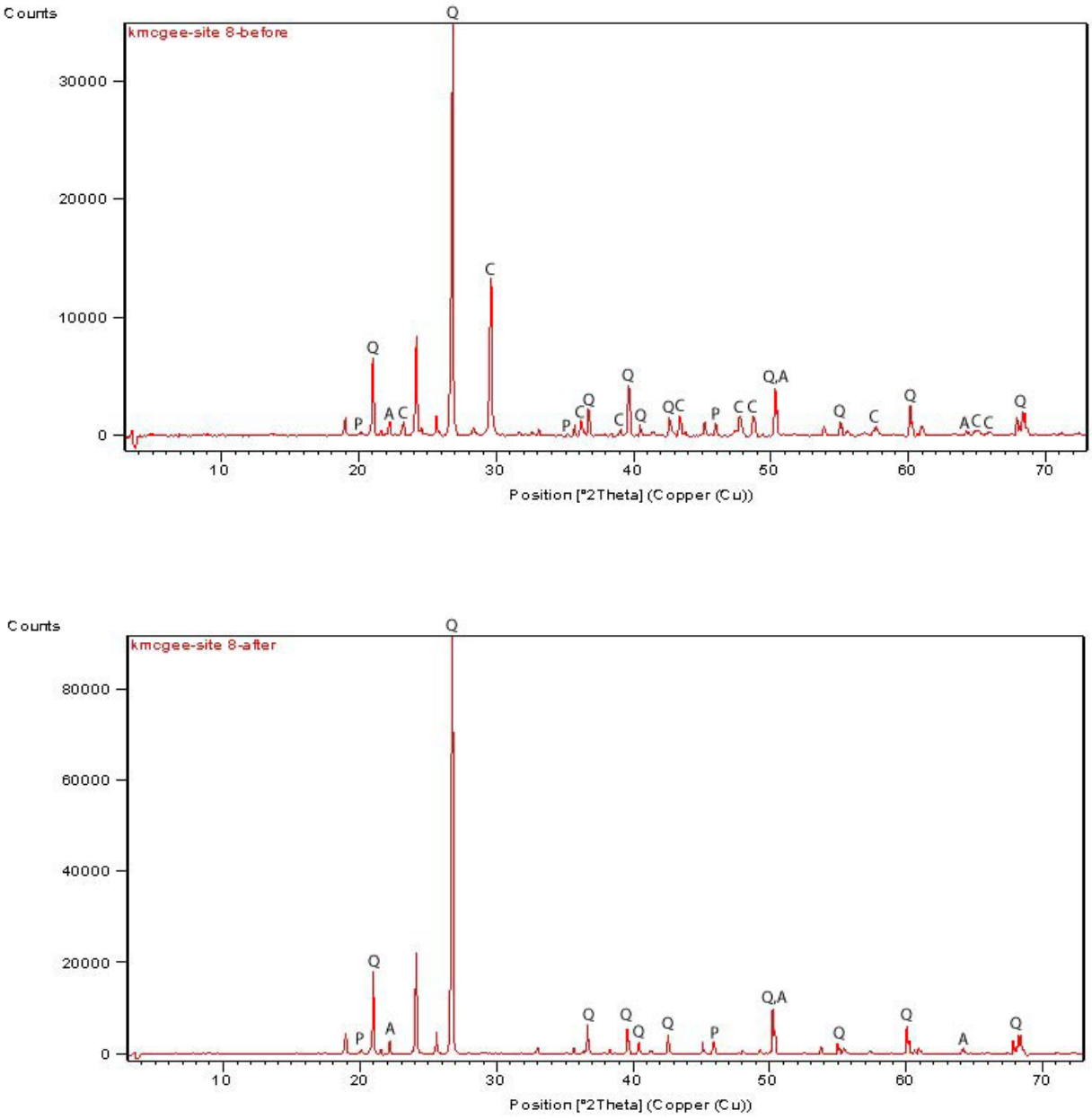

Figure F8: XRD analysis of site 8 before and after insoluble residue analysis. C-Calcite, Q-Quartz, A-Alkali feldspar, and P-Phyllosilicate.

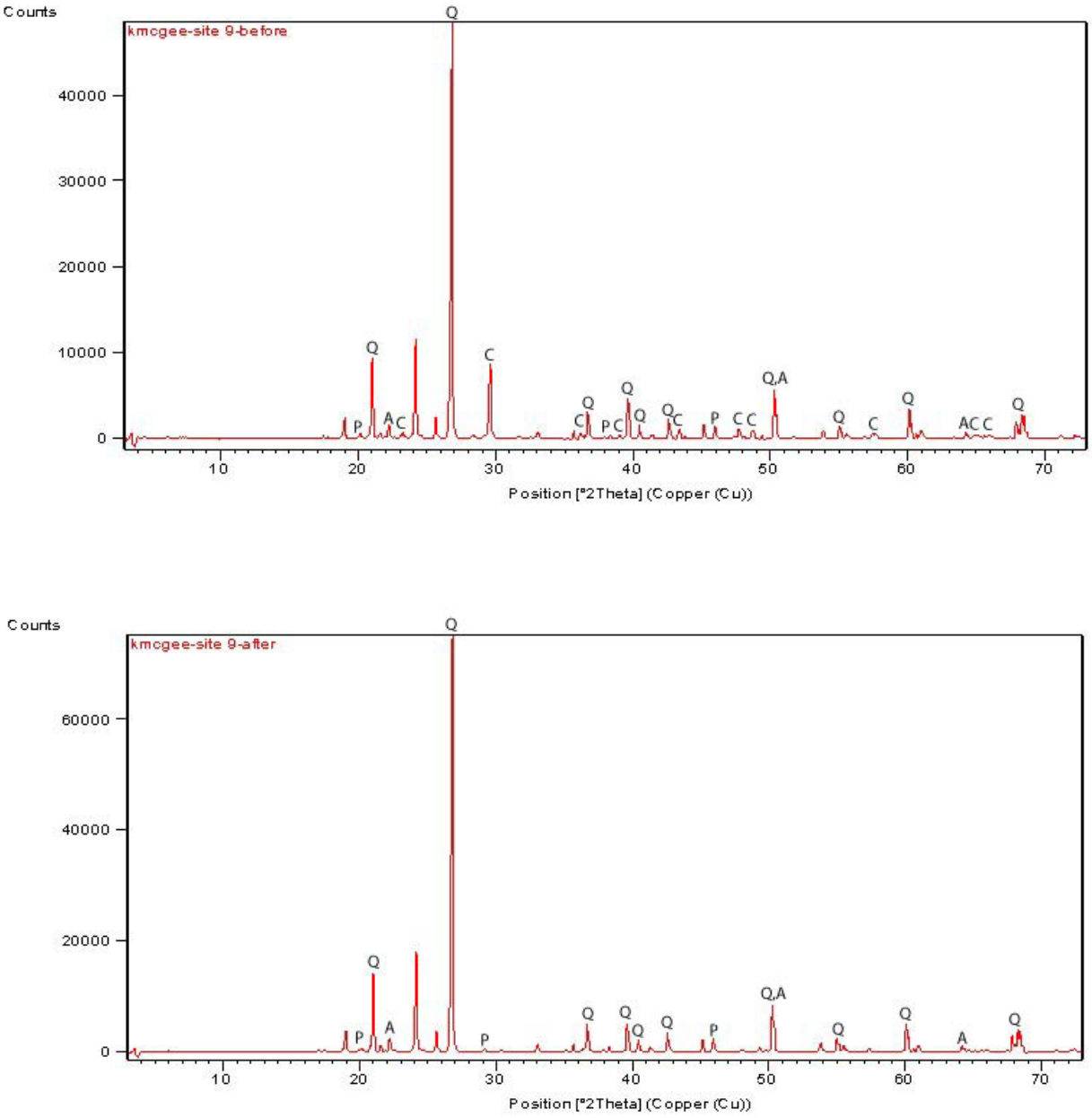

Figure F9: XRD analysis of site 9 before and after insoluble residue analysis. C-Calcite, Q-Quartz, A-Alkali feldspar, and P-Phyllosilicate.

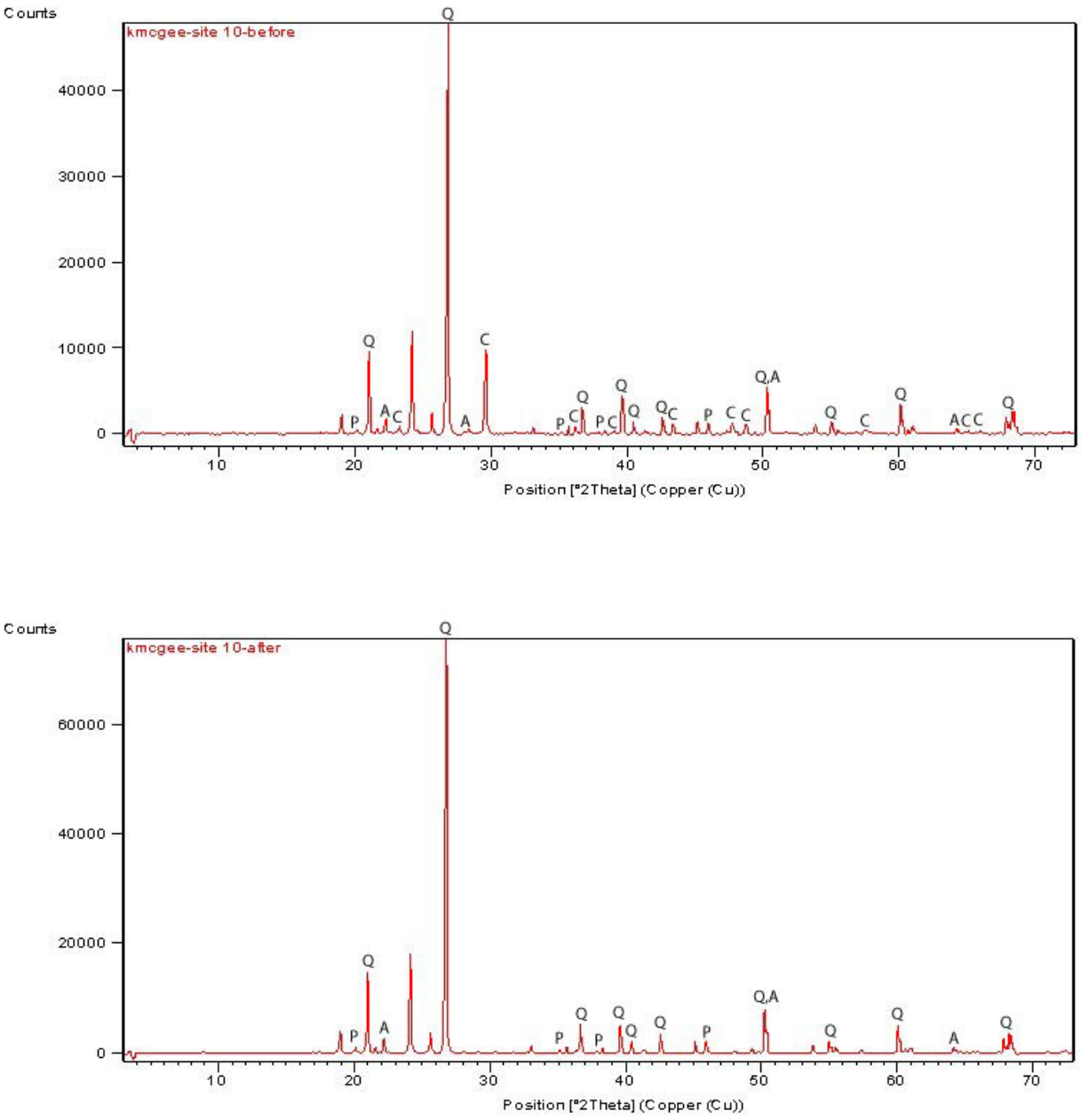

Figure F10: XRD analysis of site 10 before and after insoluble residue analysis. C-Calcite, Q-Quartz, A-Alkali feldspar, and P-Phyllosilicate.

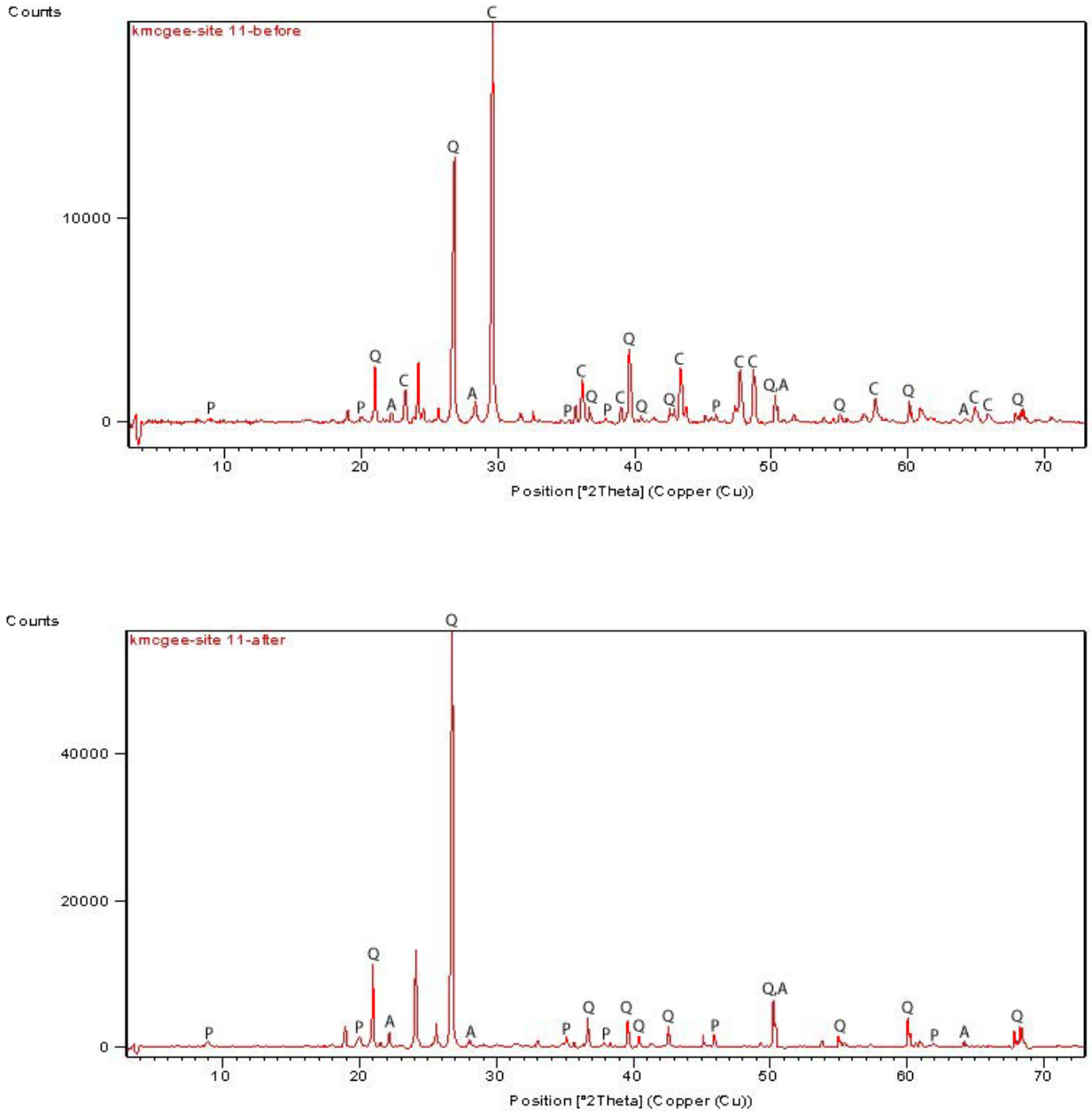

Figure F11: XRD analysis of site 11 before and after insoluble residue analysis. C-Calcite, Q-Quartz, A-Alkali feldspar, and P-Phyllosilicate.

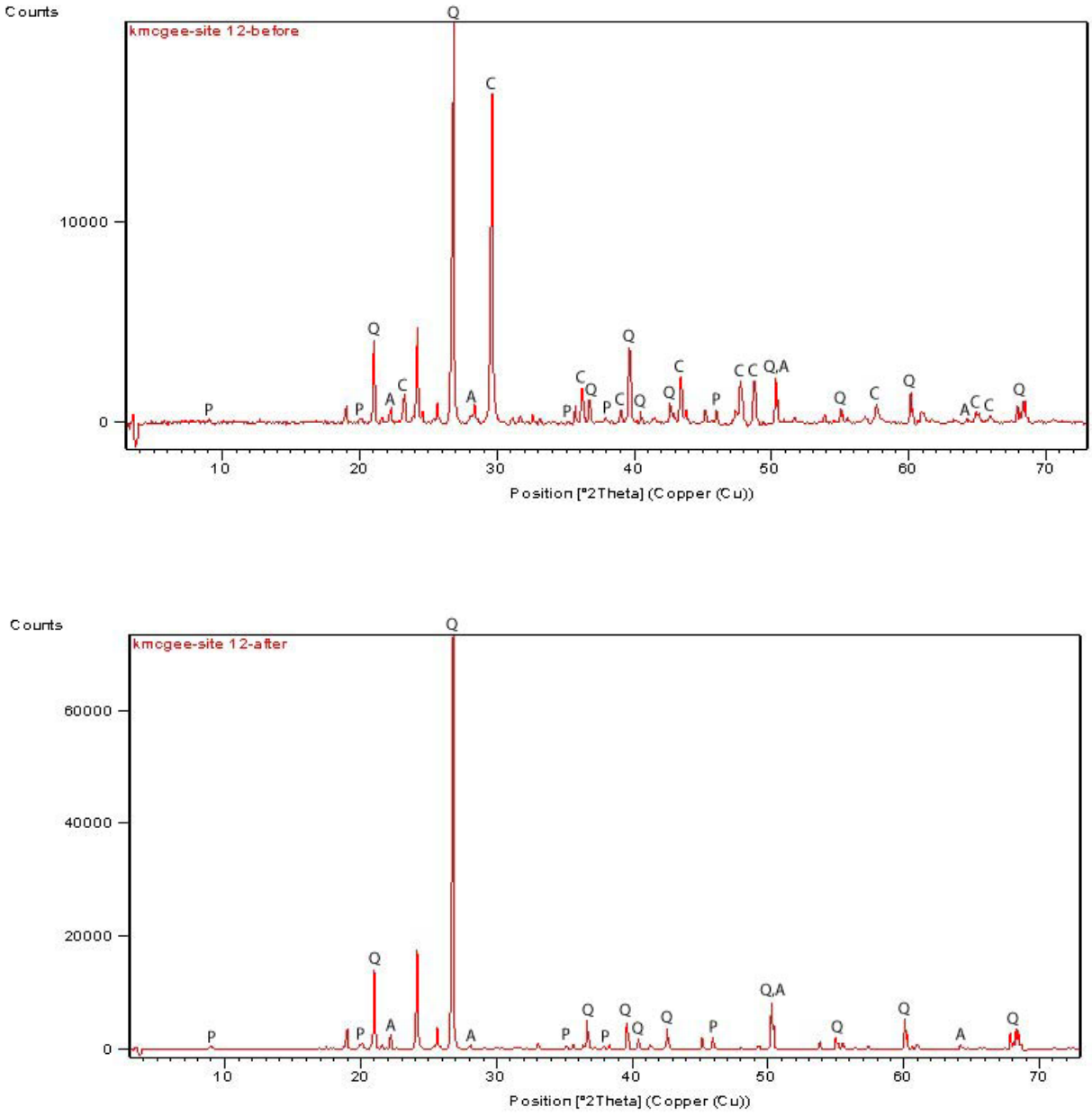

Figure F12: XRD analysis of site 12 before and after insoluble residue analysis. C-Calcite, Q-Quartz, A-Alkali feldspar, and P-Phyllosilicate.

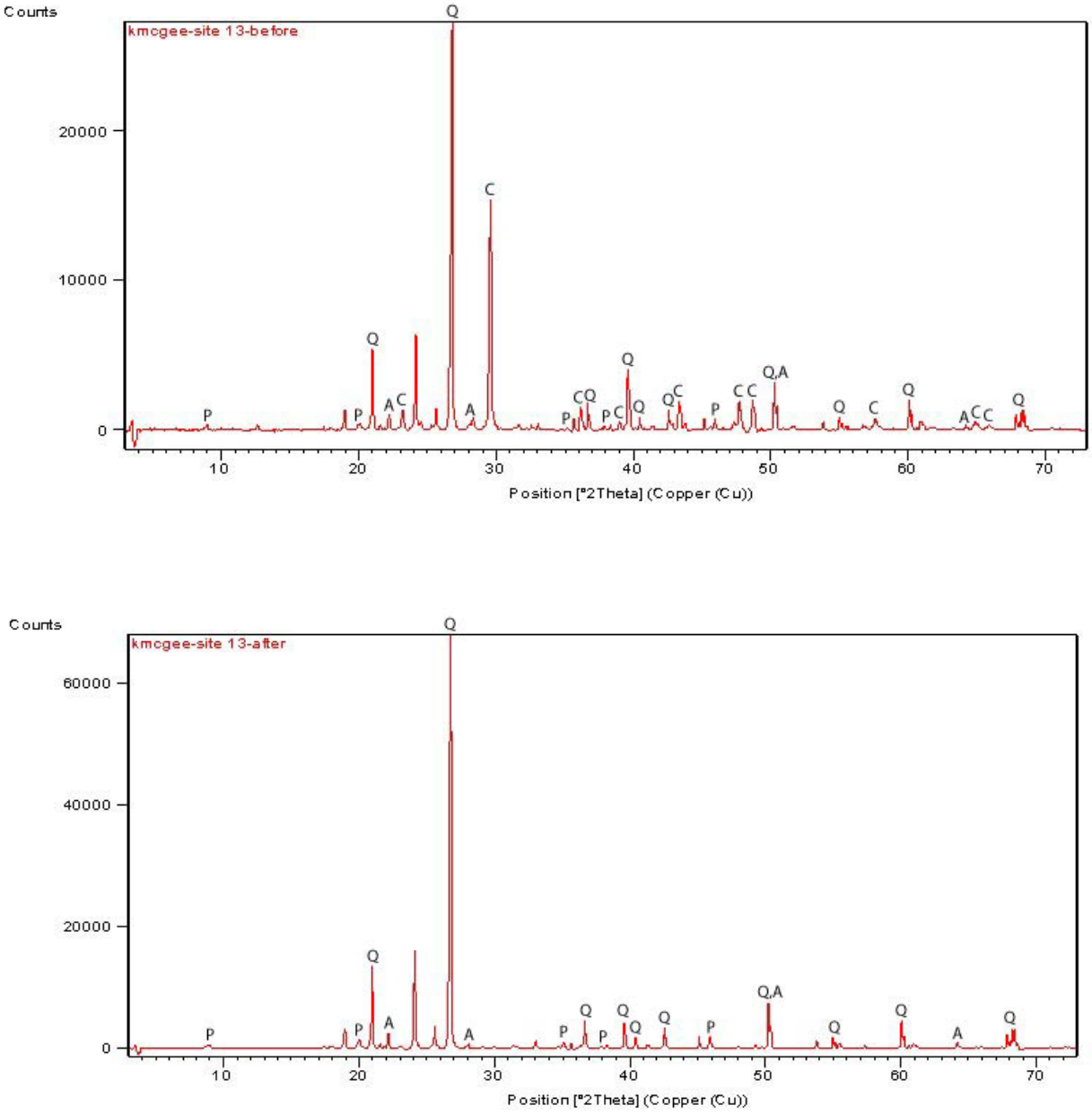

Figure F13: XRD analysis of site 13 before and after insoluble residue analysis. C-Calcite, Q-Quartz, A-Alkali feldspar, and P-Phyllosilicate.

Appendix G: Scanning Electron Microscopy/Energy Dispersive X-Ray Microanalysis (SEM-EDS) Results

Site #	Report	Mineral	Si	O	Al	K	Mg	Fe	Na	Ti	C	Ca	S	Cl	Ba	Total
1	>180um-3:2	Illite/chert	30.64	60.18	4.96	2.45	1.19	0.59								100.0
3	180-150um-1:4	Illite	28.13	52.16	12.22	4.89	0.57	1.17	0.66	0.19						100.0
3	180-150um-1:5	Illite	22.55	48.93	12.12	6.85	0.94	2.78		0.16	5.67					100.0
3	<150um-2:7	Illite/chert	13.83	39.38	1.49	0.42	0.49	5.65			38.64		0.09			100.0
3	>180um-4:1	Illite	16.29	47.74	5.83	2.81	0.96	1.01		0.17	24.83		0.15	0.2		100.0
3	>180um-4:6	Illite	18.72	46.43	9.27	4.25	0.42	0.7	0.24	0.11	19.54		0.14	0.18		100.0
8	Chert-3:2	Illite	30.05	57.49	8.44	3.17	0.26	0.59								100.0
9	180-150um-3:1	Illite	25.9	53.68	11.31	6.08	0.59	1.86	0.23	0.35						100.0
9	180-150um-4:1	Illite	25.21	51.1	13.03	7.35	0.97	2.09	0.26							100.0
9	>180um-5:1	Illite	21.38	51.71	10.75	4.91	0.73	0.45	0.26	0.14	9.69					100.0
9	Un-1:1	Illite	15.45	48.72	8.6	4.47	0.43	1.72		0.38	20.24					100.0
9	Un-1:2	Illite	13.43	45.76	5.93	2.44	1.43				32					101.0
9	Un-2:1	Illite	17.96	50.09	9.57	4.55	0.59	1.8	0.15	0.12	15.18					100.0
9	Un-3:1	Illite	17.06	47.99	8.87	3.95	0.53	0.62	0.17		20.28			0.53		100.0
9	Un-5:3	Illite	20.65	46.22	8.29	5.3	0.74	2.33			16.46					100.0
9	Un-5:4	Illite	21.28	41.45	9.9	5.94	0.28	1.7	0.21	0.65	18.59					100.0
12	<150um-1:3	Illite	20.95	58.23	11.91	5.09	1.01	2.07	0.59	0.15						100.0
12	<150um-2:3	Illite	22.77	55.18	14.24	5.88	0.64	0.81	0.48							100.0
12	<150um-3:3	Illite	24.27	54.5	11.2	5.79	1.12	2.67	0.35	0.11						100.0
12	<150um-3:4	Illite	26.2	39.59	10.85	7.51	1.06	3.59	0.17	0.38	10.65					100.0
12	>180um-1:1	Illite	23.67	56.27	11.89	5.31	0.74	1.5	0.32	0.3						100.0
12	>180um-2:3	Illite	26.1	53.07	13.07	5.94	0.72	0.64	0.26	0.19						100.0
12	>180um-4:2	Illite	22.9	48.36	9.61	6.11	1.06	3.47		0.12	8.37					100.0
12	>180um-4:3	Illite	21.75	46.58	10.36	5.57	0.31	1.02	0.33	0.25	13.84					100.0
12	>180um-4:5	Illite	22.26	50.6	12.89	6.01	0.59	1.21	0.2	0.17	6.07					100.0
12	>180um-6:2	Illite	27.29	56.28	10.46	4.31	0.43	0.71	0.33	0.2						100.0
12	>180um-6:3	Illite	25.57	59.32	8.86	3.46	1.26	1.3	0.23							100.0
12	>180um-7:3	Illite	20.88	55.37	9.96	4.19	0.53	1.13	0.33	0.09	7.53					100.0
12	>180um-7:6	Illite	24.81	44.41	9.04	6.86	0.62	2.42		0.19	11.65					100.0
12	180-150um-1:1	Illite	22.12	57.07	13.52	5.12	0.53	0.82	0.65	0.17						100.0
12	180-150um-2:1	Illite	19.64	46.8	10.63	5.48	2.55	5.24		0.34	9.31					100.0
12	180-150um-2:4	Illite/chert	33.11	55.33	6.81	3.27	0.62	0.72					0.14			100.0
12	180-150um-3:2	Illite	24.25	55.38	12.18	5.38	0.88	1.46	0.26	0.21						100.0
12	180-150um-4:2	Illite/chert	31.57	50.52	3.68	2.34	0.58	10.5		0.51			0.3			100.0
13	>180um-3:2	Illite	22.7	49.59	9.54	6.15	0.84	3.28		0.19	7.7					100.0
13	>180um-3:4	Illite	24.64	53.56	12.74	6.12	0.59	1.5	0.3	0.41				0.14		100.0
13	>180um-4:1	Illite	26.29	47.38	13.26	8.68	0.47	3.35	0.29	0.27						100.0
13	>180um-5:3	Illite	21.78	49.05	6.36	2.03	1.67	5.43			13.11	0.24	0.15	0.17		100.0
13	180-150um-2:1	Illite	23.99	56.13	10.32	5.12	1.14	2.38	0.26	0.66						100.0
13	180-150um-2:3	Illite/chert	31.02	58.46	6.21	2.72	0.69	0.67	0.22							100.0
13	<150um-4:2	Illite	22	45.76	8.76	5.82	0.58	2.72			14.36					100.0
13	<150um-4:3	Illite	20.17	47.23	10.75	3.71	0.65	1.05	0.65		15.79					100.0

Table G1: EDS analyses of illite. Values are reported in element wt. %.

Site #	Report	Mineral	Si	O	Al	K	Mg	Fe	Na	Ti	C	Ca	S	Cl	Ba	Total
3	180-150um-1:3	Chlorite	19.82	50.74	9.52	0.58	11.48	7.47		0.38						100.0
3	180-150um-2:1	Chlorite	19.09	51.77	13.66	0.31	4.18	2.34	1.39		7.26					100.0
3	180-150um-4:2	Chlorite	15.68	49.32	5.87	0.58	5.7	5.63		0.19	16.85		0.19			100.0
3	<150um-1:2	Chlorite	13.71	53.17	7.7	0.14	11.04	5.26			8.99					100.0
3	>180um-2:3	Chlorite	12.94	48.78	5.97	0.23	7.79	9.34			14.83			0.12		100.0
3	>180um-3:1	Chlorite	12.56	50.62	6.97	0.97	7.96	4.8			16.12					100.0
12	180-150um-2:3	Chlorite	14.39	41.96	5.03	0.23	4.25	11.45			22.69					100.0

Table G2: EDS analyses of chlorite. Values are reported in element wt. %.

Site #	Report	Mineral	Si	O	Al	K	Mg	Fe	Na	Ti	C	Ca	S	Cl	Ba	Total
3	<150um-1:4	Kaolinite	15.96	52.01	17.49	0.71	0.21	3.56	0.29		9.36		0.41			100.0
8	>180um-1:3	Kaolinite	22.52	52.36	11.28	1.08	0.34	1.14	0.15	0.26	10.76			0.11		100.0

Table G3: EDS analyses of kaolinite. Values are reported in element wt. %.

Site #	Report	Mineral	Si	O	Al	K	Mg	Fe	Na	Ti	C	Ca	S	Cl	Ba	Total
3	180-150um-2:2	Unknown	21.66	27.54	5.67	0.97	3.05	23.37		0.9	16.84					100.0
12	<150um-4:1	Unknown	21.61	52.67	10.02	5.85	3.77	5.87		0.2						100.0
12	<150um-4:3	Unknown	17.68	55.32	10.22	2.54	7.17	6.92		0.16						100.0
12	180-150um-1:2	Unknown	17.55	51.89	10.33	1.2	9.13	9.91								100.0
12	180-150um-3:3	Unknown	23.76	54.84	10.72	2.7	4.1	3.47	0.25	0.17						100.0

Table G4: EDS analyses of unknowns. Values are reported in element wt. %.

Site #	Report	Mineral	Si	O	Al	K	Mg	Fe	Na	Ti	C	Ca	S	Cl	Ba	Total
1	<150um-1:1	Albite	24.35	47.42	6.44			1.03	5.2		15.57					100.0
1	<150um-2:1	Albite	22.65	53.19	6.67	0.05		0.65	6.74		10.05					100.0
1	<150um-2:2	Albite	25.43	49.59	6.96	0.08	0.13	0.34	5.92		11.55					100.0
3	<150um-1:1	Albite	28.24	48.84	7.68	0.09		0.26	6.07		8.82					100.0
3	<150um-1:3	Albite	26.55	46.72	6.82	0.15	0.13	0.47	4.72		14.44					100.0
3	<150um-1:8	Albite	24.94	45.58	6.07	0.18		0.34	4.19		18.69					100.0
3	<150um-1:9	Albite	23.88	49.62	6.79	0.07		0.2	5.9		13.54					100.0
3	<150um-2:3	Albite	21.64	43.32	5.95	0.06		0.24	4.27		24.52					100.0
3	<150um-2:4	Albite/chert	21.09	39.17	5.08	0.11			2.67		31.88					100.0
3	Bio-2:2	Albite/K-fsp	18.46	47.77	6.21	1.68		0.19	3.9		21.26	0.53				100.0
12	<150um-1:2	Albite	30.37	53.72	8.11	0.11		0.31	7.38							100.0
12	<150um-1:4	Albite	35.18	51.13	7.51	0.29		0.29	5.6							100.0
12	<150um-2:1	Albite	27.5	52.83	7.33	0.12		0.13	6.61		5.48					100.0
12	<150um-3:5	Albite	30.79	54.2	7.56	0.14		0.33	6.98							100.0
12	<150um-4:5	Albite	26.01	54.53	7.19	0.1		0.13	7.13		4.91					100.0
12	<150um-5:2	Albite/chert	40.87	39.03	7.26	0.35	0.13	0.49	2.49		9.37					100.0
12	<150um-7:1	Albite	29.83	53.76	8.53	0.09		0.17	7.62							100.0
12	>180um-2:4	Albite/chert	34.09	38.59	7.04	0.48		0.61	2.3		16.89					100.0
12	>180um-4:1	Albite	23.44	53.36	6.71	0.32		0.14	5.71		10.32					100.0
12	>180um-7:4	Albite	29.39	48.4	7.37	0.21	0.15	0.27	5.43		8.78					100.0
12	>180um-7:5	Albite	30.5	44.42	6.86	0.29		0.35	4.06		13.52					100.0
12	180-150um-4:1	Albite	28.81	55.16	7.97	0.08		0.14	7.84							100.0
13	>180um-3:3	Albite	29.93	51	5.85	0.09			4.18		8.95					100.0
13	180-150um-1:3	Albite	27.02	58.88	6.64	0.18		0.16	7.13							100.0
13	<150um-3:1	Albite	23.38	52.58	6.83	0.38	0.14	0.19	5.23		11.11	0.16				100.0

Table G5: EDS analyses of albite. Values are reported in element wt. %.

Site #	Report	Mineral	Si	O	Al	K	Mg	Fe	Na	Ti	C	Ca	S	Cl	Ba	Total
3	180-150um-3:4	K-fsp	23.17	38.12	5.51	9.07	0.35	5.2	0.19		18.24			0.16		100.0
3	180-150um-3:5	K-fsp	17.97	52.93	5.79	5.78		0.36	0.25		16.93					100.0
3	Bio-2:1	K-fsp	19.82	42.61	6.47	5.22		0.22	2.23		22.48	0.31			0.63	100.0
3	Bio-3:1	K-fsp	18.24	43.05	5.88	5.06		0.24	1.96		25.57					100.0
3	Bio-3:2	K-fsp	5.7	31.65	1.85	2.92		0.57	0.54		55.97				0.81	100.0
3	Bio-4:1	K-fsp	18.15	46.9	6.08	4.11		0.1	2.5		21.8	0.35				100.0
3	Bio-4:2	K-fsp/chert	16.71	47.82	3.93	1.65	0.63	5.15	1.49	0.47	21.56	0.39		0.21		100.0
3	180-150um-5:1	K-fsp	18.95	36.15	5.62	6.17		0.72	1.16	0.12	30.84	0.26				100.0
8	<150um-3:1	K-fsp/chert	32.55	47.04	7.63	8.41	0.27	3.56		0.54						100.0
12	<150um-6:1	K-fsp/chert	23.08	50.43	3.26	5.85	0.71	4.09		0.38	12.2					100.0
13	>180um-5:1	K-fsp/chert	15.61	43.19	1.29	2.92	0.13	4.4		0.19	32.1		0.08	0.09		100.0

Table G6: EDS analyses of K-feldspar. Values are reported in element wt. %.